Enabling Secure Communications: Theoretical Tools for Quantum Repeater Systems

Inauguraldissertation

zur
Erlangung der Würde eines Doktors der Philosophie
vorgelegt der
Philosophisch-Naturwissenschaftlichen Fakultät
der Universität Basel

von

Melvyn Ho
von Singapur

Basel, 2019

Genehmigt von der Philosophisch-Naturwissenschaftlichen Fakultät auf Antrag von
Prof. Dr. Nicolas Sangouard
Dr. Mikael Afzelius

Basel, den 24 Apr 2018

Prof. Dr. Martin Spiess
Dekan

ABSTRACT

As children, whispering into the ear of a friend in the presence of others allows us to pass a secret without interception, and forms one of the simplest attempts at secret communications we can employ. However, sending secret messages becomes deeply nontrivial over long distances.

A solution for two parties to communicate securely is to encrypt and decrypt a message with two identical strings of bits, one for each party. In this case, the security of the encrypted message is provable and does not rely on assumptions on computational power. Quantum theory provides a clear solution for the initial distribution of these identical bit strings through Quantum Key Distribution. However, once long distances are involved, the corresponding loss involved in direct transmission ruins the effectiveness of quantum key distribution by reducing the effective rate exponentially with the distance.

To circumvent the losses involved in direct transmission, quantum repeater architectures have been proposed. We present our contributions towards three aspects of quantum repeater systems in this thesis. We *ensure conditions* for implementing quantum repeaters with atomic ensembles, *explore the option* of optomechanical systems for implementing quantum repeaters and *verify the success* of completed quantum repeater protocols.

In the first part of this thesis, we show how we can ensure conditions for the successful implementation of quantum repeater systems with atomic ensembles. These quantum repeater systems are formed with 1-dimensional networks, where

the nodes are made up of quantum memories connected by means of single photons. This requires memories that are highly efficient. Also, if quantum repeater systems are implemented with hybrid resources, tunable photon waveforms will be desirable. We propose a protocol to implement quantum memories with atomic ensembles using a clear recipe to optimise the efficiency. We also demonstrate that a cold ensemble of Rubidium-87 can act as an efficient tunable source of single photons, along with flexibility in the produced temporal shapes.

Next, we show how we can explore alternative options for the nodes of quantum repeater systems. We focus on optomechanical oscillators, and recognise that they can also be used as quantum memories. We present a witness to certify that this memory successfully operates in the quantum regime.

Finally, we focus on the verification of successfully implemented quantum repeater protocols. This verification will be essential for certifying that quantum repeater systems operate as instructed. We use only local homodyne measurements to witness the success of the network, and find that the witness is robust to loss.

We thus present distinct contributions towards three important aspects of quantum repeater systems. As far as a full-fledged quantum repeater system might seem to be right now, we have faith that our work brings the field of quantum-enabled secure communications forward.

ACKNOWLEDGMENTS

It is a great pleasure to be able to thank all those who supported me through the completion of this thesis.

A key factor leading to the completion of this thesis has been the people in the group. This journey would not have been possible without the patient tutelage of Nicolas Sangouard, who has mentored me through my time in the group. There has been much to learn from you, Nicolas. Also reaching back to the first work in collaboration with GAP in Geneva are Jean-Daniel and Pavel. They have somehow found themselves here in Basel at the end of this journey, which I believe is no accident. They always been eager to do more science, and bring more clarity and understanding. Special mention goes to Enky, who has been a complementary voice in so many things, even in the science! I am also especially grateful for him showing a window into a different life. I can only hope to have done the same in return. I also would like to thank Amaury and Sebastian for careful and patient discussions, so that the time spent here in this group could be always fulfilling, and the environment never dull.

Thanks goes to a long list of external collaborators from Paris, Barcelona and beyond, who have been gracious enough to work with us alongside so many other possibilities. Our 'hybrid' work between theory and experiment has been very fulfilling.

I'd like also to especially thank a different group here in Basel. The disciples in Basel Christian Fellowship, full of strangers and foreigners, have been a strong encouragement in faith and deed.

While much support has come from Basel, support has also come from Singapore. There is absolutely no doubt that the hopes, prayers and well-wishes of family and friends have contributed immeasurably to this event.

No words can completely express the appreciation I have for Kimberley. Her love has been a source of strength in this endeavour.

In this journey God has been Author, Perfector, and the One who reveals all mysteries in His time.

For now we see in a mirror dimly, but then face to face; now I know in part, but then I will know fully just as I also have been fully known.

1 Cor 13:12
New American Standard Version

CONTENTS

LIST OF PUBLICATIONS

1. Witnessing trustworthy single-photon entanglement with local homodyne measurements
   Physical Review Letters **110**, 130401 (2013)

2. Witnessing single-photon entanglement with local homodyne measurements: analytical bounds and robustness to losses
   New Journal of Physics **16**, 103035 (2014)

3. Generation of single photons with highly tunable wave shape from a cold atomic quantum memory
   Nature Communications **7**, 13556 (2016)

4. Probing wave function collapse models with a classically driven mechanical oscillator
   New Journal of Physics, **18**, 033025 (2016)

5. Optimal photon generation from spontaneous Raman processes in cold atoms
   New Journal of Physics **20**, 123018 (2018)

6. Witnessing opto-mechanical entanglement with photon-counting
   Physical Review Letters **121**, 023602 (2018)

INTRODUCTION

With the birth [1, 2] and subsequent mathematical formulation [3, 4, 5] of quantum mechanics in the early 20th century, consequent scientific advances have led to new and unpredicted advances in our understanding of nature. This distinct break from the then well-understood realm of classical physics has allowed us to see quantisation, complementarity, superposition and probability amplitudes as valuable ingredients in the description of many physical effects, including the radiation of black bodies [1], the photoelectric effect [2] and the Young's double slit experiment with individual particles [6].

In addition to providing a detailed description of physical phenomena, quantum theory has also provided new applications. For example, the quantum mechanical prediction that the simple photon's detection after a 50-50 beam-splitter being perfectly random has been invaluable for implementing sources of random numbers. Companies such as ID Quantique and Quintessence have already been commercialising devices for randomness generation based on such a principle. Quantum theory has also brought about new possibilities in computing, with quantum systems being able to simulate the behaviour of other, difficult-to-implement quantum systems, in order to study their behaviour [7]. Furthermore, quantum computers also offer the promise of an exponential speedup in some computational tasks. Building a quantum computer is currently the single-minded focus of some departments within IBM, Google and Microsoft, and also various labs and startups all over the world [8].

The last point has been especially worrying to many. This exponential speedup threatens to nullify the security of communication protocols based on the difficulty

of certain mathematical problems. A clear example is the commonly used RSA [9] protocol, which relies on the difficulty of factorising large numbers, and forms the guarantee for the security of internet browsers and other transactions. If any adversaries possess a quantum computer, they could use Shor's algorithm [10] to efficiently find the factors of any large integer, rendering the RSA scheme insecure. The aforementioned surge of recent efforts by both academia and industry towards a quantum computer have resulted in successive increases of the range over which large integers can be factored with quantum devices [11, 12, 13]. These systematic improvements make it clear that the security of communication protocols cannot continue to rely on computational complexity alone.

Thankfully, quantum theory offers a solution for secure communications that does not rely on an assumed limitation of adversarial computational power. There is a protocol in classical cryptography dating back to 1882 [14], which states that if Alice and Bob share a secret key, all that remains for them to securely send messages is to encrypt and decrypt their message with that key. If this secret key is truly completely random, and not reused, then this encryption/decryption protocol (known as One Time Pad) is completely secure. The remaining issue is that of securely distributing the secret keys in the first place, which has to be as long as the message to be encrypted [15]. The requirement to securely share a key between the two parties thus presents a problem as large as that of sending the original message in the first place. Thankfully, Quantum Key Distribution (QKD) offers a way to avoid this issue. Let us first describe the basic principles of the well-known BB84 protocol [16] first (see Fig 1).

Consider the scenario where Alice would like to send Bob an encryption key composed of a string of random bits. She encodes each classical bit in the form of a qubit in either the X or Z basis,

$$Z \text{ basis} : \begin{cases} 0 \rightarrow |0\rangle \\ 1 \rightarrow |1\rangle \end{cases} \quad X \text{ basis} : \begin{cases} 0 \rightarrow |+\rangle \\ 1 \rightarrow |-\rangle \end{cases} ,$$

and sends the resulting qubits to Bob. Bob proceeds to randomly perform measurements in the Z or X basis. They both publicly reveal the bases they had used, and keep only the bits where they had used the same basis choices. These bits are ideally perfectly identical, and can thus define a shared raw key. At the quantum level, since we are using two different measurement bases, the no-cloning theorem [17, 18] prevents Eve from always making a perfect copy of the sent bit. At the

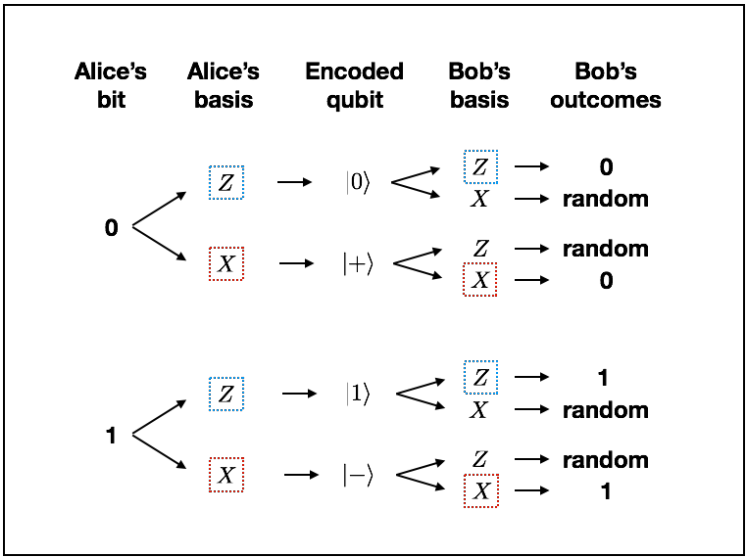

Figure 1: Schematic of the BB84 protocol. For each classical bit in her original random string, Alice selects a random basis for encoding (shown in different coloured boxes). For runs where Bob selects the same basis as Alice (marked in coloured boxes as well), he observes the outcome corresponding to the bit that Alice wanted to send.

classical level, the knowledge of the basis after the measurements have been done do not help her to infer Alice's inputs, nor the outcomes of Bob's measurement, since they are both completely random. Classical post-processing steps (such as error correction and privacy amplification) can be applied if the error rate is low enough, allowing them to refine the raw key into a useable secret key. This protocol can thus provide secure communications with qubits, without any assumptions on computational power [15].

Another QKD scheme related to the above protocol is the E91 protocol [19], which requires the use of entangled states. The basic idea is the following. If Alice and Bob share a singlet state, and Alice measures her qubit in the X basis, she projects Bob's qubit into one of the eigenstates of the X measurement. If Bob also measures his qubit in the same basis, he obtains a perfectly anticorrelated measurement outcome. As such, by simply choosing one out of two settings at random (See Fig 2), Alice and Bob can get a raw key from their outcomes after comparing their bases, similar to the BB84 scenario. The advantage of E91 relies on the possibility of using Bell tests to check the quality of their entangled state. In particular, the maximal violation of the Bell-CHSH inequality [20] certifies that the singlet state has been measured, without any assumptions on either the underlying Hilbert space or on the proper calibration of the measurement device.

This sets the framework for device-independent QKD (DIQKD) [21, 22, 23], which offers security guarantees without assumptions on the shared quantum state or measurement, and again without assumptions on computational power.

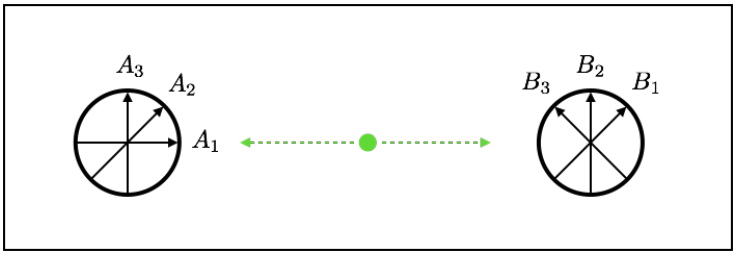

Figure 2: Schematic of the E91 protocol. Alice and Bob make measurements along randomly chosen measurement directions on a singlet state of two qubits. After their measurements they announce their basis choices. Measurement runs where they had the same basis can be used to form the basis for the raw key. Other runs can be used to ascertain the value of a Bell inequality to assess the quality of their shared state.

The security guarantees provided by QKD have inspired efforts worldwide to benefit from this technology, beginning with the first proof-of-principle experiment spanning just 30cm [24]. From there, keys have been distributed between increasingly distant sites via fiber [25, 26, 27], reaching past 300km while managing losses greater than 50dB. Further lengthening of the distance will result in an unavoidable exponential increase in the loss, and hinder the effectiveness of QKD by severely limiting the distributed key rate. Attempts have been made to overcome these losses with the use of satellites, as the advantage here is that atmospheric attenuation at high altitudes ($\sim$0.07 dB/km) can be much lower than fiber, with negligible attenuation from the vacuum of space [28]. Despite recent successes with satellites [29, 30], there are several considerations to watch for. Even after successfully launching a satellite, ensuring an always-open communications window requires the satellite to be geostationary, for which there are limited orbital paths. Furthermore, the time of day can also change the background noise level of the transmitted photon wavelength [31]. Although satellite implementations offer some options, direct transmission remains an issue in QKD protocols.

What else can one do to overcome the problem of losses involved in direct transmission? Classical communication networks involve the use of amplifier stations along the transmission path to boost the degraded signal. However, direct amplification techniques are not directly applicable to QKD protocols, again due to the no-cloning theorem [17, 18]. Quantum repeater architectures [32, 33] offer

a promising solution. The basic principle is as follows. The global distance is divided into n links, where entanglement is established within each link. This step is made efficient by using quantum memories so that attempts at entanglement creation are being done independently in each link. This drastically reduces the losses, since the relevant efficiency is that of the efficiency of a single link η, as compared to the direct transmission efficiency η^n. Successive entanglement swapping operations can be performed by the repeater stations to establish entanglement between the far away stations (see Fig 3).

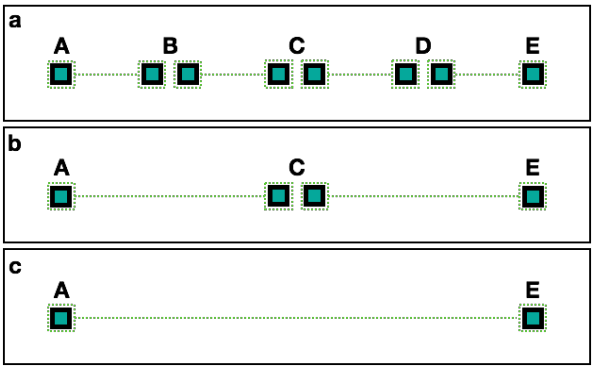

Figure 3: Schematic of successive entanglement swapping across 4 links. (a) Distant users (A, E) wish to share entanglement, and can make use of quantum repeater stations (B-D) situated between them. Consider the situation where the stations have established entanglement between neighbouring systems, as shown in green dotted lines. For example, station B has established entanglement via direct transmission with A and C separately. (b) Stations B and D perform entanglement swapping operations to allow station C to share entanglement with A and E. (c) Next, station C performs swapping, establishing entanglement between the distant users.

For the above quantum repeater architecture to be useful, it requires the entanglement within each link to be created in a heralded way. Also, neighbouring stations must be able to perform entanglement swapping, and this requires efficient retrieval operations. These requirements are necessary for the quantum repeater system to efficiently distribute entanglement.

The following protocol proposed by Duan, Lukin, Cirac and Zoller [34], known as the DLCZ protocol, allows one to build a quantum repeater while satisfying the requirements above, requiring only the use of atomic ensembles and linear optical elements (see Figs 4 and 5).

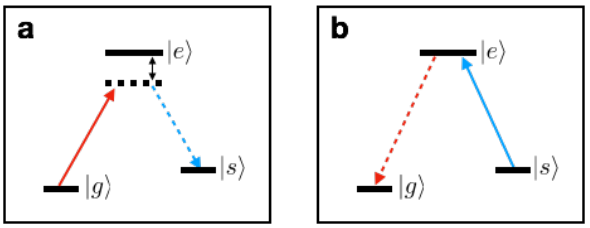

Figure 4: Write and read operations on a 3-level atomic system with excited level $|e\rangle$ and two metastable states $|g\rangle$ and $|s\rangle$. (a) A far-detuned write laser pulse (solid red arrow) creates a single delocalised excitation on $|s\rangle$, accompanied by a write photon emission (blue dotted arrow) (b) The delocalised excitation can be retrieved with the use of a resonant read laser pulse (blue solid arrow), accompanied by a read photon emission (red dotted arrow).

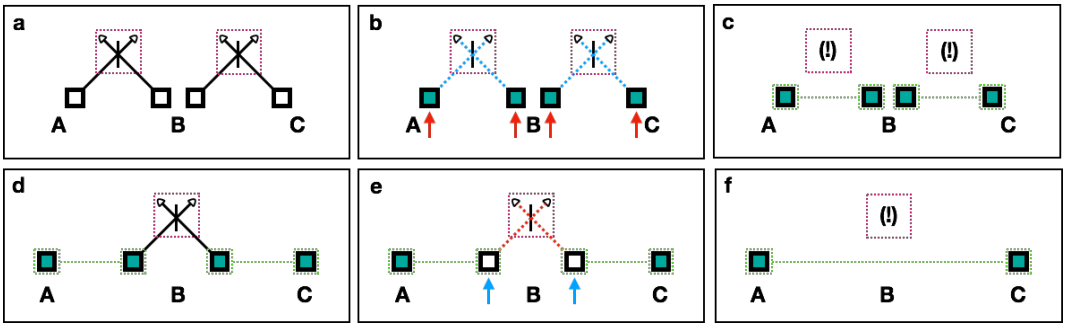

Figure 5: Schematic of DLCZ protocol for building a quantum network. (a) Users A and C wish to set up entanglement between their atomic ensembles (black boxes) with the help of repeater station B. (b) Each site sends a far-detuned write laser pulse onto one atomic transition, and they interfere the emitted write photons in a beamsplitter, which might be situated closer to one of the sites. (c) Upon a detection, each individual link has successfully created a delocalised atomic excitation between the two ensembles (entangled ensembles are connected with dotted green lines). (d) To connect entanglement, repeater station B has to perform swapping. (e) Read laser pulses are sent into the atomic ensembles in order to interfere the emitted read photons in a beamsplitter. (f) A detction indicates that entanglement has been successfully swapped.

In the DLCZ repeater architecture, each link is made up of two atomic ensembles (one at each node), and a central station with linear optics and photon counting. Each ensemble of 3-level atoms is initially prepared in the ground state. Far-detuned write laser pulses produce Raman scattered write photons correlated with spin excitations. The write modes are combined using a 50-50 beamsplitter in a central station, erasing the which-path information so that a single detector after the beamsplitter heralds a single delocalised excitation in one of the two

ensembles. These steps create entanglement between the two ensembles, which share a single excitation. After two neighbouring links have been successfully set up, read laser pulses are sent into atomic ensembles at the intermediate repeater stations. The resulting read modes are then combined into a 50-50 beamsplitter. The subsequent detection after the beamsplitter heralds the entanglement connection between the far away locations. Since the two links involved in the swapping each share a delocalised single excitation, the click after the beamsplitter projects the remote sites into an entangled state. Crucially, the entanglement needs to be swapped at a beamsplitter. This can be done, since the initial write process imprints a momentum-dependent phase on the atomic ensemble, allowing for retrieval into a well-defined spatial mode. Finally, once the desired sites have been entangled with successive swapping operations, retrieval can be performed on the entangled atomic ensembles to obtain a path-entangled state, which is an entangled state of 2 optical modes sharing a single delocalised photon.

These simple ingredients that make up the DLCZ protocol are experimentally appealing, and can even be used to constitute more effective architectures [33]. However, ensuring that these ingredients result in the successful distribution of entanglement across long distances can require some investigation and fine-tuning. Firstly, for a working quantum repeater system, high retrieval efficiencies of $\sim 90\%$ are crucial. Depending on the architecture, a reduction of the retrieval efficiency by 1% can reduce the repeater distribution rate by $10 - 20\%$ [33], highlighting the retrieval efficiency as a critical factor. This motivates work on optimising the retrieval efficiency from stored atomic excitations. Secondly, in order to make the DLCZ repeater system more efficient, one might include a combination of different systems as ingredients. This requires the ability to address each of these systems using photons of different waveforms. We describe our results towards studying and *ensuring* these conditions in **Chapter 1: Atomic Ensembles for Quantum Repeaters**.

Instead of the atomic ensembles described in the original DLCZ protocol, one might also explore the possibility of performing the DLCZ protocol with mechanical resonators. To do this, one has to be sure that there is an initial process creating correlated excitations between the resonator and the write photon mode, and afterwards a subsequent process for retrieving the stored excitation into a read photon mode. We recognise that these processes are possible with mechanical resonators, and go on to design an entanglement witness to certify that these

correlated excitations have been formed. These tools show that optomechanical devices can form the cornerstone of future quantum repeaters. We *explore* such an alternative platform in **Chapter 2: Optomechanical Devices for Quantum Repeaters**.

Upon the successful setup of remote entanglement using quantum repeaters, one might want to verify the quality of the resulting entanglement. The original DLCZ article prescribes a method based on having an additional chain of DLCZ repeater systems, and then relying on postselection showing that entanglement was present. This requirement for extra repeaters makes entanglement verification logistically prohibitive. Postselection is also not useful in the implementation of applications like device-independent QKD. A simple method of verifying entanglement using local measurements would allow users to easily verify if the distributed state is entangled. We present this method of *verifying* the success of the repeater system in **Chapter 3: Certifying Quantum Repeaters**.

CHAPTER 1

ATOMIC ENSEMBLES FOR QUANTUM REPEATERS

As we have shown in the Introduction, the DLCZ protocol allows for quantum repeaters to be set up while taming the losses from direct transmission. The use of atomic ensembles allows for the entanglement in each link to be created independently. Swapping operations can connect entanglement once neighbouring links have been established, so that entanglement can be established over long distances. The distributed entanglement can then be used for the desired task.

So far we have described the use of atomic ensembles acting as the nodes of the network. Eventually, distributing entangled states over intercontinental distances might well involve dissimilar nodes so as to benefit from their respective advantages [35]. Optimising the coupling within such hybrid networks would require the careful matching of linewidths between the photons and respective devices [36]. In addition, optimisation of the retrieval efficiency from the quantum memory is needed so as to minimise any losses from the swapping operations.

To address concerns with regards to the spectrum of the read photons, we explore the control of the emission profile from a cold atomic ensemble [37]. We have shown that a cold atomic ensemble of Rubidium-87 can act as a tunable source of single photons, with controllable emission times varying over 3 orders of magnitude (up to several tens of μs in duration) while maintaining the retrieval efficiency. Aside from creating long duration gaussian-profiled single photons, we also produced single photons of other shapes, including exponentially rising shapes and double-peaked wave shapes. This further demonstrates a flexibility in controlling photon waveforms for coupling within quantum networks.

Having explored the limits of a particular atomic sample with regards to the emission duration, we go on to investigate the limits with regards to the retrieval efficiency [38]. Taking close reference from the work of [39], we first examine the dependence of the retrieval efficiency on given experimental parameters. For a given optimal depth of an atomic ensemble, there is an optimal spin shape with which to perform retrieval from. We thus propose a simple recipe for creating near-optimal spin shapes in the sample so as to allow for high retrieval efficiencies. This involves the use of a resonant exponentially rising write pulse that undergoes significant attenuation by the sample. By optimising the duration of the resonant write pulse we can create spin excitations that yield near-optimal retrieval efficiencies for a given optical depth.

Paper A

Generation of single photons with highly tunable wave shape from a cold atomic ensemble

Pau Farrera, Georg Heinze, Boris Albrecht, Melvyn Ho, Matías Chávez, Colin Teo, Nicolas Sangouard and Hugues de Riedmatten

Nature Communications **7**, 13556 (2016)

nature COMMUNICATIONS

ARTICLE

Received 4 May 2016 | Accepted 13 Oct 2016 | Published 25 Nov 2016

DOI: 10.1038/ncomms13556 OPEN

Generation of single photons with highly tunable wave shape from a cold atomic ensemble

Pau Farrera[1], Georg Heinze[1], Boris Albrecht[1,†], Melvyn Ho[2], Matías Chávez[2], Colin Teo[3,4,†], Nicolas Sangouard[2] & Hugues de Riedmatten[1,5]

The generation of ultra-narrowband, pure and storable single photons with widely tunable wave shape is an enabling step toward hybrid quantum networks requiring interconnection of remote disparate quantum systems. It allows interaction of quantum light with several material systems, including photonic quantum memories, single trapped ions and opto-mechanical systems. Previous approaches have offered a limited tuning range of the photon duration of at most one order of magnitude. Here we report on a heralded single photon source with controllable emission time based on a cold atomic ensemble, which can generate photons with temporal durations varying over three orders of magnitude up to 10 μs without a significant change of the readout efficiency. We prove the nonclassicality of the emitted photons, show that they are emitted in a pure state, and demonstrate that ultra-long photons with nonstandard wave shape can be generated, which are ideally suited for several quantum information tasks.

[1] ICFO-Institut de Ciencies Fotoniques, The Barcelona Institute of Science and Technology, 08860 Castelldefels, Barcelona, Spain. [2] Department of Physics, University of Basel, Klingelbergstrasse 82, 4056 Basel, Switzerland. [3] Institute for Quantum Optics and Quantum Information of the Austrian Academy of Sciences, A-6020 Innsbruck, Austria. [4] Institute for Theoretical Physics, University of Innsbruck, A-6020 Innsbruck, Austria. [5] ICREA-Institució Catalana de Recerca i Estudis Avançats, 08015 Barcelona, Spain. † Present addresses: Niels Bohr Institute, University of Copenhagen, Denmark (B.A.); Singapore University of Technology and Design, 8 Somapah Road, 487372 Singapore (C.T.). Correspondence and requests for materials should be addressed to G.H. (email: georg.heinze@icfo.es) or to H.d.R. (email: hugues.deriedmatten@icfo.es).

A vast range of experiments in quantum information science and technology rely on single photons as carriers of information[1]. Single photon sources are thus key components and have been continuously improved over the past years[2]. The spectrum and temporal shape of the emitted photons are important parameters of such sources[3]. The generation of ultra-long single photons is for example an essential requirement for precise interactions with media exhibiting a sharp energy structure like trapped atoms, ions or doped solids, which have been proposed as quantum memories for light[4–6] and also with cavity opto-mechanical systems[7–11].

Several approaches to achieve narrow linewidth photons have been investigated, including for example, cavity-enhanced spontaneous parametric down conversion[12–14], cold atomic ensembles[15–22], single atoms[23,24], quantum dots[25] or trapped ions[26,27]. Moreover, significant efforts have been devoted to generate single photons with tunable temporal shapes[20,26,28–34], which is important for many applications in quantum information science[35,36]. However, most of the previous approaches offered only a limited tuning range of the photon duration up to at most one order of magnitude[20,26,32].

In this paper, we demonstrate a single photon source with a wide tuning range of three orders of magnitude, up to single photon durations of 10 μs. To our knowledge, this represents the longest photons generated from an atomic ensemble. Our source is based on a cold atomic ensemble quantum memory (QM) following the scheme of Duan, Lukin, Cirac, and Zoller (DLCZ)[37], which allows us to release the single photons on demand after a programmable delay. This is essential for temporal synchronization tasks as for example needed for quantum repeater architectures[38,39] or synchronization of photon pair sources[40]. In contrast to most former DLCZ experiments, we apply readout pulses with very flexible temporal shapes, which are accurately controlled over several orders of magnitude in amplitude and time. This enables the generation of ultra-long single photons with very flexible wave shapes and coherence times much longer than the lifetime of the involved excited state. We characterize the emitted photons by measuring their heralded and unheralded autocorrelation functions, demonstrating a high degree of anti-bunching and purity.

Results

Heralded single photon source with controllable emission time. Our heralded single photon source is based on a cold ensemble of N identical ^{87}Rb atoms in a magneto-optical trap. Each atom exhibits a Λ-type level scheme consisting of a ground state $|g\rangle=|5^2S_{1/2},\ F=2,\ m_F=2\rangle$ a storage state $|s\rangle=|5^2S_{1/2},\ F=1,\ m_F=0\rangle$ and an excited state $|e\rangle=|5^2P_{3/2},\ F=2,\ m_F=1\rangle$ (see Fig. 1b). The atoms are initially prepared in the ground state $|g\rangle$ by optical pumping. A weak write pulse, detuned from the $|g\rangle\rightarrow|e\rangle$ transition, probabilistically creates a delocalized single-collective spin excitation (spin-wave) in the memory by transferring a single atom into the $|s\rangle$ state. This process is heralded by a Raman scattered write photon. The state of the spin-wave is to first order given by

$$|1_s\rangle=\frac{1}{\sqrt{N}}\sum_{j=1}^{N}e^{i\mathbf{x}_j\cdot(\mathbf{k}_W-\mathbf{k}_w)}|g_1\ \ldots\ s_j\ \ldots\ g_N\rangle, \qquad (1)$$

where $\mathbf{x}_j$ denotes the spatial position of the jth atom and $\mathbf{k}_W$ and $\mathbf{k}_w$ are the wave vectors of the write pulse and the write photon, respectively. Neglecting noise, the joint state of the write photon and the associated spin-wave is described by a two-mode squeezed state as

$$|\phi\rangle=\sqrt{1-p}\left(|0_w\rangle|0_s\rangle+\sqrt{p}|1_w\rangle|1_s\rangle+p|2_w\rangle|2_s\rangle+o\left(p^{3/2}\right)\right), \qquad (2)$$

with p the probability to create a spin-wave correlated with a write photon in the detection mode. After a programmable delay, the spin-wave is converted back to a single read photon by a read pulse, which is resonant with the $|s\rangle\rightarrow|e\rangle$ transition. Due to collective interference of all atoms, the read photon is emitted in a well defined spatial mode given by the phase matching condition $\mathbf{k}_r=\mathbf{k}_R+\mathbf{k}_W-\mathbf{k}_w$, where $\mathbf{k}_R$ and $\mathbf{k}_r$ are the wave vectors of the read pulse and read photon, respectively. The noise-corrected retrieval efficiency is defined as $\eta_{\rm ret}=(p_{w,r}-p_{w,nr})/p_w$, where $p_{w,r}$ is the probability to detect a coincidence between a write and a read photon, $p_{w,nr}$ is the probability to detect a coincidence due to background noise and p_w is the probability to detect a write photon per trial.

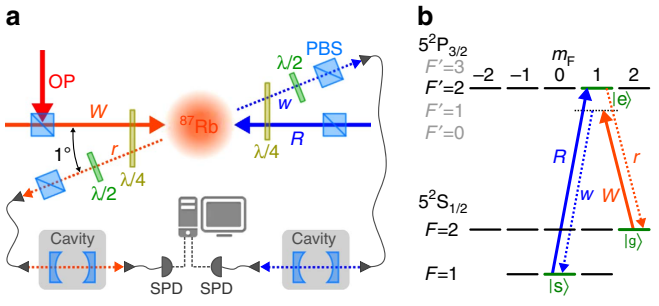

Figure 1 | Experimental set-up and level scheme. (**a**) Experimental set-up. Write pulse (*W*) and read pulse (*R*) are sent counterpropagating into the atomic cloud. Write and read photons (denoted by *w* and *r*) are sent after polarization filtering via fibres to frequency filtering cavities before being detected by SPDs. (**b**) Energy levels of the D2 line of ^{87}Rb and coupling scheme for the DLCZ experiment.

Experimental set-up. The experimental set-up is shown in Fig. 1a. All light beams are derived from diode lasers resonant to the D_2 line of ^{87}Rb at 780 nm. To generate the desired laser pulses, the beams are modulated by acousto-optic modulators in double-pass configuration driven by an arbitrary waveform generator (Signadyne AWG-H3384) with a sampling frequency of 1 GS s^{-1} and amplifiers (AA Optoelectronic AMPA-B-34). We combine a magnetic gradient of 20 G cm^{-1} with cooling light (red detuned from the $|F=2\rangle\rightarrow|F'=3\rangle$ transition) and repumping light (resonant with the $|F=1\rangle\rightarrow|F'=2\rangle$ transition) to load $N\approx10^8$ Rubidium atoms into the MOT. After a 1.6 ms long optical molasses phase, we prepare all population in the $|g\rangle$ Zeeman sublevel by applying repumping light and σ^+ polarized optical pumping (OP) light on the $|F=2\rangle\rightarrow|F'=2\rangle$ transition. The spin-wave is generated by sending a write pulse of 15 ns duration (full-width at half-maximum, FWHM), which is red detuned by 40 MHz from the $|g\rangle\rightarrow|e\rangle$ transition. The heralding write photon is collected at an angle of 1° with respect to the write/read pulse axis. By changing the intensity of the write pulse, we can adjust the probability p_w to detect a write photon per trial. For the experiments presented in this paper, p_w ranges between 0.25% and 1% depending on the measurement. The read pulse, counterpropagating with the write pulse, is resonant with the $|s\rangle\rightarrow|e\rangle$ transition and its temporal shape can be precisely controlled. The read photon is collected in the same spatial mode but opposite direction of the write photon. By measuring the transmission of classical light sent through the photons axis and by comparison of experimental and theoretical data in Figs 2 and 5, we infer a coupling efficiency of the read photon into the first fibre of $\eta_{\rm fibre}\approx60\%$. The polarization of the write and read pulses

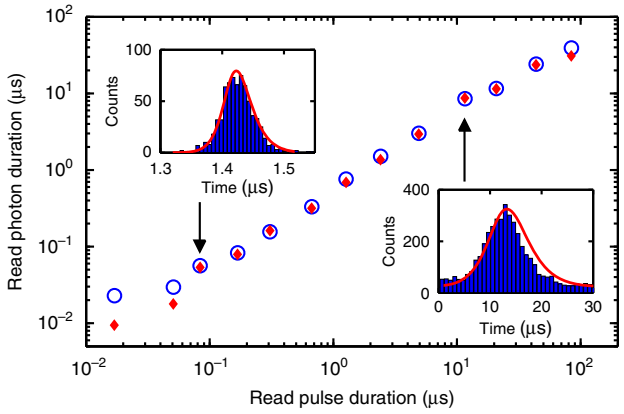

Figure 2 | Temporal duration of the read photon versus the duration of the driving read pulse. Experimentally measured durations (FWHM) (blue circles, errorbars smaller than symbol size) are compared with numerical simulations (red diamonds). The insets show two examples of the read photon wave shape as reconstructed from the number of counts and arrival times in the SPDs (blue histograms) as well as the simulated wave shapes (red lines) for which we allowed at most 10% adjustment of the input parameters to account for experimental inaccuracies.

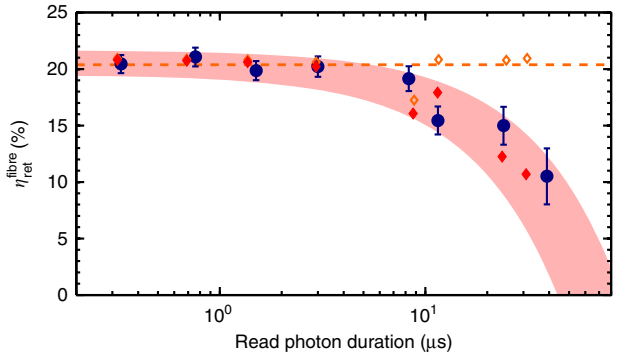

Figure 3 | Retrieval efficiency. Fibre-coupled retrieval efficiency η_{ret}^{fibre} versus read photon duration (FWHM) for $p_w = 0.5\%$. Experimental data (blue dots) are compared with numerical simulations (see Supplementary Note 2) for realistic (red diamonds) and ideal (orange diamonds) conditions. The red shaded area depicts the expected range if the input parameters of the simulation are varied by ±10%. The errorbars (±1 s.d.) correspond to the propagated Poissonian error of the photon counting statistics.

in the frame of the atoms is σ^- and σ^+, respectively, while the detected write and read photons are σ^+ and σ^- polarized. We use a combination of quarter- and half-waveplates with polarization beamsplitters to transmit only the photons with the correct polarizations. The write and read photons are moreover spectrally filtered by identical monolithic Fabry–Perot cavities with $\eta_{filter} \approx 20\%$ total transmission (including cavity transmission and subsequent fibre coupling), before being detected by single photon detectors (SPDs) with $\eta_{det} = 43\%$ efficiency and a dark count rate of 130 Hz.

Measurements. We now present the experimental results and compare them to detailed theoretical calculations. To generate read photons of variable length, we change the duration of the Gaussian-shaped read pulse as well as the storage time over several orders of magnitude (see Fig. 2). The shortest read pulse duration of ~17 ns leads to a read photon of around 23 ns duration. After that initial data point, we observe a quite linear increase of the read photon duration with the read pulse duration up to several tens of microseconds. The lower limit of photon duration is given by the limited optical depth OD = 5.5 in our experiment, which leads to limited superradiant emission of the read photon[41]. A further technical limitation is given by the finite bandwidth of the spectral filtering cavity of about 60 MHz, which additionally increases the detected duration for short read photons. This effect, together with the deviation from the adiabatic condition, partly explains the slight difference of the first data points in Fig. 2 from the theoretical prediction (see below). The upper limit of photon duration is given by the spin-wave linewidth, which is mainly determined by thermal atomic motion and spurious external magnetic fields. This currently limits the maximal storage time in the memory to about 50 μs (see Supplementary Note 1 and Supplementary Fig. 1). In addition, the photon duration will also be limited by the coherence time of the read laser, which has a specified linewidth of 20 kHz. However, within the above limits, we demonstrate that the photon duration is fully tunable and that the Gaussian wave shape of the driving read pulse is preserved in the readout process (see insets).

The dynamics of the write and read photon pairs is modelled using the Heisenberg–Langevin equations. For slowly varying optical fields propagating in a pencil-shape atomic ensemble, explicit expressions for both the write and read photon fields can be obtained in the adiabatic approximation[42]. These field expressions can be subsequently used to reproduce the read photon emissions conditioned on the detection of a write photon from first and second order correlation functions (see Supplementary Note 2). The result of these simulations which are based on independent measurements reproduce very well the experimental data presented in Fig. 2.

To characterize the retrieval efficiency of the photon source, we optimized the intensity of the driving read pulse for each duration (see Supplementary Note 1 and Supplementary Fig. 2). Figure 3 shows the highest achievable fibre-coupled retrieval efficiency $\eta_{ret}^{fibre} = \eta_{ret}/(\eta_{filter} \cdot \eta_{det})$ versus the read photon duration, which corresponds to the probability of finding a read photon in the optical fibre after the vacuum cell, that is, corrected for filtering and detector efficiencies only. We observe a constant retrieval efficiency of about $\eta_{ret}^{fibre} = 20\%$ up to a read photon duration of ~10 μs. Our numerical simulations match very well with the experimental data and also show that the efficiency in the constant region is just limited by the finite OD of our atomic cloud. We verify numerically that in the absence of technical noise and considering infinite spin-wave coherence, for OD = 50 an intrinsic retrieval efficiency of 80% can be achieved while maintaining control of the photon shape. The decrease of the efficiency at around 10 μs is due to dephasing of the spin-wave induced by atomic motion, spurious external magnetic field gradients[43] and the finite read laser coherence time. In particular, our numerical simulations show clearly that in the absence of technical noise and in the limit of infinite spin coherence, the efficiency is kept constant (see orange diamonds and dashed line in Fig. 3).

Next, we characterized the state of the emitted read photons by measuring their heralded and unheralded second order autocorrelation functions depending on the read photon duration. To perform these measurements, we inserted a balanced fibre beamsplitter into the read photon arm after the spectral filtering cavity, with both output ports connected to SPDs $r1$ and $r2$. First, we recorded the autocorrelation function conditioned on the detection of a write photon, defined as[44]:

$$g^{(2)}_{r1,r2|w} = \frac{p_{r1,r2|w}}{p_{r1|w} \cdot p_{r2|w}} \quad (3)$$

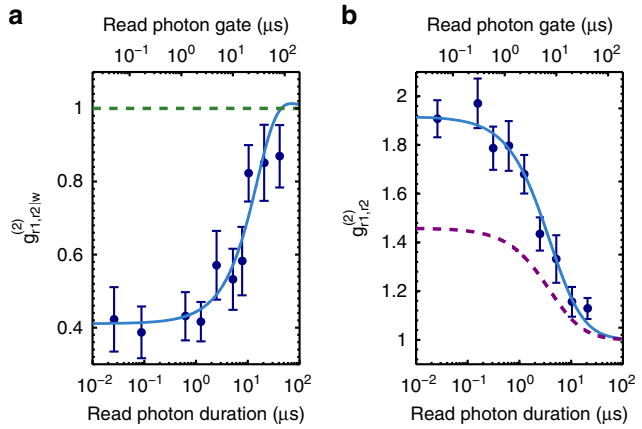

Figure 4 | Measurement of correlation functions. Second order autocorrelation function of the generated read photons, (**a**) conditioned on the detection of a write photon in the same experimental trial at $p_w = 0.25\%$ and (**b**) not conditioned on a write photon detection at $p_w = 1\%$. The experimental data (blue dots) are compared with a theoretical model accounting for detector imperfections, that is, a measured dark count rate of 130 Hz (blue lines). The dashed green line in (**a**) represents the classical bound of a coherent state and the dashed purple line in (**b**) shows the expected trace for a photon state with two modes. The errorbars (±1 s.d.) correspond to the propagated Poissonian error of the photon counting statistics.

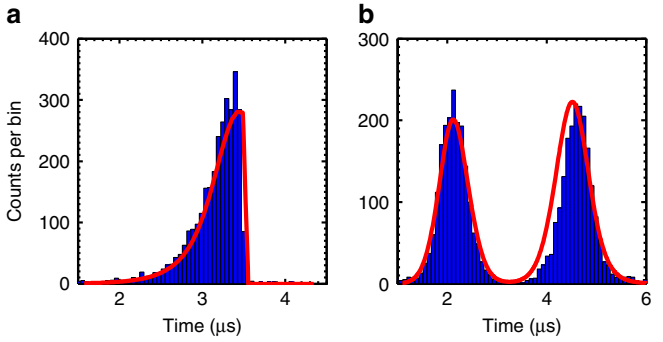

Figure 5 | Single photons with nonstandard wave shapes. Temporal wave shape of the read photon for (**a**) a rising exponential and (**b**) a doubly peaked (time-bin) read pulse wave shape. Experimental data (blue histograms) are compared with numerical simulations (red line) for which we allowed at most 10% adjustment of the input parameters with respect to the measured data. Both histograms were taken at $p_w = 0.5\%$.

where $p_{r1,r2|w}$ denotes the probability to measure a coincidence between both read photon detections conditioned on a write photon detection, and $p_{r1|w}$, $p_{r2|w}$ are the probabilities to detect a read photon via $r1$ or $r2$ conditioned on a write photon detection. The data shown in Fig. 4a clearly demonstrate the nonclassicality of the photons (that is, $g^{(2)}_{r1,r2|w} < 1$) up to photon durations of $> 10\,\mu s$. However, we do not reach the ideal value of $g^{(2)}_{r1,r2|w} = 0$ of perfect single photons. For short read photon durations, we are still limited by noise due to higher-order components of the spin-wave, which can be addressed by reducing p_w. In fact, the observed $g^{(2)}_{r1,r2|w} \approx 0.4$ is consistent with former measurements at similar values for p_w and read pulse durations[43]. For longer read photon durations, we observe an increase of $g^{(2)}_{r1,r2|w}$, which can be simply explained by a higher number of dark counts of the SPDs for longer read photon detection gates (see upper axis in Fig. 4). The solid blue line shows the prediction of a non-perturbative theoretical model accounting for detector imperfections[45]. The agreement between the model and the experimental data is excellent.

The single mode nature of the photon state is characterized by the unconditional autocorrelation function $g^{(2)}_{r,r}$ (see Fig. 4b). For an ideal two-mode squeezed state, where the write and read photons are each emitted in a single temporal mode, one expects $g^{(2)}_{r,r} = 2$, which is quite well fulfilled by the measured data up to a read photon duration of roughly 1 μs. For longer durations, we observe a drop, which can be attributed to either an increasing temporal multimodality of the read photon ($g^{(2)}_{r,r}$ scales as $1 + 1/K$ with K denoting the number of photon modes[46]) or to measurement imperfections because of higher dark counts for larger detection gates. The solid blue line shows the theoretical prediction, assuming read photons emitted in a single mode. The excellent agreement between experiment and theory suggests that the read photons are emitted mostly in a single mode. For comparison, we also plotted the expected behaviour for a single photon with $K = 2$ modes (see purple dashed line), which significantly differs from the measured data, therefore, confirming the single mode nature of the emitted read photons. Consequently, the read photons are close to being Fourier transform limited, giving linewidths ranging from around 20 MHz to < 100 kHz. This, together with the conditional $g^{(2)}_{r1,r2|w}$, allows us to conclude that the heralded read emission is close to a pure single photon.

Finally, we investigate the flexibility of the temporal shape of the generated read photons. Instead of a Gaussian-shaped read pulse, we apply read pulses with a rising exponential envelope or a doubly peaked wave shape. These two examples are important for a broad class of applications in quantum information science. Photons with rising exponential wave shape exhibit the highest possible absorbance when interacting with two-level systems[35,47] and can be very efficiently loaded in optical cavities[36,48]. The temporal shape of the generated rising exponential read photon is shown in Fig. 5a. The driving read pulse had a $1/e$ width of 300 ns. We observe a similar retrieval efficiency of $\eta^{\mathrm{fibre}}_{\mathrm{ret}} = 19.8\%$ as for a standard Gaussian-shaped pulse of same duration (*c.f.* Fig. 3). The conditioned autocorrelation function of the rising exponential photon is $g^{(2)}_{r1,r2|w} = 0.31 \pm 0.14$ (taken at $p_w = 0.25\%$) and $g^{(2)}_{r1,r2|w} = 0.73 \pm 0.12$ (taken at $p_w = 0.5\%$), which is clearly in the nonclassical regime.

As a final example, we send a doubly peaked read pulse into the prepared QM. The intensity and duration of the first readout peak was chosen such that the stored spin-wave is read out with half of the maximal efficiency and for the second peak the retrieval efficiency is maximized. This leads to a read photon with a shape shown in Fig. 5b. Photons with such a delocalized shape can be used to create time-bin qubits, which have applications in robust long-distance quantum communication[49,50]. The efficiency of the generated time-bin photon is $\eta^{\mathrm{fibre}}_{\mathrm{ret}} = 25\%$, comparable to the standard Gaussian-shaped photons, and the conditioned autocorrelation function is $g^{(2)}_{r1,r2|w} = 0.54 \pm 0.11$ (taken at $p_w = 0.25\%$) and $g^{(2)}_{r1,r2|w} = 0.75 \pm 0.08$ (taken at $p_w = 0.5\%$), which is clearly in the nonclassical regime.

Discussion

We demonstrated a highly flexible heralded single photon source with intrinsic storage capability following the DLCZ protocol[37] in a cold ^{87}Rb ensemble. Compared with other approaches for narrowband single photon generation, such as cavity-enhanced spontaneous down conversion[12–14], single atoms and ions in cavities[23,24,26,27] and four-wave mixing in atomic ensembles[20,22], our single photon source offers an unprecedented photon duration tunability of three orders of magnitude and the possibility to generate photons of highly flexible wave shape and an efficient emission on a single spatial and temporal mode

without the need of a high-finesse cavity (see Supplementary Note 4 for a more detailed discussion).

Another important feature of our approach is that our single photon source has intrinsic storage capability, which naturally enables synchronization with other identical sources. In the following, we discuss that possibility with our current set-up. A deterministic synchronization of two such sources depends on the average time separation between successful heralding events (write photon detections) and the maximal storage time of the source. The time between heralding events depends on several parameters: First, the power of the write pulse determines the probability p_w and hence the detection rate of the Raman scattered write photons. However, one cannot just arbitrarily increase the write power to increase that rate because it would also lead to a degradation of the nonclassical correlations between both photons. Second, the various losses from the vacuum cell toward the final detection (mainly fibre coupling, filtering and detector efficiencies) decrease the probability and hence the rate to detect an emitted write photon quite significantly (factor ~ 20). However, these are mainly technical issues, which could be improved by better equipment.

In our experiment, we typically operate the single photon source with a p_w of around 0.5%. Using a heralded sequence (that is, sending the read pulse only when a write photon was detected), we can generate 500 trials per 1 ms interrogation time for read photon lengths of a few microseconds, which gives an average time separation between heralding events of 400 μs. This is of course much longer than the current storage time of about 50 μs and would not allow for a deterministic synchronization of two single photon sources with the current status of the experiment.

However, note that, first, it is not necessary to be in the regime where the storage time is longer than the delay between two write photon detections to start improving the synchronization time while using the QM. The important parameter is the number of write attempts that can be done during the storage time[51,52]. Even with the current set-up ($N \approx 25$ trials per 50 μs storage time), we would reduce the synchronization time between two sources by a factor $2N+1 \approx 50$ compared with single shot attempts[51]. Second, with quite moderate improvements (a storage time of 1 ms[53,54] and a filtering efficiency of $\eta_{\mathrm{filter}} = 80\%$), the time separation between heralding events would be 100 μs, which would be 10 times shorter than the storage time, immediately enabling the deterministic synchronization of several single photon sources.

In conclusion, we demonstrated a highly flexible single photon source with intrinsic storage capability following the DLCZ protocol[37] in a cold ^{87}Rb ensemble. By varying the temporal width of the driving read pulse, the duration of the read photons could be changed over three orders of magnitude up to several tens of microseconds. Up to a read photon duration of 10 μs, we obtain a fibre-coupled retrieval efficiency of $\eta_{\mathrm{ret}}^{\mathrm{fibre}} = 20\%$, which is just limited by the OD in our experiment. We verified numerically that for OD = 50 under ideal conditions, an intrinsic retrieval efficiency of 80% can be achieved while maintaining control of the photon shape. The drop in retrieval efficiency at around 10 μs is mainly due to spin-wave dephasing induced by thermal motion, which could be improved by a more sophisticated trapping of the atoms[32,53]. The generated read photons show a nonclassical behaviour up to durations of >10 μs for the heralded autocorrelation function and up to 1 μs we detect single photons in a pure state, currently just limited by the dark counts of our detectors. Finally, we create single photons with a nonstandard envelope like rising exponential or time-bin wave shapes, which have important applications in quantum information science. Our approach allows the generation of ultra-narrow single photons with unprecedented duration tunability and highly flexible wave shape. This will enable the interconnection of our cold atom QM with other physical systems exhibiting sharp resonances, like for example, Rb atoms prepared in a highly excited Rydberg state under the condition of EIT. Moreover, combining our approach with quantum frequency conversion techniques[53,55] paves the way to the optical interconnection of the cold atom QM with different types of quantum systems, which typically demand very different photon shapes, like long-lived solid state quantum memories or opto-mechanical systems. Finally, also applying the ability to generate single photons with doubly peaked wave shapes (as shown in Fig. 5b), one could demonstrate quantum state transfer via time-bin qubits between different systems, which would be an important step toward the creation of heterogeneous quantum networks[56].

Data availability. The data that support the findings of this study are available from the corresponding author on request.

References

1. Sangouard, N. & Zbinden, H. What are single photons good for? *J. Mod. Opt.* **59,** 1458–1464 (2012).
2. Eisaman, M. D., Fan, J., Migdall, A. & Polyakov, S. V. Invited review article: single-photon sources and detectors. *Rev. Sci. Instrum.* **82,** 071101 (2011).
3. Raymer, M. G. & Srinivasan, K. Manipulating the color and shape of single photons. *Phys. Today.* **65,** 32–37 (2012).
4. Simon, C. *et al.* Quantum memories. *Eur. Phys. J. D* **58,** 1–22 (2010).
5. Bussières, F. *et al.* Prospective applications of optical quantum memories. *J. Mod. Opt.* **60,** 1519–1537 (2013).
6. Afzelius, M., Gisin, N. & de Riedmatten, H. Quantum memory for photons. *Phys. Today.* **68,** 42–47 (2015).
7. Bose, S., Jacobs, K. & Knight, P. L. Scheme to probe the decoherence of a macroscopic object. *Phys. Rev. A.* **59,** 3204–3210 (1999).
8. Marshall, W., Simon, C., Penrose, R. & Bouwmeester, D. Towards quantum superpositions of a mirror. *Phys. Rev. Lett.* **91,** 130401 (2003).
9. Sekatski, P., Aspelmeyer, M. & Sangouard, N. Macroscopic optomechanics from displaced single-photon entanglement. *Phys. Rev. Lett.* **112,** 080502 (2014).
10. Ghobadi, R. *et al.* Optomechanical micro-macro entanglement. *Phys. Rev. Lett.* **112,** 080503 (2014).
11. Aspelmeyer, M., Kippenberg, T. J. & Marquardt, F. Cavity optomechanics. *Rev. Mod. Phys.* **86,** 1391–1452 (2014).
12. Bao, X.-H. *et al.* Generation of narrow-band polarization-entangled photon pairs for atomic quantum memories. *Phys. Rev. Lett.* **101,** 190501 (2008).
13. Haase, A., Piro, N., Eschner, J. & Mitchell, M. W. Tunable narrowband entangled photon pair source for resonant single-photon single-atom interaction. *Opt. Lett.* **34,** 55–57 (2009).
14. Fekete, J., Rieländer, D., Cristiani, M. & de Riedmatten, H. Ultranarrow-band photon-pair source compatible with solid state quantum memories and telecommunication networks. *Phys. Rev. Lett.* **110,** 220502 (2013).
15. Chou, C. W., Polyakov, S. V., Kuzmich, A. & Kimble, H. J. Single-photon generation from stored excitation in an atomic ensemble. *Phys. Rev. Lett.* **92,** 213601 (2004).
16. Laurat, J. *et al.* Efficient retrieval of a single excitation stored in an atomic ensemble. *Opt. Express* **14,** 6912–6918 (2006).
17. Thompson, J. K., Simon, J., Loh, H. & Vuletic, V. A high-brightness source of narrowband, identical-photon pairs. *Science* **313,** 74–77 (2006).
18. Matsukevich, D. N. *et al.* Deterministic single photons via conditional quantum evolution. *Phys. Rev. Lett.* **97,** 013601 (2006).
19. Chen, S. *et al.* Deterministic and storable single-photon source based on a quantum memory. *Phys. Rev. Lett.* **97,** 173004 (2006).
20. Du, S., Kolchin, P., Belthangady, C., Yin, G. Y. & Harris, S. E. Subnatural linewidth biphotons with controllable temporal length. *Phys. Rev. Lett.* **100,** 183603 (2008).
21. Srivathsan, B. *et al.* Narrow band source of transform-limited photon pairs via four-wave mixing in a cold atomic ensemble. *Phys. Rev. Lett.* **111,** 123602 (2013).
22. Zhao, L. *et al.* Photon pairs with coherence time exceeding 1 μs. *Optica* **1,** 84–88 (2014).
23. McKeever, J. *et al.* Deterministic generation of single photons from one atom trapped in a cavity. *Science* **303,** 1992–1994 (2004).
24. Hijlkema, M. *et al.* A single-photon server with just one atom. *Nat. Phys.* **3,** 253–255 (2007).
25. Matthiesen, C., Vamivakas, A. N. & Atatüre, M. Subnatural linewidth single photons from a quantum dot. *Phys. Rev. Lett.* **108,** 093602 (2012).

26. Almendros, M. *et al.* Bandwidth-tunable single-photon source in an ion-trap quantum network. *Phys. Rev. Lett.* **103,** 213601 (2009).
27. Stute, A. *et al.* Tunable ionphoton entanglement in an optical cavity. *Nature* **485,** 482–485 (2012).
28. Eisaman, M. D. *et al.* Shaping quantum pulses of light via coherent atomic memory. *Phys. Rev. Lett.* **93,** 233602 (2004).
29. Keller, M., Lange, B., Hayasaka, K., Lange, W. & Walther, H. Continuous generation of single photons with controlled waveform in an ion-trap cavity system. *Nature* **431,** 1075–1078 (2004).
30. Balić, V., Braje, D. A., Kolchin, P., Yin, G. Y. & Harris, S. E. Generation of paired photons with controllable waveforms. *Phys. Rev. Lett.* **94,** 183601 (2005).
31. Nisbet-Jones, P. B. R., Dilley, J., Ljunggren, D. & Kuhn, A. Highly efficient source for indistinguishable single photons of controlled shape. *New. J. Phys.* **13,** 103036 (2011).
32. Bao, X.-H. *et al.* Efficient and long-lived quantum memory with cold atoms inside a ring cavity. *Nat. Phys.* **8,** 517–521 (2012).
33. Matthiesen, C. *et al.* Phase-locked indistinguishable photons with synthesized waveforms from a solid-state source. *Nat. Commun.* **4,** 1600 (2013).
34. Zhao, L. *et al.* Shaping the biphoton temporal waveform with spatial light modulation. *Phys. Rev. Lett.* **115,** 193601 (2015).
35. Aljunid, S. A. *et al.* Excitation of a single atom with exponentially rising light pulses. *Phys. Rev. Lett.* **111,** 103001 (2013).
36. Liu, C. *et al.* Efficiently loading a single photon into a single-sided fabry-perot cavity. *Phys. Rev. Lett.* **113,** 133601 (2014).
37. Duan, L. M., Lukin, M. D., Cirac, J. I. & Zoller, P. Long-distance quantum communication with atomic ensembles and linear optics. *Nature* **414,** 413–418 (2001).
38. Briegel, H.-J., Dür, W., Cirac, J. I. & Zoller, P. Quantum repeaters: the role of imperfect local operations in quantum communication. *Phys. Rev. Lett.* **81,** 5932–5935 (1998).
39. Sangouard, N., Simon, C., de Riedmatten, H. & Gisin, N. Quantum repeaters based on atomic ensembles and linear optics. *Rev. Mod. Phys.* **83,** 33–80 (2011).
40. Nunn, J. *et al.* Enhancing multiphoton rates with quantum memories. *Phys. Rev. Lett.* **110,** 133601 (2013).
41. de Oliveira, R. A. *et al.* Single-photon superradiance in cold atoms. *Phys. Rev. A.* **90,** 023848 (2014).
42. André, A. *Nonclassical States of Light and Atomic Ensembles: Generation and New Applications* (PhD thesis, Harvard University, 2005).
43. Albrecht, B., Farrera, P., Heinze, G., Cristiani, M. & de Riedmatten, H. Controlled rephasing of single collective spin excitations in a cold atomic quantum memory. *Phys. Rev. Lett.* **115,** 160501 (2015).
44. Grangier, P., Roger, G. & Aspect, A. Experimental evidence for a photon anticorrelation effect on a beam splitter: a new light on single-photon interferences. *Europhys. Lett.* **1,** 173–179 (1986).
45. Sekatski, P. *et al.* Detector imperfections in photon-pair source characterization. *J. Phys. B* **45,** 124016 (2012).
46. Christ, A., Laiho, K., Eckstein, A., Cassemiro, K. N. & Silberhorn, C. Probing multimode squeezing with correlation functions. *New. J. Phys.* **13,** 033027 (2011).
47. Stobińska, M., Alber, G. & Leuchs, G. Perfect excitation of a matter qubit by a single photon in free space. *Europhys. Lett.* **86,** 14007 (2009).
48. Bader, M., Heugel, S., Chekhov, A. L., Sondermann, M. & Leuchs, G. Efficient coupling to an optical resonator by exploiting time-reversal symmetry. *New. J. Phys.* **15,** 123008 (2013).
49. Brendel, J., Gisin, N., Tittel, W. & Zbinden, H. Pulsed energy-time entangled twin-photon source for quantum communication. *Phys. Rev. Lett.* **82,** 2594–2597 (1999).
50. Marcikic, I. *et al.* Time-bin entangled qubits for quantum communication created by femtosecond pulses. *Phys. Rev. A* **66,** 062308 (2002).
51. Felinto, D. *et al.* Conditional control of the quantum states of remote atomic memories for quantum networking. *Nat. Phys.* **2,** 844–848 (2006).
52. Yuan, Z.-S. *et al.* Synchronized independent narrow-band single photons and efficient generation of photonic entanglement. *Phys. Rev. Lett.* **98,** 180503 (2007).
53. Radnaev, A. G. *et al.* A quantum memory with telecom-wavelength conversion. *Nat. Phys.* **6,** 894–899 (2010).
54. Yang, S.-J., Wang, X.-J., Bao, X.-H. & Pan, J.-W. An efficient quantum lightmatter interface with sub-second lifetime. *Nat. Photonics* **10,** 381–384 (2016).
55. Albrecht, B., Farrera, P., Fernandez-Gonzalvo, X., Cristiani, M. & de Riedmatten, H. A waveguide frequency converter connecting rubidium-based quantum memories to the telecom C-band. *Nat. Commun.* **5,** 3376 (2014).
56. Kimble, H. J. The quantum internet. *Nature* **453,** 1023–1030 (2008).

Acknowledgements

Research at ICFO is supported by the ERC starting grant QuLIMA, by the Spanish Ministry of Economy and Competitiveness (MINECO) and the Fondo Europeo de Desarrollo Regional (FEDER) through grant FIS2012-37569 and FIS2015-69535-R, by MINECO Severo Ochoa through grant SEV-2015-0522, by AGAUR via 2014 SGR 1554 and by Fundació Privada Cellex. P.F. acknowledges the International PhD fellowship programme 'la Caixa'-Severo Ochoa @ ICFO. G.H. acknowledges support by the ICFOnest + international postdoctoral fellowship programme. Research at the University of Basel is supported by the Swiss National Science Foundation (SNSF) through the grant number PP00P2-150579 and the Army Research Laboratory Center for Distributed Quantum Information via the project SciNet. C.T. was supported by the Austrian Federal Ministry of Science, Research, and Economy (BMWFW) and would like to thank the hospitality of the quantum optics theory group at the University of Basel.

Author contributions

P.F. and G.H. performed the experiments and analysed the data. B.A. built the experimental set-up. M.H., M.C. and C.T. performed the numerical simulations. G.H. and H.d.R. wrote the paper, with inputs from all co-authors. N.S and H.d.R initiated and supervised the project.

Additional information

Supplementary Information accompanies this paper at http://www.nature.com/naturecommunications

Competing financial interests: The authors declare no competing financial interests.

Reprints and permission information is available online at http://npg.nature.com/reprintsandpermissions/

How to cite this article: Farrera, P. *et al.* Generation of single photons with highly tunable wave shape from a cold atomic ensemble. *Nat. Commun.* **7,** 13556 doi: 10.1038/ncomms13556 (2016).

Publisher's note: Springer Nature remains neutral with regard to jurisdictional claims in published maps and institutional affiliations.

Supplementary Figures

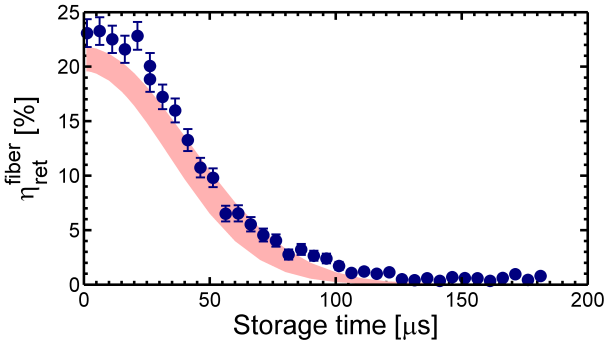

Supplementary Figure 1: **Fiber-coupled conditional retrieval efficiency $\eta_{\rm ret}^{\rm fiber}$ vs the delay between the write and read pulses.** Experimental data (blue dots) are compared with numerical simulations (red shaded area). In order to account for the observed Gaussian decay reflecting an inhomogeneous broadening of the $|g\rangle \rightarrow |s\rangle$ transition, the exponential decay term $e^{-\gamma_0 t}$ in Eq. (5) is replaced with a Gaussian decay $e^{-\frac{1}{2}(t/\gamma_0)^2}$, with $\gamma_0 = 53\,\mu$s. The simulation is performed from Eq. (7) and uses the following measured values: The write pulse has a Rabi frequency of $\Omega_W = 25.1\,$MHz and a FWHM of 15 ns, detuned by $-40\,$MHz from the $|e\rangle \rightarrow |g\rangle$ transition. The peak Rabi frequency of the read pulse is at 23.5 MHz with a FWHM of 35 ns. We take $d_w = 7.5$ and $d_r = 5$. An error of 10% on the Rabi frequencies, pulse widths, optical depths and spin coherence time was assumed in order to obtain the bounds on the simulation.

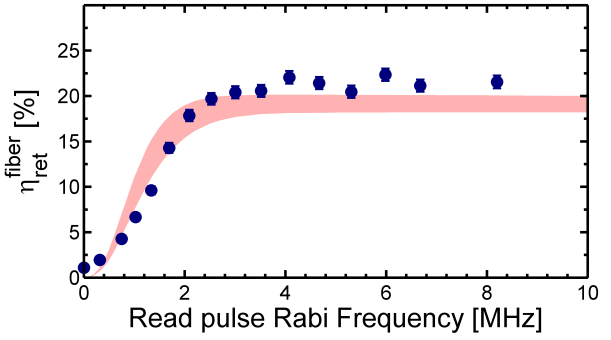

Supplementary Figure 2: **Fiber-coupled conditional retrieval efficiency $\eta_{\rm ret}^{\rm fiber}$ vs read Rabi frequency Ω_R.** Experimental data (blue dots) are compared with numerical simulations (red shaded area). The simulation is performed from Eq. (7) and uses the values of the write pulse presented in the caption of Supplementary Figure 1. The peak Rabi frequency of the read pulse is varied and its FWHM is $1.27\,\mu$s. It has a delay of $2.16\,\mu$s from the write peak frequency. We take $d_w = 4.4$ and $d_r = 2.9$. An error of 10% on the Rabi frequencies, pulse widths, optical depths and spin coherence time was assumed in order to obtain the bounds on the simulation.

Supplementary Notes

Supplementary Note 1: CHARACTERIZATION OF THE QUANTUM MEMORY

In this section, we present additional experimental characterizations of the quantum memory and compare them to simulations based on the formalism introduced in the former section. Note first that for simulating the experimental data, we use the following conventions for the write (read) Rabi frequencies and optical depths: $\Omega_W = 2\bar{\Omega}_W = \langle e|\mathbf{d}\cdot\mathbf{E}_W|g\rangle$ ($\Omega_R = 2\bar{\Omega}_R$) with $\mathbf{d}$ the dipole operator and $\mathbf{E}_W$ the electric field amplitude of the write pulse and $d_w = 2\bar{d}_w$ ($d_r = 2\bar{d}_r$) such that the attenuation of the outgoing light intensity decreases as $I(L) = e^{-\bar{d}_w(\bar{d}_r)} I(0)$.

Supplementary Figure 1 shows the fiber-coupled conditional retrieval efficiency as a function of the delay between the write and read pulses. To account for the observed Gaussian decay of the retrieval efficiency, reflecting an inhomogeneous broadening of the $|g\rangle \rightarrow |s\rangle$ transition, all the simulations are performed by replacing the exponential decay term $e^{-\gamma_0 t}$ in Eq. (5) with a Gaussian decay $e^{-\frac{1}{2}(t/\gamma_0)^2}$.

To optimize the retrieval efficiency, we scanned the intensity of the driving read pulse for fixed photon durations. For short photon durations, we observe the expected Rabi oscillations in the retrieval efficiency vs. read pulse power [2]. If we generate photons with durations longer than the natural decay time, the oscillations are damped and the efficiency approaches a constant value for high read pulse intensities. Supplementary Figure 2 shows such an example of the fiber-coupled conditional retrieval efficiency as a function of the Rabi frequency Ω_R of the driving read pulse. Note that the results of Supplementary Figure 1 and Supplementary Figure 2 have been taken with slightly modified setups, hence the differing optical depths.

Supplementary Note 2: PRINCIPLE OF NUMERICAL SIMULATION

Here, we explain how one can compute the read photon properties conditioned on a write emission. We begin by solving the dynamics of the write field and the spin-wave. We then provide the explicit expression of the read field before showing how it can be used to obtain the conditional read photon characteristics.

A. Write field and spin-wave expressions

Working with a Λ-scheme for a three level system, we consider a writing pulse $\bar{\Omega}_W(t)$ detuned by Δ from the $|g\rangle \rightarrow |e\rangle$ transition. The $|e\rangle \rightarrow |s\rangle$ transition is characterized by an optical depth $\bar{d}_w$. γ_{es} describes the decay of coherence in the $|e\rangle \rightarrow |s\rangle$ transition, and γ_0 describes the decay of the $|g\rangle \rightarrow |s\rangle$ coherence. In the limit where the write field $\hat{\mathcal{E}}_w$ is slowly varying, propagating in a pencil-shaped atomic ensemble in which the $|g\rangle \rightarrow |e\rangle$ transition is driven by a off-resonant write pulse of duration τ_W satisfying $\gamma_{es}\tau_W \bar{d}_w \ll 1$, and also operating in the regime where $\Delta \gg |\bar{\Omega}_W|, \gamma_{es}$, the Raman scattering process results in the emission of a write field and the creation of a correlated spin-wave $\hat{S}$, whose dynamics are described with the Heisenberg-Langevin equations

$$\begin{aligned} c\partial_{z'}\hat{\mathcal{E}}_w &= i\chi\hat{S}^\dagger \\ \partial_{t'}\hat{S}^\dagger &= -\Gamma_S\hat{S}^\dagger - i\chi\hat{\mathcal{E}}_w + \hat{F}_S^\dagger \end{aligned} \tag{1}$$

Here, we introduced shifted coordinates $z' = z$ and $t' = t - z/c$. $\chi(t) = (\sqrt{\bar{d}_w\gamma_{es}c/L})\frac{\bar{\Omega}_W(t)}{\Delta}$, where L is the length of the atomic medium, $\Gamma_S(t) = \gamma_S(t) + i\delta_S(t)$, $\gamma_S(t) = \gamma_0 + \gamma_{es}\frac{|\bar{\Omega}_W(t)|^2}{\Delta^2}$, $\delta_S(t) = -\frac{|\bar{\Omega}_W(t)|^2}{\Delta}$ and $\hat{F}_S$ is the Langevin noise operator for the write process. The commutation relations for the relevant operators are given by

$$\begin{aligned} &[\hat{\mathcal{E}}_w(z,t), \hat{\mathcal{E}}_w^\dagger(z',t')] = L\delta[z - z' - c(t-t')] \\ &[\hat{S}(z,t), \hat{S}^\dagger(z',t)] = L\delta(z-z') \\ &\langle\hat{F}_S(z,t)\hat{F}_S^\dagger(z',t')\rangle = 2\gamma_S L\delta(z-z')\delta(t-t') \\ &\langle\hat{F}_S^\dagger(z,t)\hat{F}_S(z',t')\rangle = 0 \end{aligned} \tag{2}$$

The equations of motion can be solved as shown in Ref. [1]. The solutions for the spin-wave and write field are

$$\begin{aligned} \hat{S}^\dagger(z',t') &= e^{-\Gamma(t')}\hat{S}^\dagger(z',0) \\ &+ \int_0^{t'} e^{-[\Gamma(t')-\Gamma(t'')]}\hat{F}_S^\dagger(z',t'')dt'' \\ &- i\int_0^{t'} \chi(t'')e^{-[\Gamma(t')-\Gamma(t'')]}H(z',0,t',t'')\hat{\mathcal{E}}_w(0,t'')dt'' \\ &+ e^{-\Gamma(t')}\int_0^{z'} G_s(z',z'',t',0)\hat{S}^\dagger(z'',0)dz'' \\ &+ \int_0^{t'} e^{-[\Gamma(t')-\Gamma(t'')]}\int_0^{z'} G_s(z',z'',t',t'')\hat{F}_S^\dagger(z'',t'')dz''dt'' \end{aligned} \tag{3}$$

and

$$\begin{aligned}\hat{\mathcal{E}}_w(z',t') &= \hat{\mathcal{E}}_w(0,t') \\ &+ i(\chi(t')/c)e^{-\Gamma(t')}\int_0^{z'} H(z',z'',t',0)\hat{S}^\dagger(z'',0)dz'' \\ &+ i(\chi(t')/c)\int_0^{t'} e^{-[\Gamma(t')-\Gamma(t'')]}\int_0^{z'} H(z',z'',t',t'')\hat{F}_S^\dagger(z'',t'')dz''dt'' \\ &+ (\chi(t')/c)\int_0^{t'} \chi(t'')e^{-[\Gamma(t')-\Gamma(t'')]}G_e(z',0,t',t'')\hat{\mathcal{E}}_w(0,t'')dt'', \end{aligned} \tag{4}$$

where

$$\begin{aligned}H(z',z'',t',t'') &= I_0\left(2\sqrt{[g(t')-g(t'')]\frac{z'-z''}{c}}\right) \\ G_s(z',z'',t',t'') &= \sqrt{\frac{g(t')-g(t'')}{c(z'-z'')}}I_1\left(2\sqrt{[g(t')-g(t'')]\frac{z'-z''}{c}}\right) \\ G_e(z',z'',t',t'') &= \left(\frac{c(z'-z'')}{g(t')-g(t'')}\right)G_s(z',z'',t',t'').\end{aligned}$$

Here, $I_n(x)$ refers to the modified Bessel function of the first kind, and here we have defined $\Gamma(t) = \int_0^t \Gamma_S(t)dt$, $g(t) = \int_0^t \chi(t')^2 dt'$.

B. Read field expression

During the retrieval process, a read pulse with Rabi frequency $\bar{\Omega}_R(t)$ is applied resonant with the $|e\rangle \to |s\rangle$ transition, converting the spin-wave in the atomic medium into a read field resonant with the $|e\rangle \to |g\rangle$ transition. The $|e\rangle \to |g\rangle$ transition is characterized by an optical depth $\bar{d}_r$. γ_{eg} describes the decay of coherence in the $|e\rangle \to |g\rangle$ transition. Following similar arguments as Ref. [1], we can find the explicit expression of the read field $\hat{\mathcal{E}}_r$ as a function of the spin-wave resulting from the write process. Here, we consider a write emission at time t_i, and a non-zero read field at time t_d after the write pulse ends. For the retrieval, the read field is emitted backwards, towards the z=0 position of the atomic medium. In the regime of $\bar{d}_r \gg 1$ and sufficiently long read field duration $\tau_r \gg \frac{1}{\gamma_{eg}\bar{d}_r}$,

$$\begin{aligned}&\hat{\mathcal{E}}_r(0, t = t_d + \xi) \\ =\ & -\frac{\bar{\Omega}_R(t)}{g\sqrt{N}}e^{-\gamma_0(t-\xi)}\int_{c\Delta\tau(t,\xi)}^{L+c\Delta\tau(t,\xi)}\frac{1}{\sqrt{2\pi}\Delta l(t,\xi)}\exp\left[-\frac{1}{2}\left(\frac{L-z}{\Delta l(t,\xi)}\right)^2\right]\hat{S}\left(L-z+c\Delta\tau(t,\xi),\xi\right)dz \\ -\ & \frac{\bar{\Omega}_R(t)}{g\sqrt{N}}\int_\xi^t\int_{c\Delta\tau(t,\xi))}^{L+c\Delta\tau(t,\xi)}\frac{e^{-\gamma_0(t-t')}}{\sqrt{2\pi}\Delta l(t,t')}\exp\left[-\frac{1}{2}\left(\frac{L-z}{\Delta l(t,t')}\right)^2\right]\times \\ & \Bigg[\hat{F}_S(L-z+c\Delta\tau(t,t'),t') \\ & + i\frac{\Delta l^2(t,t')+(L-z)(2c(\Delta\tau(t,t'))+L-z)}{4\gamma_{eg}c^2(\Delta\tau(t,t'))^2}\bar{\Omega}_R(t')\hat{F}_P(L-z+c\Delta\tau(t,t'),t')\Bigg]dz \\ +\ & \frac{i}{g\sqrt{N}}e^{-\gamma_0 t}\hat{F}_P(0,t),\end{aligned} \tag{5}$$

where the commutation relations are

$$\begin{aligned}&[\hat{\mathcal{E}}_r(z,t),\hat{\mathcal{E}}_r^\dagger(z',t')] = L\delta[z-z'-c(t-t')] \\ &\langle\hat{F}_P(z,t)\hat{F}_P^\dagger(z',t')\rangle = 2\gamma_{eg}L\delta(z-z')\delta(t-t') \\ &\langle\hat{F}_P^\dagger(z,t)\hat{F}_P(z',t')\rangle = 0.\end{aligned}$$

Here, $\Delta\tau(t,t') = \frac{L}{\bar{d}_r\gamma_{eg}c}\int_{t'}^{t}\bar{\Omega}_R^2(t'')dt''$, and $\Delta l(t,t') = \sqrt{\frac{2Lc}{\bar{d}_r}\Delta\tau(t,t')}$. g refers to the coupling constant between a single atom and a single read photon, and N corresponds to the number of interacting atoms. This can be expressed as $g^2N = \frac{\bar{d}_r\gamma_{eg}c}{L}$. ξ indicates a suitable time after the write pulse has ended, and where the read pulse is considered to begin, so as to perform the numerical integration for the retrieval. $\hat{F}_P$ is the Langevin noise operator for the retrieve process.

C. Conditional retrieval efficiency

Equipped with the above expressions for the optical fields and spin-wave, we can compute the expectation of read photon emissions conditioned on the emission of a write photon from

$$\eta_{r|w} = \frac{c}{L}\frac{\int\int\langle\hat{\mathcal{E}}_w^\dagger(L,t_i)\hat{\mathcal{E}}_r^\dagger(0,t)\hat{\mathcal{E}}_r(0,t)\hat{\mathcal{E}}_w(L,t_i)\rangle dt_i dt}{\int\langle\hat{\mathcal{E}}_w^\dagger(L,t_i)\hat{\mathcal{E}}_w(L,t_i)\rangle dt_i}. \tag{6}$$

Evaluating the expression $\langle\hat{\mathcal{E}}_w^\dagger(L,t_i)\hat{\mathcal{E}}_r^\dagger(0,t)\hat{\mathcal{E}}_r(0,t)\hat{\mathcal{E}}_w(L,t_i)\rangle$ requires the expression in Eq. (4) and only the first term in Eq. (5), which one in turn develops using Eq. (3). A tedious but straightforward computation then results in 12 nonzero terms, of which 3 terms are 4-point noise correlators. Such 4-point noise correlations can be evaluated with use of Isserlis' theorem, which allows a decomposition into 2-point noise correlators for Gaussian random variables.

This gives, for example,

$$\begin{aligned}\langle\hat{F}_S(z_1,t_1)\hat{F}_S^\dagger(z_2,t_2)\hat{F}_S(z_3,t_3)\hat{F}_S^\dagger(z_4,t_4)\rangle &= \langle\hat{F}_S(z_1,t_1)\hat{F}_S^\dagger(z_2,t_2)\rangle\,\langle\hat{F}_S(z_3,t_3)\hat{F}_S^\dagger(z_4,t_4)\rangle\\ &+ \langle\hat{F}_S(z_1,t_1)\hat{F}_S(z_3,t_3)\rangle\,\langle\hat{F}_S^\dagger(z_2,t_2)\hat{F}_S^\dagger(z_4,t_4)\rangle\\ &+ \langle\hat{F}_S(z_1,t_1)\hat{F}_S^\dagger(z_4,t_4)\rangle\,\langle\hat{F}_S^\dagger(z_2,t_2)\hat{F}_S(z_3,t_3)\rangle,\end{aligned}$$

where only the first term survives since the normal-ordered 2-point noise correlators are zero.

Finally, from the coupling efficiency of the read emission into the first fiber η_{fiber}, we can reproduce the fiber-coupled conditional retrieval efficiency $\eta_{\text{ret}}^{\text{fiber}}$ using

$$\eta_{\text{ret}}^{\text{fiber}} = \eta_{r|w}\eta_{\text{fiber}}, \tag{7}$$

valid in the low photon number regime ($\eta_{r|w} \ll 1$).

D. Read photon shape

The explicit expression of the fields also allows us to predict the temporal dependence of the conditional read emission, in a similar way as above. In particular, the conditional read photon flux inside the first fiber is given by

$$n_r^{cond}(t) = \frac{c}{L}\frac{\int\langle\hat{\mathcal{E}}_w^\dagger(L,t_i)\hat{\mathcal{E}}_r^\dagger(0,t)\hat{\mathcal{E}}_r(0,t)\hat{\mathcal{E}}_w(L,t_i)\rangle dt_i}{\int\langle\mathcal{E}_w^\dagger(L,t_i)\mathcal{E}_w(L,t_i)\rangle dt_i}\eta_{\text{fiber}}. \tag{8}$$

Supplementary Note 3: QUANTUM FEATURES AND PURITY OF THE READ PHOTONS

To prove that the conditional read emission takes the form of single photons, we have measured the second order autocorrelation function conditioned on the detection of a write photon. Assuming that the write-read photon pairs are described by a two-mode squeezed vacuum state, an explicit expression of the conditional second order autocorrelation function can be derived in a non-perturbative way while taking the detector imperfections into account (non-unit, noisy and non-photon number resolving detectors), see Eqs. (24)-(25) in Ref. [3]. The agreement between this model and the experimental data shows that the heralded second order autocorrelation function is mainly limited by dark counts, see Fig. 4(a) in the main text.

To conclude about the purity of the heralded read emission, we have also measured the (unconditional) second order autocorrelation function. Assuming again that the state of the write-read photon pairs corresponds to a two-mode squeezed vacuum, the exact expression of the second order autocorrelation function can be derived taking the detector imperfection into account, see formula $\tilde{g}^{(2)}_{\sum_n a_n}$ after Eq. (39) in Ref. [3]. In particular, in the absence of noise and for small detection efficiencies, the auto-correlation function is given by $1+1/K$, i.e. depends on the number of modes K. The full (blue) and dashed (purple) lines in Fig. 4 (b) of the main text are obtained by assuming that the read photons are emitted in a single mode and in two possible modes respectively (with the detector imperfections). This shows that the read emission is single mode and together with the result of the conditional auto-correlation measurement, we conclude that the heralded emission is close to a pure single photon.

Supplementary Note 4: COMPARISON WITH OTHER APPROACHES

In this section, we briefly compare our approach with other investigated experimental platforms to generate ultra-narrowband photons.

Cavity-enhanced spontaneous parametric down conversion (SPDC) has been proven to allow for generation of single photons pairs at high rates and spectral brightness [4–6]. However, single photons with ultra-narrow bandwidth in the range of 100 kHz have not been demonstrated yet via SPDC. The narrowest single photons in single mode generated by SPDC so far has a bandwidth of around 2 MHz [6]. Although narrower linewidths are in principle possible, it will be challenging to reach a linewidth as narrow as 100 kHz, because of the limited cavity finesse achievable due to the optical loss in the non-linear crystal. Also the tunability of the photon waveshape, as demonstrated in our manuscript, would be very challenging using SPDC, as it would require a dynamic and highly accurate control of the cavity finesse. To the best of our knowledge, such tunable SPDC experiments have not been presented yet. Finally, the SPDC approach alone doesn't enable a controllable emission time for the heralded photon.

Another common approach is based on spontaneous four wave mixing (SFWM) by which bi-photon coherence times up to 1 μs could be obtained [7]. Although that approach offers a tunability of the photon duration of about one order of magnitude [8], i.e. two orders of magnitude less than demonstrated here, photon durations are intrinsically limited by the coherence times of the involved levels, which might be limited by dephasing due to a magnetic gradient in the experiment. Also the delay between the generated anti-Stokes and the Stokes photons relies on slow light via electromagnetically induced transparency (EIT). In our case, the magnetic field is switched off during the experiment, leading to much longer coherence time. Also, the achievable delay between the two photons depends only on the ground state coherence time. Finally, in contrast to the FWM case we also don't need to deal with optical precursors.

Single photons of tunable length have also been produced by spontaneous Raman transitions in trapped single ions [9]. Here, the photon length could be varied depending on the laser-controlled Raman transition rate. The longest coherence time observed was 1.6 μs limited by the natural lifetime of the particular transition in $^{40}Ca^{+}$.

Finally, there have been also attempts to realize DLCZ-type quantum memories in hot atomic vapors. But their performance is limited due to high background noise and collisional decoherence during the write and read-out process [10]. A possible route to overcome these problems could be the use of micro-cells [11]. However, the generation of ultra-narrow single photons still has to be demonstrated using that approach.

In other systems like in rare-earth doped solids, DLCZ-like experiments are currently being investigated [12–16]. Whether ultra-narrow single photons with widely tunable waveshape can be produced with that approach is still an open question and needs to be further investigated.

Supplementary References

[1] André, A. *Nonclassical states of light and atomic ensembles: Generation and New Applications.* PhD thesis, Harvard University (2005).

[2] Mendes, M. S., Saldanha, P. L., Tabosa, J. W. R. & Felinto, D. Dynamics of the reading process of a quantum memory. *New Journal of Physics* **15**, 075030 (2013).

[3] Sekatski, P. *et al.* Detector imperfections in photon-pair source characterization. *Journal of Physics B: Atomic, Molecular and Optical Physics* **45**, 124016 (2012).

[4] Bao, X.-H. *et al.* Generation of Narrow-Band Polarization-Entangled Photon Pairs for Atomic Quantum Memories. *Physical Review Letters* **101**, 190501 (2008).

[5] Haase, A., Piro, N., Eschner, J. & Mitchell, M. W. Tunable narrowband entangled photon pair source for resonant single-photon single-atom interaction. *Optics Letters* **34**, 55–57 (2009).
[6] Fekete, J., Rieländer, D., Cristiani, M. & de Riedmatten, H. Ultranarrow-Band Photon-Pair Source Compatible with Solid State Quantum Memories and Telecommunication Networks. *Physical Review Letters* **110**, 220502 (2013).
[7] Zhao, L. *et al.* Photon pairs with coherence time exceeding 1 μs. *Optica* **1**, 84–88 (2014).
[8] Du, S., Kolchin, P., Belthangady, C., Yin, G. Y. & Harris, S. E. Subnatural Linewidth Biphotons with Controllable Temporal Length. *Physical Review Letters* **100**, 183603 (2008).
[9] Almendros, M. *et al.* Bandwidth-Tunable Single-Photon Source in an Ion-Trap Quantum Network. *Physical Review Letters* **103**, 213601 (2009).
[10] Manz, S., Fernholz, T., Schmiedmayer, J. & Pan, J.-W. Collisional decoherence during writing and reading quantum states. *Physical Review A* **75**, 040101 (2007).
[11] Borregaard, J. *et al.* Scalable photonic network architecture based on motional averaging in room temperature gas. *Nature Communications* **7**, 11356 (2016).
[12] Ledingham, P. M., Naylor, W. R. & Longdell, J. J. Nonclassical photon streams using rephased amplified spontaneous emission. *Physical Review A* **81**, 012301 (2010).
[13] Sekatski, P., Sangouard, N., Gisin, N., de Riedmatten, H. & Afzelius, M. Photon-pair source with controllable delay based on shaped inhomogeneous broadening of rare-earth-metal-doped solids. *Physical Review A* **83**, 053840 (2011).
[14] Ledingham, P. M., Naylor, W. R. & Longdell, J. J. Experimental Realization of Light with Time-Separated Correlations by Rephasing Amplified Spontaneous Emission. *Physical Review Letters* **109**, 093602 (2012).
[15] Beavan, S. E., Hedges, M. P. & Sellars, M. J. Demonstration of Photon-Echo Rephasing of Spontaneous Emission. *Physical Review Letters* **109**, 093603 (2012).
[16] Ferguson, K. R., Beavan, S. E., Longdell, J. J. & Sellars, M. J. Generation of Light with Multimode Time-Delayed Entanglement Using Storage in a Solid-State Spin-Wave Quantum Memory. *Physical Review Letters* **117**, 020501 (2016).

Paper B

Optimal photon generation from spontaneous Raman processes in cold atoms

Melvyn Ho, Colin Teo, Hugues de Riedmatten and Nicolas Sangouard

New Journal of Physics **20**, 123018 (2018)

New Journal of Physics
The open access journal at the forefront of physics

Deutsche Physikalische Gesellschaft DPG
IOP Institute of Physics

Published in partnership with: Deutsche Physikalische Gesellschaft and the Institute of Physics

OPEN ACCESS

RECEIVED
6 July 2018

REVISED
6 November 2018

ACCEPTED FOR PUBLICATION
26 November 2018

PUBLISHED
18 December 2018

PAPER

Optimal photon generation from spontaneous Raman processes in cold atoms

Melvyn Ho[1,5], **Colin Teo**[1,2], **Hugues de Riedmatten**[3,4] **and Nicolas Sangouard**[1]

[1] Quantum Optics Theory Group, University of Basel, Klingelbergstrasse 82, 4056 Basel, Switzerland
[2] Centre for Bioimaging Sciences, Department of Biological Sciences, National University of Singapore, 14 Science Drive 4, 117543, Singapore
[3] ICFO-Institut de Ciencies Fotoniques, The Barcelona Institute of Science and Technology, E-08860, Castelldefels (Barcelona), Spain
[4] ICREA-Institució Catalana de Recerca i Estudis Avançats, E-08015, Barcelona, Spain
[5] Present address: Group of Applied Physics, University of Geneva, Chemin de Pinchat 22, CH-1211 Geneva 4, Switzerland.

E-mail: melvyn.ho@unibas.ch

Keywords: single photon sources, quantum networks, quantum communication

Abstract

Spontaneous Raman processes in cold atoms have been widely used in the past decade for generating single photons. Here, we present a method to optimise their efficiencies for given atomic coherences and optical depths. We give a simple and complete recipe that can be used in present-day experiments, attaining near-optimal single photon emission.

1. Introduction

On-demand single photon sources are appealing ingredients for many quantum information tasks. Examples include the distribution of entanglement over long distances using quantum repeaters or quantum communications with security guarantees which remain valid, independent of the details of the actual implementation [1, 2]. These tasks necessitate stringent purity and efficiency requirements on the performance of the single photon sources used. Techniques based on spontaneous Raman processes in cold atoms are among the most advanced single-photon sources with such characteristics. The basic principle is to use an ensemble of three-level atoms in a Λ-configuration and two pulsed laser fields (see figure 1(a)). The first write pulse—the write control field—off-resonantly excites one transition, which can spontaneously produce a frequency-shifted photon—the write photon field—along the second transition through a Raman process. Since all the interacting atoms participate in the process, and there is no information about which atom emitted the photon, the detection of this write photon heralds the existence of a single delocalised excitation across the sample—an atomic spin wave. Once the spin wave has been prepared, the atomic sample is ready to be used as a source, and a second pulse—the read control field—along the second transition performs a conversion of the atomic spin wave into a second photon—the read photon field. If the duration of the process is short enough with respect to the atomic coherence times, and the optical depth of the sample sufficiently high, then the read photon is emitted efficiently in a well defined mode and the protocol provides a viable single photon source.

Such sources have been at the core of numerous experiments during the last decade following the seminal paper of Duan, Lukin, Cirac and Zoller [3], showing how they could be used for long-distance quantum communication based on quantum repeater architectures (for reviews, see [4–7]). Recently, they have been used as quantum memories with storage times up to 200 ms [8, 9] or as a source producing pure single photons with a temporal duration that can be varied over up to 3 orders of magnitude while maintaining constant efficiencies [10]. We stress that the efficiency of such a source is a critical parameter for the implementation of efficient quantum repeater architectures. While very high efficiencies of $\sim$90% are essential, a reduction of the source efficiency by 1% can reduce the repeater distribution rate by 10%–20%, depending on the specific architecture [4].

Several solutions can be envisioned to ensure high efficiencies. One solution relies on the use of an optical cavity to enhance the spinwave–light conversion efficiency. Experimental efforts along this direction have

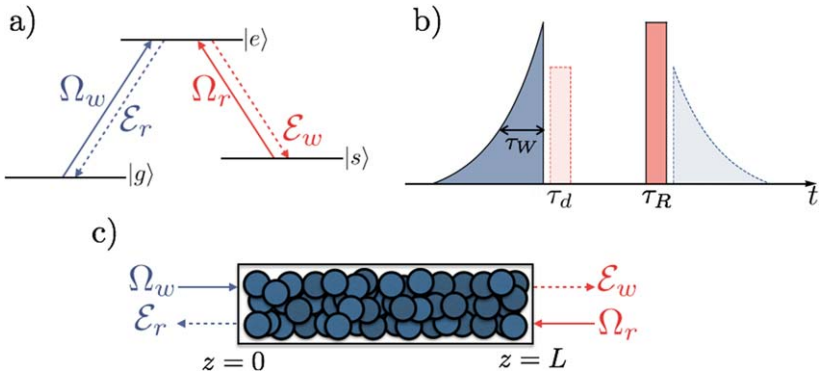

Figure 1. Λ energy level scheme and schematic of the proposed single photon source. (a) Write (read) control fields are indicated with Rabi frequencies Ω_W (Ω_R) and write (read) photon fields are indicated with quantum fields $\mathcal{E}_w$ ($\mathcal{E}_r$), each along their respective transitions. In our model the excited level $|e\rangle$ is capable of spontaneous emission to the metastable states $|g\rangle$ and $|s\rangle$. (b) A schematic of the protocol indicates the sequence of events. A fast resonant write control field of duration τ_W followed by a write photon field detection in a short time window τ_d heralds a spatially varying spin wave. A fast π-pulse of duration τ_R then enables the retrieval of the stored excitation. Laser pulses are shaded darker to indicate their stronger intensities as compared to the weaker photon emissions. (c) A backward retrieval configuration with counterpropagating control fields results in photon field emissions in opposing directions.

resulted in efficiencies of up to 84% [11, 12]. An alternative solution involves increasing the atomic density in order to obtain a larger optical depth [13]. This however makes operations like optical pumping and noise free operations more challenging. This naturally raises the following question: *What is the optimal efficiency that can be achieved with a bulk atomic ensemble having a certain optical depth?* This question has been previously addressed for memory protocols where single photons are first absorbed before subsequently retrieved in a well defined mode [14, 15].

Inspired by these works, we first examine the conditions on the spin wave shape for achieving optimal photon retrieval efficiencies given the optical depths and specified energy levels in the atomic species. We observe that the optimal spin waves are decreasing functions in space whose decay depends on the optical depth. The intuition is that the reemission process is a collective effect in which the fields emitted by each atom interfere with each other. The best possible way for these fields to add up constructively is that the field amplitude increases as it propagates into the medium. After finding the optimal spin wave shapes, we recognise that current approaches using off-resonant write control fields create non-ideal flat spin excitations in the sample (previously studied in works such as [16]), since such control fields do not experience significant intensity depletion during propagation. To achieve better retrieval efficiencies, we propose a concrete solution (see figure 1(b)) to spatially shape the spin wave using resonant, temporally shaped write control fields. Combined with fast read control fields during the retrieval process, we show that our recipe achieves near-optimal retrieval efficiencies.

This paper is structured as follows: in the first section we discuss the optimal retrieval efficiency from a spin excitation. For completeness, we first quickly review derivations in [15] that allow us to find the expression for the retrieval efficiency of a complete retrieval process, where we begin with only $|g\rangle - |s\rangle$ coherences and transfer all atoms to $|g\rangle$. We then find the shapes of the spin excitation that yield the optimal retrieval efficiency when complete retrieval is performed. In the second section we propose the use of a resonant write control field to create heralded spin excitations similar to those that allow for optimal retrieval. We then give explicit expressions for retrieval when using a quick read control field with a constant Rabi frequency. Finally, we include a feasibility study in the case of a gas of Rubidium-87.

2. Optimal retrieval

2.1. Efficiency of a complete retrieval process

We first review a derivation in [15] giving the dependency of the efficiency of the retrieval process on the relevant quantities in the physical setup. This yields an expression for the retrieval efficiency, that depends only on the shape of the spin wave from which the retrieval is performed, and on the optical depth of the relevant transition.

We emphasise that the work in [15] focuses on absorptive memory protocols where a field is first absorbed in an atomic medium, creating a spin wave that can be read out later to re-emit the field in a well defined spatio-temporal mode. To justify the relation to [15], in our proposal the spin wave creation is instead heralded by the detection of the write photon field, but the readout process is analogous, allowing us to make use of [15] to deduce the spin wave shapes that maximise the retrieval efficiency.

We consider a three-level atomic system in a Λ-configuration (see figure 1(a)) with spin excitations present in the form of $|g\rangle - |s\rangle$ coherences. In the situation where almost all the atoms remain in $|g\rangle$ and in a rotating frame, the backward wave propagation equation (see figure 1(a)) along with the Heisenberg–Langevin equations of motion yield

$$\begin{aligned}\partial_z \mathcal{E}_r(z,\,t) &= -\mathrm{i}\sqrt{\frac{d\gamma_{eg}}{cL}}\,P(z,\,t),\\ \partial_t P(z,\,t) &= -(\gamma_{eg}+\mathrm{i}\Delta)P(z,\,t)+\mathrm{i}\sqrt{\frac{d\gamma_{eg}c}{L}}\,\mathcal{E}_r(z,\,t)\\ &\quad+\mathrm{i}\Omega_R(t)S(z,\,t)+F_P(z,\,t),\\ \partial_t S(z,\,t) &= -\gamma_0 S(z,\,t)+\mathrm{i}\Omega_R^*(t)P(z,\,t)+F_S(z,\,t),\end{aligned} \tag{1}$$

where $P(z,\,t)=\sqrt{N}\sigma_{ge}(z,\,t)\mathrm{e}^{-\mathrm{i}\omega_1\frac{L-z}{c}}$ and $S(z,\,t)=\sqrt{N}\sigma_{gs}(z,\,t)\mathrm{e}^{-\mathrm{i}(\omega_1-\omega_2)\frac{L-z}{c}}$ are rescaled and slowly varying atomic operators (see appendix for details), with ω_1 (ω_2) referring to the energy transition of the $|e\rangle - |g\rangle$ ($|e\rangle - |s\rangle$) transition. γ_{eg} (γ_0) refers to the decay rate of the $|e\rangle - |g\rangle$ ($|g\rangle - |s\rangle$) transition. L denotes the length of the atomic sample and N the number of atoms within this sample. F_S and F_P indicate the noise operators associated to S and P, respectively. Ω_R (Δ) refers to the Rabi frequency (detuning) of the classical write control field on the $|e\rangle - |g\rangle$ transition, and $\mathcal{E}_\mathrm{r}$ denotes the quantum field of the retrieval emission. The optical depth d characterises the absorption of resonant light in the sample, such that the outgoing light intensity is $I_0(z=L)=e^{-2d}I(z=0)$, valid when the spectrum of the incoming light is well contained within the atomic bandwidth.

Here, we consider the situation where retrieval is completed well within the spin wave decoherence time, and thus ignore γ_0. In computing the spin and photon numbers, we also ignore the Langevin noise terms F_S and F_P as they appear in normal ordered form, and in the situation where almost all the atoms are in the ground state these do not contribute.

Defining first the reversed functions $\bar{P}(L-z,\,t)=P(z,\,t)$, $\bar{S}(L-z,\,t)=S(z,\,t)$ and $\bar{\mathcal{E}}_\mathrm{r}(L-z,\,t)=\mathcal{E}_\mathrm{r}(z,\,t)$, then taking the Laplace transforms of equations (1) from $L-z=z'\to u$, we begin with the following set of transformed equations

$$\bar{\mathcal{E}}_\mathrm{r}(u,\,t)=\mathrm{i}\sqrt{\frac{\gamma_{eg}d}{cL}}\,\frac{1}{u}\bar{P}(u,\,t), \tag{2}$$

$$\partial_t\bar{P}(u,\,t)=-\left[\gamma_{eg}\left(1+\frac{d}{Lu}\right)+\mathrm{i}\Delta\right]\bar{P}(u,\,t)+\mathrm{i}\Omega_\mathrm{R}(t)\bar{S}(u,\,t) \tag{3}$$

$$\partial_t\bar{S}(u,\,t)=\mathrm{i}\Omega_\mathrm{R}^*(t)\bar{P}(u,\,t). \tag{4}$$

From equations (3) and (4) we first obtain the following result

$$\begin{aligned}&\frac{\mathrm{d}}{\mathrm{d}t}(\langle\bar{P}^\dagger(u_1,\,t)\bar{P}(u_2,\,t)+\bar{S}^\dagger(u_1,\,t)\bar{S}(u_2,\,t)\rangle)\\ &\quad=\gamma_{eg}\left(-2-\frac{d}{Lu_1}-\frac{d}{Lu_2}\right)\langle\bar{P}^\dagger(u_1,\,t)\bar{P}(u_2,\,t)\rangle.\end{aligned} \tag{5}$$

With equation (2) we can then rewrite the number of emitted photons η in terms of $P(u,t)$

$$\begin{aligned}\eta&=\frac{c}{L}\int_0^\infty \mathrm{d}t\ \langle\mathcal{E}_r^\dagger(z=0,\,t)\mathcal{E}_r(z=0,\,t)\rangle\\ &=\frac{c}{L}\mathcal{L}_2^{-1}\int_0^\infty \mathrm{d}t\ \frac{\gamma_{eg}d}{cL}\frac{1}{u_1u_2}\langle\bar{P}^\dagger(u_1,\,t)\bar{P}(u_2,\,t)\rangle\ \Big|_{\substack{z_1'\to L\\ z_2'\to L}},\end{aligned}$$

where $\mathcal{L}_2^{-1}$ indicates the instruction to take the Laplace inverses of both u_1 and u_2 separately. With the use of equation (5) we can next rewrite $\langle\bar{P}^\dagger(u_1,\,t)\bar{P}(u_2,\,t)\rangle$ as a full derivative and perform the integral to get

$$\begin{aligned}\eta&=\mathcal{L}_2^{-1}\frac{d}{L}\frac{-1}{(u_1+u_2)d+2Lu_1u_2}\\ &\quad\times(\langle\bar{P}^\dagger(u_1,\,t)\bar{P}(u_2,\,t)\rangle+\langle\bar{S}^\dagger(u_1,\,t)\bar{S}(u_2,\,t)\rangle)\,|_{t=0}^\infty\,|_{\substack{z_1'\to L\\ z_2'\to L}}\\ &=\frac{1}{L^2}\mathcal{L}_2^{-1}\frac{dL}{d(u_1+u_2)+2Lu_1u_2}\langle\bar{S}^\dagger(u_1,\,0)\bar{S}(u_2,\,0)\rangle\ \Big|_{\substack{z_1'\to L\\ z_2'\to L}},\end{aligned}$$

where the last equality comes from the conditions we assume in a complete retrieval process, i.e. that we begin with only $|g\rangle - |s\rangle$ coherences and at the end of the process all atoms are in $|g\rangle$. By performing the inverse

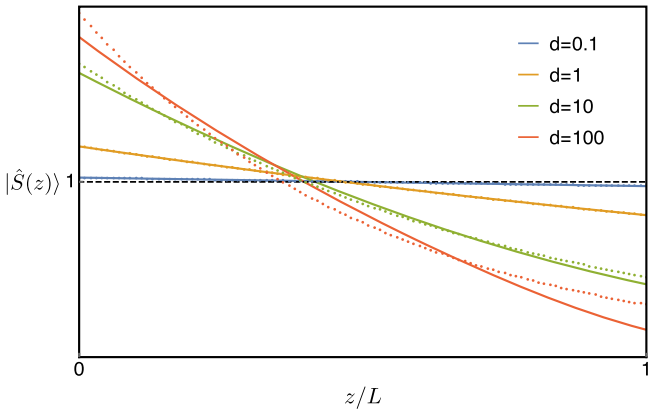

Figure 2. Optimised spin wave shapes for retrieval in the backward direction (solid lines) when compared to the best fitting exponential shapes created by our resonant write protocol (dotted lines).

Laplace transforms one sees that for complete retrieval in the backward direction[6],

$$\eta = \frac{1}{L}\int_0^L \mathrm{d}z_1 \frac{1}{L}\int_0^L \mathrm{d}z_2\; k_r(L - z_1, L - z_2) \times \langle S^\dagger(L - z_1, 0) S(L - z_2, 0)\rangle, \tag{6}$$

where $k_r(z_1, z_2) = \frac{d}{2}\mathrm{e}^{-d\frac{z_1+z_2}{2L}} I_0\left(\frac{d}{L}\sqrt{z_1 z_2}\right)$ and $I_n(x)$ indicates the modified nth Bessel function of the first kind. We proceed by considering the situation where there is originally a single spin wave in the sample (such that $\frac{1}{L}\int_0^L S^\dagger(z, 0) S(z, 0)\; \mathrm{d}z = 1$), and thus interpret η as the efficiency of the retrieval process. The retrieval efficiency η is independent of the details of the read control field used, and is a result of the ratio between desired and undesired modes that are retrieved from the spin wave.

2.2. Optimal spin shapes for complete retrieval

Having shown the dependence of the retrieval efficiency on the spin wave shape and optical depth, we now look to gain some intuition on how one might obtain the optimal retrieval efficiencies, by plotting the spin shapes that maximise the retrieval efficiency for given depths.

To do this, we recognise equation (6) as the continuous form of a product of discretised versions of k_r (in the form of a matrix) and $|S\rangle$ (in the form of a vector). Cast in this light, this integral can be computed by performing a matrix multiplication between the discretised versions of k_r and $|S\rangle$, and in this discrete approximation the optimal spin shape is the eigenvector of k_r with the largest eigenvalue. One can then interpolate the resulting vector to obtain optimised spin shapes, which are shown as solid coloured lines in figure 2.

The best spin shapes for optimal retrieval show a clear spatial dependence with a bias (depending on the optical depth d) towards placing larger excitation probabilities towards the retrieval direction (backwards in this case). Intuitively, we see these shapes representing the best way to obtain constructive interference throughout the retrieval process. As the optical field is converted from the spin wave towards the retrieval direction, it benefits from encountering a higher excitation from the atoms it next encounters. We will denote the retrieval efficiencies from these optimal spin shapes as η^*.

3. Practical recipe for achieving near-optimal retrieval efficiencies

3.1. Heralding spatially varying excitations from write photon detections

In the previous section, we have outlined how the retrieval efficiency depends on the shape of the given spin excitation, and also how the optimal spin shapes can be computed. Here we propose a method of conveniently creating spin shapes that yield near-optimal retrieval efficiencies. In contrast to creating spin excitations using spontaneous Raman processes enabled by far-detuned write control fields, we explore the use of resonant control fields instead, which create spin excitations with significantly position-dependent excitation profiles. These profiles can be controlled by tuning the duration of the write control field, which is in turn related to the

[6] In [15], equation (6) is said to describe the *optimal retrieval efficiency* from a given spin wave. For us, we see this retrieval efficiency function as a description of *complete retrieval* in the absence of spin wave decoherence, which is made optimal only when provided with the correct spin excitation.

frequency spread. A shorter (longer) write field duration implies that it has a wider (sharper) spread in frequency, and this thus affects how quickly the write pulse is depleted within the sample.

We give a detailed derivation of the write process in appendix B.1. To summarise (see figure 1(b)), beginning with all atoms in the $|g\rangle$-level, we send a short rising exponential resonant write pulse with Rabi frequency $\Omega_W(0,\,t) = \Omega_W^{\max} e^{t/\tau_W}$ that does not significantly excite the atoms to the $|e\rangle$ level ($\Omega_W^{\max}\tau_W \ll 1$). If sent with a sufficiently short duration ($\tau_W \ll 1/\gamma_{eg}, \tau_W \ll 1/\gamma_{es}$) and shut off at $t = 0$, one can consider only the dynamics along the $|g\rangle - |e\rangle$ transition, and obtain atomic coherences of the form (see appendix B.2)

$$\sigma_{ge}(z,\,0) = e^{ik_w z}\theta_0 e^{-\frac{\alpha z}{2}}, \tag{7}$$

where $\theta_0 = i\frac{\Omega_W^{\max}\tau_W}{1+\gamma_{eg}\tau_W}$, $\alpha/2 = d\frac{\gamma_{eg}\tau_W}{1+\gamma_{eg}\tau_W}\frac{1}{L}$ and k_w indicates the wave vector for the write photon, which is described using a quantum field $\mathcal{E}_w$. Immediately after the preparation, we look for the detection of write photons within a short detection window τ_d as a herald for single spin excitations. This avoids potential dephasing effects from the decoherence of the $|e\rangle$ level. In this short detection window of duration $\tau_d \ll \min\left(\frac{1}{2\gamma_{es}}, \frac{1}{2\gamma_{eg}}\right)$, and where $\tau_d \ll \left\{\bar{d}\ \gamma_{es}|\theta_0|^2\frac{1-e^{-\alpha L}}{\alpha L}\right\}^{-1}$, ensuring the number of emitted write photons n_w is much smaller than 1, we obtain (see appendices B.3 and B.4)

$$n_w = (\bar{d}\ \gamma_{es}\tau_d)|\theta_0|^2\frac{1-e^{-\alpha L}}{\alpha L}, \tag{8}$$

where γ_{es} ($\bar{d}$) refers to the decay rate (optical depth) of the $|e\rangle - |s\rangle$ transition. The write photon number η_w is simply the product of $\bar{d}\ \gamma_{es}\tau_d$ and the fraction of excited atoms (averaged across the sample).

In this same regime for τ_d, to leading order the corresponding heralded spin state is (see appendix B.5)

$$S^\dagger(z,\,\tau_d) = -i\sqrt{\frac{\bar{d}\gamma_{es}c}{L}}\,\theta_0 e^{-\alpha z/2}\int_0^{\tau_d} e^{-\gamma_0(\tau_d - t_a)}\mathcal{E}_w(0,\,t_a)\,dt_a, \tag{9}$$

which has an exponentially decaying spatial dependence from the $z = 0$ side of the sample. The extent of this spatial decay is characterised by α, which does depend on the given properties of the atomic sample, but can be controlled by varying the write control field duration τ_W. One can compare this class of heralded spin shapes (created from exponentially rising write pulses) to the optimal spin shapes in figure 2.

3.2. Performing fast retrieval

We now proceed with the retrieval process, and spell out the exact requirements for a certain implementation of retrieval—the fast π-pulse using a square waveform of duration τ_R. Once again, we focus on retrieval processes completed well within the spin wave decoherence time and performed under relevant experimental conditions. We thus ignore both the spin decoherence and Langevin noise terms in equation (1). Here we have implicitly assumed that the energy levels of the $|g\rangle$ and $|s\rangle$ levels are degenerate[7]. See [15, 17] for details.

With a resonant square retrieve pulse in the backward direction (see figure 1(c)) one finds the following simple expression for the dynamics of the spin wave (details given in appendix A.1)

$$\ddot{\bar{S}}(u,\,t) + A\dot{\bar{S}}(u,\,t) + B\bar{S}(u,\,t) = 0, \tag{10}$$

where $A = \gamma_{eg}\left(1 + \frac{d}{Lu}\right)$ and $B = \Omega_R^2$ (for real Ω_R), and we have taken the Laplace transform $L - z = z' \to u$.

In the regime[8] where $2\Omega_R \gg \gamma_{eg}(1+d)$, we find $4B \gg A^2$, and obtain the following solution

$$\bar{S}(u,\,t) = e^{-At/2}\cos(\Omega_R t)\bar{S}(u,\,t=\tau_d), \tag{11}$$

which yields the following expression

$$\begin{aligned}\bar{P}(u,\,t) &= \frac{1}{i\Omega_R}\partial_t\bar{S}(u,\,t)\\ &= \frac{i}{\Omega_R}e^{-\frac{A}{2}t}\left(\frac{A}{2}\cos(\Omega_R t) + \Omega_R\sin(\Omega_R t)\right)\bar{S}(u,\,t=\tau_d),\end{aligned} \tag{12}$$

where we then see that with a sufficiently fast π-pulse (such that $2\Omega_R\tau_R = \pi$) obeying $\gamma_{eg}(1+d)\,\tau_R \ll 2$, one can convert S to P without loss, yielding

[7] The phase-matching condition in one dimension is fully satisfied for co-propagating pulses and emissions, even in the non-degenerate case. For counterpropagating strategies like the one we suggest, one requires the condition $|\Delta k|L \ll 1$, where $\Delta k = k_w - k_w(=k_R - k_r)$ refers to the difference in wave vector along our 1-dimensional system for the write (read) control and photon fields (see appendix C).

[8] In considering the lossless preparation of $\bar{P}(u,\,t)$ from $\bar{S}(u,\,t=\tau_d)$, requiring $2\Omega_R \gg \gamma_{eg}(1+d)$ for the π-pulse can be demanding. However, we show in appendix A.3 that one can achieve the same retrieval efficiency even in the slow readout regime where we do not separate the P preparation process from the emission.

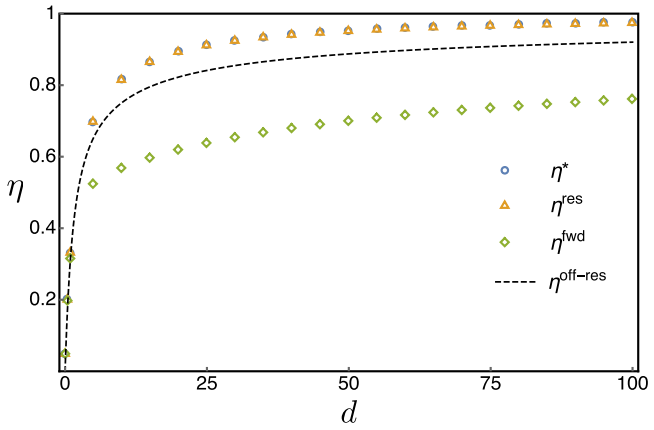

Figure 3. Retrieval efficiency as a function of the optical depth. Blue circles indicate the retrieval efficiency from the optimal spin wave. Yellow triangles (green diamonds) indicate the efficiency from backward (forward) retrieval for the proposed recipe that uses an exponentially rising write control field. The black dashed line indicates the retrieval efficiency using the standard approach with off-resonant write control fields.

$$\bar{P}(u,\ \tau_{\mathrm{R}}+\tau_{\mathrm{d}}) \approx \mathrm{i}\bar{S}(u,\ t=\tau_{\mathrm{d}}). \tag{13}$$

The emitted read photon field can then be obtained by solving the set of equations in (1) after the fast read control field has ended (see appendix A.2), giving

$$\mathcal{E}_{\mathrm{r}}(0,\ t) = \mathrm{i}\sqrt{\frac{\gamma_{eg}\,d}{cL}}\,\mathrm{e}^{-\gamma_{eg}t}\int_0^L J_0\left[2\sqrt{\frac{\gamma_{eg}\,d}{L}t(L-z_1'')}\right] P(L-z_1'',\ \tau_{\mathrm{R}}+\tau_{\mathrm{d}})\,\mathrm{d}z_1''. \tag{14}$$

Along with equation (13) and noting that $\int_0^\infty \mathrm{e}^{-\alpha x}J_\nu(2\beta\sqrt{x})J_\nu(2\gamma\sqrt{x})\mathrm{d}x = \frac{1}{\alpha}I_\nu\left(\frac{2\beta\gamma}{\alpha}\right)\exp\left(-\frac{\beta^2+\gamma^2}{\alpha}\right)$ [18], this emitted field then yields a retrieval efficiency given by equation (6).

3.3. Comparison

We have seen that the proposed retrieval protocol yields a dependence on the spin shape, as described by equation (6). Hence we now compare the retrieval efficiencies attainable with our protocol and compare them to the optimal ones.

We can estimate the achievable efficiency of our protocol by choosing a write pulse duration such that the heralded spin shape best fits the optimal spin shape. A good approximation to this write pulse duration is well described in [19], and given by

$$\tau_{\mathrm{W}}^{\mathrm{approx}} = \frac{1}{\gamma_{eg}}\frac{1}{1+\frac{d}{2}}. \tag{15}$$

As we show below, this simple expression for the write pulse duration essentially produces the optimal efficiency available for a given optical depth. This is hence the write pulse duration we recommend.

We also compute the retrieval efficiencies η^{fwd} that would be obtained if the resonant write pulse of duration τ_W^{approx} were to be followed by a co-propagating retrieve pulse instead. This would result in a situation where the spin wave would be far from optimal with respect to the retrieval direction. In figure 3, we compare the optimal efficiency η^*, the efficiencies η^{res} and η^{fwd} obtained with our proposal (from a spin wave created from a resonant exponential pulse with duration τ_W^{approx}) together with the efficiency of the standard approach using far off-resonant write pulses, for which the efficiency is bounded by the complete retrieval efficiency from a flat spin wave [15]

$$\eta^{\mathrm{off-res}} = 1 - \mathrm{e}^{-d}(I_0(d) + I_1(d)), \tag{16}$$

which we have verified numerically. This retrieval efficiency is valid for retrieval from both the forward and backward directions from a flat spin wave.

Our proposal approaches optimal efficiencies, performing within $\sim 10^{-3}$ of η^* and compares favourably with respect to the standard off-resonant case. The improvement in efficiency is dependent on the optical depth, and we present some values in table 1.

Table 1. Comparison of retrieval efficiency from different spin shapes.

d	η^{fwd}	$\eta^{\mathrm{off-res}}$	η^{res}	η^{*}
0.1	0.047 6	0.047 6	0.047 6	0.047 6
1	0.314 0	0.326 3	0.330 5	0.330 5
10	0.567 1	0.750 9	0.813 4	0.814 2
20	0.618 3	0.822 7	0.892 1	0.897 3
100	0.760 0	0.920 3	0.972 8	0.974 5

Finally, we have also investigated the on-resonance retrieval with an exponentially increasing write pulse using non optimised pulse widths ($\tau_W = \gamma_{eg}^{-1}$), but find a saturation of only ~67 % of the retrieval efficiency for high optical depths.

3.4. Retrieval into a single mode

For a single photon source to be useful, one needs to not only efficiently emit a single photon, but also to ensure that the said photon is emitted in a single mode. In our model we have assumed that the write and read photons are each in a single mode.

For an actual implementation, one way to check that a single mode for the write and read photons are collected and detected, is to perform an autocorrelation measurement with two detectors after a 50-50 beamsplitter (see appendix D). Under the assumption that the write and read photons are correlated through vacuum squeezing processes, this measurement allows us to determine the number of emission modes K, as it gives $g^{(2)} \sim 1 + \frac{1}{K}$ [20] (valid in the absence of detector noise and for small emission probabilities).

4. Feasibility study of Rubidium-87

For a feasibility study we consider a Λ-system consisting of the following energy levels from the D-2 transition of Rubidium-87: $|g\rangle = |5^2S_{1/2}, F = 2, m_F = 2\rangle$, $|s\rangle = |5^2S_{1/2}, F = 1, m_F = 0\rangle$ and $|e\rangle = |5^2P_{3/2}, F = 2, m_F = 1\rangle$. By taking into account the relevant branching ratios, we take $\gamma_{eg} = \frac{1}{12}(2\pi)6.067$ MHz and $\gamma_{es} = \frac{1}{8}(2\pi)6.067$ MHz.

We first consider an optical depth of $d = 20$ on the $|e\rangle - |g\rangle$ transition. From equation (15), we find that a suitable write control field duration is given by $\gamma_{eg}\tau_W^{\mathrm{approx}} = 0.09$. This implies a field duration of $\tau_W^{\mathrm{approx}} \approx 29$ ns. Further considering an optical depth of $\bar{d} = 20$ on the $|e\rangle - |s\rangle$ transition and a weak write control field such that $\Omega_W^{\max}\tau_W = 0.01$, the number of write photons is $n_w = 2 \times 10^{-4}$ within a short detection window of $\tau_d \approx 100$ ns. We note that the ability to create pulses with a rising exponential shape with field amplitude duration as low as 20 ns has already been demonstrated in works such as [21, 22].

Subsequently, the retrieval pulse on the $|e\rangle - |g\rangle$ transition requires a Rabi frequency of $\Omega_R \gg (2\pi)5.3$ MHz, with a predicted retrieval efficiency of 89%, essentially achieving η^* (see table 1). This compares favourably to the retrieval efficiency from a flat spin wave $\eta^{\mathrm{off-res}} = 82\%$.

5. Conclusion

In this work, we have discussed conditions for the optimal generation of single photons from spontaneous Raman processes in cold atoms.

We have first recognised that the ability to create favourable spin wave shapes can significantly improve the heralded retrieval efficiency. Since the reemission process is collective, the retrieval process benefits from all atoms participating favourably, in this case benefitting from a particular optimal spin shape. A resonant write pulse offers the option to create spatially varying waves due to its significant interaction through the sample. We have thus proposed a detailed recipe to create single photons with efficiencies that compare favourably to standard strategies utilising flat spin waves.

The recipe focuses on cases where the spin coherence time is longer than the optical coherence times and consists in first specifying the decay rates γ_{eg} and γ_{es} from the excited states and the optical depths d and $\bar{d}$ on the $|e\rangle - |g\rangle$ and $|e\rangle - |s\rangle$ transitions. Then the recipe fixes the duration of the detection window to be smaller than the shortest decoherence times, that is, the minimum of $1/\gamma_{eg}$ and $1/\gamma_{eg}$ while maintaining that the number of write photons is sufficiently low. Finally, the recipe proposes to take for the write pulse an exponential rising function in time, whose duration is given by $\tau_W^{\mathrm{approx}} = \gamma_{eg}^{-1}\left(1 + \frac{d}{2}\right)^{-1}$. To estimate the heralding rates, one can

next compute the write photon number with the formula in equation (8) given the Rabi frequency of the write pulse. The readout efficiency obtained with a fast readout pulse, that is a readout pulse with a duration much smaller than the atomic coherence times, reaches the values given in figure 3 (yellow triangles) as soon as the corresponding Rabi frequency defines essentially a π-pulse. This recipe describes a convenient way to come close to the optimal efficiency of single photon sources with given optical depths based on spontaneous Raman processes. This work could help in the implementation of the first quantum repeater protocol successfully outperforming the direct transmission of photons [4].

Acknowledgements

We would like to acknowledge Mikael Afzelius, Jean-Daniel Bancal, Lucas Beguin, Pau Farrera, Georg Heinze, Enky Oudot, Tan Peng Kian, Philipp Treutlein and Janik Wolters for useful discussions. Research at the University of Basel is supported by the Swiss National Science Foundation (SNSF) through the grant number PP00P2-150579 and the Army Research Laboratory Center for Distributed Quantum Information via the project SciNet. H de R acknowledges financial support by the Spanish Ministry of Economy and Competitiveness (MINECO) and Fondo Europeo de Desarrollo Regional (FEDER) (FIS2015-69535-R), by MINECO Severo Ochoa through Grant No. SEV-2015-0522, by Fundació Cellex, and by CERCA programme/Generalitat de Catalunya.

Appendix A. Retrieval process

A.1. Retrieval emission dynamics

We begin from the Hamiltonian $H = H_0 + V$ (see [15]), where we consider an atomic sample of length L, and a classical field sent from the $z = L$ side of the sample. Choosing $|g\rangle$ to be the energy level reference for the atomic states, we have

$$H_0 = \int \mathrm{d}\omega \hbar\omega \hat{a}^\dagger_\omega \hat{a}_\omega + \sum_{i=1}^{N} (\hbar\omega_s \sigma^j_{ss} + \hbar\omega_e \sigma^j_{ee}) \tag{17}$$

$$V = -\hbar \sum_{i=1}^{N} \left(\Omega_\mathrm{R}\left(t - \frac{L - z_i}{c}\right) \sigma^i_{es} \mathrm{e}^{-\mathrm{i}\omega_2 t} \mathrm{e}^{+\mathrm{i}\omega_2 \left(\frac{L-z_i}{c}\right)} + g\sqrt{\frac{L}{2\pi c}} \int \mathrm{d}\omega \; a_\omega \mathrm{e}^{\mathrm{i}\omega \frac{L-z_i}{c}} \sigma^i_{eg} + \mathrm{h.c.} \right), \tag{18}$$

where $\sigma^i_{\mu\nu} = |\mu\rangle_i \langle\nu|$ indicates atomic level operators for the ith atom, and a_w indicates the annihilation operator for the photonic mode at frequency ω. ω_2 (ω_1) indicates the frequency of the read control (photon) field, respectively. Note that we are considering resonant pulses, so we have ω_1 (ω_2) = ω_e (ω_s). Using

$$A = \sum_{i=1}^{N} [\hbar(\omega_1 - \omega_2)\sigma^i_{ss} + \hbar\omega_1 \sigma^i_{ee}] + \hbar\omega_1 \int \mathrm{d}\omega \; \mathcal{E}^\dagger_r(z, t)\mathcal{E}_r(z, t),$$
$$U = \mathrm{e}^{-\mathrm{i}At/\hbar},$$

for the change of frame, then in the continuum limit, we obtain

$$\begin{aligned} H_\mathrm{new} &= U^\dagger H U - A \\ &= \int \mathrm{d}\omega \; \hbar\omega a^\dagger_\omega a_\omega - \hbar\omega_1 \int \mathrm{d}z \; \mathcal{E}^\dagger_r(z, t)\mathcal{E}_r(z, t) \\ &\quad + \frac{N}{L} \int \mathrm{d}z \{ -\hbar\Omega_\mathrm{R}(z, t)\sigma_{es}(z, t)\mathrm{e}^{+\mathrm{i}\omega_2 \frac{L-z}{c}} + \mathrm{H.c.} \\ &\quad - g\mathcal{E}_r(z, t)\sigma_{eg}(z, t)\mathrm{e}^{+\mathrm{i}\omega_1 \frac{L-z}{c}} + \mathrm{H.c.} \}, \end{aligned}$$

where we have defined a real Rabi frequency $\Omega_\mathrm{R}(z, t) = \Omega_\mathrm{R}(t - \frac{L-z}{c})$ and $\mathcal{E}_\mathrm{r}(z, t) = \sqrt{\frac{L}{2\pi c}} \int \mathrm{d}\omega \; \mathrm{e}^{\mathrm{i}\omega_1 t} a_\omega \mathrm{e}^{\mathrm{i}(\omega-\omega_1)\frac{L-z}{c}}$. Using the field propagation equation along with the Heisenberg–Langevin equations of motion, we have in a moving coordinate frame, ignoring spinwave decoherence and the noise terms, and also considering that $\sigma_{gg} \sim 1$,

$$\begin{aligned} \partial_z \mathcal{E}_\mathrm{r}(z, t) &= -\frac{\mathrm{i}g\sqrt{N}}{c} P(z, t) \\ \partial_t P(z, t) &= -\gamma_{eg} P(z, t) + \mathrm{i}g\sqrt{N}\mathcal{E}_\mathrm{r}(z, t) + \mathrm{i}\Omega_\mathrm{R}(t) S(z, t) \\ \partial_t S(z, t) &= \mathrm{i}\Omega_\mathrm{R}(t) P(z, t), \end{aligned}$$

where $g^2N = \frac{d\gamma_{eg}c}{L}$, $P(z,\,t) = \sqrt{N}\sigma_{ge}(z,\,t)\mathrm{e}^{-\mathrm{i}\omega_1\frac{L-z}{c}}$ and $S(z,\,t) = \sqrt{N}\sigma_{gs}(z,\,t)\mathrm{e}^{-\mathrm{i}(\omega_1-\omega_2)\frac{L-z}{c}}$. In the continuum limit, the spin and field operators obey the following commutation relations

$$[\sigma_{\alpha\beta}(z,\,t),\,\sigma_{\mu\nu}(z',\,t)] = \frac{L}{N}\delta(z-z')(\delta_{\beta\mu}\sigma_{\alpha\nu}(z,\,t) - \delta_{\nu\alpha} \tag{19}$$

$$[\mathcal{E}_{\mathrm{r}}(z,\,t),\,\mathcal{E}_{\mathrm{r}}^{\dagger}(z,\,t')] = \frac{L}{c}\delta(t-t'). \tag{20}$$

Rewriting equations (A.1) in the reverse direction e.g. $\bar{\mathcal{E}}_{\mathrm{r}}(z',\,t) = \bar{\mathcal{E}}_{\mathrm{r}}(L-z,\,t) = \mathcal{E}_{\mathrm{r}}(z,\,t)$, and taking the Laplace transform from $z' \to u$ we obtain

$$\begin{aligned}
\bar{\mathcal{E}}_{\mathrm{r}}(u,\,t) &= \frac{\mathrm{i}g\sqrt{N}}{cu}\bar{P}(u,\,t) + \frac{1}{u}\bar{\mathcal{E}}_{\mathrm{r}}(z'=0,\,t),\\
\partial_{\mathrm{t}}\bar{P}(u,\,t) &= -\gamma_{eg}\bar{P}(u,\,t) + \mathrm{i}g\sqrt{N}\bar{\mathcal{E}}_{\mathrm{r}}(u,\,\mathrm{t}) + \mathrm{i}\Omega_{\mathrm{R}}(t)\bar{S}(u,\,t),\\
\partial_{\mathrm{t}}\bar{S}(u,\,t) &= \mathrm{i}\Omega_{\mathrm{R}}(\mathrm{t})\bar{P}(u,\,t).
\end{aligned} \tag{21}$$

We can combine these three equations into a single differential equation, where we have ignored the boundary term $\bar{\mathcal{E}}_{\mathrm{r}}(z'=0,\,t)$ since we send the read control field into the $z = L$ side of the atoms. On resonance ($\Delta = 0$), let $A = \gamma_{eg} + \frac{g^2N}{cu}$ and $B = \Omega_{\mathrm{R}}^2$ to see

$$\ddot{\bar{S}}(u,\,t) + A\dot{\bar{S}}(u,\,t) + B\bar{S}(u,\,t) = 0. \tag{22}$$

A.2. Fast retrieval

In the strong regime for the read control field, one requires $2|\Omega_{\mathrm{R}}| \gg \gamma_{eg}(1+d)$, which implies

$$\begin{aligned}
2\Omega_{\mathrm{R}} &\gg \gamma_{eg}\left(1 + \frac{dz'}{L}\right)\\
\Rightarrow 2\Omega_{\mathrm{R}} &\gg \gamma_{eg}\left(1 + \frac{d}{Lu}\right),
\end{aligned}$$

which then yields the regime $4B \gg A^2$.

The solution for equation (22) in this regime is

$$\bar{S}(u,\,t) = \mathrm{e}^{-At/2}\cos(\Omega_{\mathrm{R}}t)C_1(u) + \mathrm{e}^{-At/2}\sin(\Omega_{\mathrm{R}}t)C_2(u),$$

where the initial condition implies

$$\bar{S}(u,\,t) = \mathrm{e}^{-At/2}\cos(\Omega_{\mathrm{R}}t)\bar{S}(u,\,t=0).$$

One can then find the prepared polarisation in terms of the intial spin condition,

$$\begin{aligned}
\bar{P}(u,\,t) &= \frac{1}{\mathrm{i}\Omega_R}\partial_t\bar{S}(u,\,t)\\
&= \frac{\mathrm{i}}{\Omega_R}\mathrm{e}^{-\frac{A}{2}t}\left[\frac{A}{2}\cos(\Omega_R t) + \Omega_R\sin(\Omega_R t)\right]\bar{S}(u,\,t=0).
\end{aligned}$$

In the limit where we have a sufficiently strong read control field ($2\Omega_{\mathrm{R}} \gg \frac{\pi}{2}\gamma_{eg}(1+d)$), the π-pulse is completed quickly and we obtain a lossless preparation of $\bar{P}(u,\,t)$ from $\bar{S}(u,\,t=0)$ in the form

$$\bar{P}(u,\,\tau_{\mathrm{R}}) = \mathrm{i}\bar{S}(u,\,t=0). \tag{23}$$

Once the polarisation is prepared, we find the emission by solving for the dynamics in the absence of the laser,

$$\begin{aligned}
\partial_z\bar{\mathcal{E}}_{\mathrm{r}}(z,\,t) &= -\mathrm{i}\frac{g\sqrt{N}}{c}\bar{P}(z,\,t),\\
(\partial_t + \gamma_{eg})\bar{P}(z,\,t) &= \mathrm{i}g\sqrt{N}\bar{\mathcal{E}}_{\mathrm{r}}(z,\,t).
\end{aligned}$$

Taking the Laplace transform from $L - z = z' \to u$ and neglecting the boundary term since it does not contribute to the photon number, we have

$$\begin{aligned}
\bar{\mathcal{E}}_{\mathrm{r}}(u,\,t) &= \mathrm{i}\frac{g\sqrt{N}}{cu}\bar{P}(u,\,t),\\
(\partial_t + \gamma_{eg})\bar{P}(u,\,t) &= \mathrm{i}g\sqrt{N}\bar{\mathcal{E}}_{\mathrm{r}}(u,\,t) = -\frac{g^2N}{cu}\bar{P}(u,\,t).
\end{aligned}$$

This yields the evolution of $P(u, t)$ after its preparation from $S(u, t)$,

$$\bar{P}(u, t) = \mathrm{e}^{-\left(\gamma_{eg}+\frac{g^2N}{cu}\right)(t-\tau_{\mathrm{R}})}\bar{P}(u, \tau_{\mathrm{R}}), \tag{24}$$

and gives an emitted field of

$$\bar{\mathcal{E}}_{\mathrm{r}}(z', t) = \mathrm{i}\frac{g\sqrt{N}}{c}\mathrm{e}^{-\gamma_{eg}(t-\tau_{\mathrm{R}})} \times \int_0^{z'} \mathrm{d}z'' J_0\left[2\sqrt{\frac{g^2N}{c}(t-\tau_{\mathrm{R}})(z'-z'')}\right]\bar{P}(z', \tau_{\mathrm{R}}),$$

where $J_n[x]$ refers the nth Bessel function of the first kind. Now with $z' = L - z$, we require the field at $z = 0$ for backward retrieval, and we finally obtain

$$\mathcal{E}_r(0, t) = -\frac{g\sqrt{N}}{c}\mathrm{e}^{-\gamma_{eg}t} \times \int_0^{L} \mathrm{d}z'' J_0\left[2\sqrt{\frac{g^2N}{c}t(L-z'')}\right]S(L-z'', 0), \tag{25}$$

where we have used equation (23) for a lossless preparation.

A.3. Slow retrieval

In the weak regime for the read control field, one requires $2|\Omega_{\mathrm{R}}| \ll \gamma_{eg}$, which implies

$$2\Omega_R \ll \gamma_{eg}\left(1 + \frac{dz}{L}\right)$$
$$\Rightarrow 2\Omega_R \ll \gamma_{eg}\left(1 + \frac{d}{Lu}\right),$$

which then yields the regime $4B \ll A^2$.

The solution for equation (22) in this regime is

$$\bar{S}(u, t) = \mathrm{e}^{-\frac{1}{2}(A+\sqrt{A^2-4B})t}C_u(1) + \mathrm{e}^{-\frac{1}{2}(A-\sqrt{A^2-4B})t}C_u(2).$$

When there is no laser ($B = 0$), there should be no spinwave decay since we have considered zero spin wave decoherence, so we set $C_u(1) = 0$ and obtain

$$\bar{S}(u, t) = \mathrm{e}^{-\frac{1}{2}(A-\sqrt{A^2-4B})t}\bar{S}(u, t = 0).$$

Now, in this regime when the Rabi frequency is small, we have

$$\begin{aligned}\mathrm{e}^{-\frac{1}{2}(A-\sqrt{A^2-4B})t} &= \mathrm{e}^{-\frac{1}{2}(A-A\sqrt{1-\frac{4B}{A^2}})t}\\ &\approx \mathrm{e}^{-\frac{B}{A}t}\\ &= \mathrm{e}^{-\frac{\Omega^2}{\gamma_{eg}(1+\frac{d}{Lu})}t}\end{aligned}$$

This gives

$$\bar{S}(u, t) = \mathrm{e}^{-Kt\frac{1}{1+s/u}}\bar{S}(u, t = 0),$$

where $K = \frac{\Omega_{\mathrm{R}}^2}{\gamma_{eg}}$ and $s = \frac{d}{L}$. One can proceed to find $\bar{P}(u, \mathrm{t}) = \frac{1}{\mathrm{i}\Omega_{\mathrm{R}}}\partial_{\mathrm{t}}\bar{S}(u, \mathrm{t})$ and $\bar{\mathcal{E}}(u, t) = \mathrm{i}\frac{g\sqrt{N}}{cu}\bar{P}(u, t)$, giving

$$\bar{\mathcal{E}}(u, t) = -\frac{g\sqrt{N}}{c}\frac{K}{\Omega_{\mathrm{R}}}\left[\frac{1}{u+s}\mathrm{e}^{-Kt+Kt\left(\frac{s}{s+u}\right)}\right]\bar{S}(u, t = 0).$$

This yields

$$\bar{\mathcal{E}}(z', t) = -\frac{g\sqrt{N}}{c}\frac{K}{\Omega}\mathrm{e}^{-Kt} \times \int_0^{z'} \mathrm{e}^{-s(z'-z'')}I_0(2\sqrt{Kts(z'-z'')})\bar{S}(z'', t = 0)\mathrm{d}z''. \tag{26}$$

One can then compute the retrieval efficiency from a single spin wave, and this is found to yield the optimal retrieval efficiency.

$$\int_0^\infty \mathrm{d}t\ \frac{c}{L}\langle \mathcal{E}^\dagger(0,\ t)\mathcal{E}(0,\ t)\rangle$$
$$= \int_0^\infty \mathrm{d}t\ \frac{d}{L^2}\frac{\Omega_R^2}{\gamma_{eg}}\mathrm{e}^{-2Kt}\int_0^L \mathrm{d}z_1''\int_0^L \mathrm{d}z_2''\ \mathrm{e}^{-\frac{d}{L}(2L-z_1''-z_2'')}$$
$$\times I_0\left[2\sqrt{Kt\frac{d}{L}(L-z_1'')}\right]I_0\left[2\sqrt{Kt\frac{d}{L}(L-z_2'')}\right]$$
$$\times \langle S^\dagger(L-z_1'',\ t=0)S(L-z_2'',\ t=0)\rangle$$
$$= \frac{1}{L}\int_0^L \mathrm{d}z_1''\ \frac{1}{L}\int_0^L \mathrm{d}z_2''\ \frac{d}{2}\mathrm{e}^{-\frac{d}{2}\frac{(L-z_1'')+(L-z_2'')}{L}}$$
$$\times I_0\left[\mathrm{d}\sqrt{\frac{L-z_1''}{L}}\sqrt{\frac{L-z_2''}{L}}\right]\langle S^\dagger(L-z_1'',\ t=0)S(L-z_2'',\ t=0)\rangle$$

where $I_n[x]$ denotes the nth modified Bessel function of the first kind. We have made use of the fact that $I_n(z) = \mathrm{i}^{-n}J_n(\mathrm{i}z)$ and also $\int_0^\infty \mathrm{e}^{-\alpha x}J_\nu(2\beta\sqrt{x})J_\nu(2\gamma\sqrt{x})\mathrm{d}x = \frac{1}{\alpha}I_\nu\left(\frac{2\beta\gamma}{\alpha}\right)\exp\left(-\frac{\beta^2+\gamma^2}{\alpha}\right)$.

Appendix B. Write process

B.1. Heisenberg–Langevin equations for the atomic coherences

The goal here is to first derive the expressions for the evolution of the atomic coherences in the write process. We begin from the Hamiltonian $\bar{H} = \bar{H}_0 + \bar{V}$

$$\bar{H}_0 = \int \mathrm{d}\omega\hbar\omega a_\omega^\dagger a_\omega + \sum_{i=1}^N(\hbar\omega_s\sigma_{ss}^j + \hbar\omega_e\sigma_{ee}^j) \tag{27}$$

$$\bar{V} = -\hbar\sum_{i=1}^N(\Omega_{\mathrm{W}}(t-z_i/c)\sigma_{eg}^i\mathrm{e}^{-\mathrm{i}\omega_1(t-z_i/c)} + \bar{g}\sqrt{\frac{L}{2\pi c}}\int \mathrm{d}\omega\ \hat{a}_\omega\mathrm{e}^{\mathrm{i}\omega z_i/c}\sigma_{es}^i + \mathrm{H.c.}\Big). \tag{28}$$

Using

$$\bar{A} = \sum_{i=1}^N(\hbar\omega_s\sigma_{ss}^i + \hbar\omega_e\sigma_{ee}^i) + \hbar\omega_2\int \mathrm{d}z\ \mathcal{E}_w^\dagger(z,\ t)\mathcal{E}_w(z,\ t),$$
$$\bar{U} = \mathrm{e}^{-\mathrm{i}\bar{A}t/\hbar}$$

for the change of frame, then in the continuum limit, we obtain

$$\bar{H}_{\mathrm{new}} = \bar{U}^\dagger\bar{H}\bar{U} - \bar{A}$$
$$= \int \mathrm{d}\omega\ \hbar a_\omega^\dagger a_\omega - \hbar\omega_2\int \mathrm{d}z\ \mathcal{E}_w^\dagger(z,\ t)\mathcal{E}_w(z,\ t)$$
$$+ \frac{N}{L}\int \mathrm{d}z\{-\hbar\,\Omega_{\mathrm{W}}(t-z/c)\sigma_{eg}(z,\ t)\mathrm{e}^{\mathrm{i}\omega_1 z/c} + \mathrm{H.c.}$$
$$- g\mathcal{E}_w(z,\ t)\sigma_{es}(z,\ t)\mathrm{e}^{\mathrm{i}\omega_2 z/c} + \mathrm{H.c.}\}, \tag{29}$$

where we have defined $\mathcal{E}_{\mathrm{w}}(z,\ t) = \sqrt{\frac{L}{2\pi c}}\mathrm{e}^{\mathrm{i}\omega_2 t}\int d\omega\ a_\omega\mathrm{e}^{\mathrm{i}(\omega-\omega_2)z/c}$.

Assuming a real Rabi frequency Ω_{W}, this yields the Heisenberg–Langevin equations as follows:

$$\partial_{\mathrm{t}}\sigma_{se} = -\gamma_{es}\sigma_{se} + \mathrm{i}\Omega_W\mathrm{e}^{\mathrm{i}\omega_1 z/c}\sigma_{sg} - \mathrm{i}\bar{g}\mathcal{E}_w\mathrm{e}^{\mathrm{i}\omega_2 z/c}(\sigma_{ee}-\sigma_{ss}) + F_{se}$$
$$\partial_{\mathrm{t}}\sigma_{sg} = -\gamma_0\sigma_{sg} + \mathrm{i}\Omega_W\mathrm{e}^{-\mathrm{i}\omega_1 z/c}\sigma_{se} - \mathrm{i}\bar{g}\mathcal{E}_w\mathrm{e}^{\mathrm{i}\omega_2 z/c}\sigma_{eg} + F_{sg}$$
$$\partial_{\mathrm{t}}\sigma_{eg} = -\gamma_{eg}\sigma_{eg} - \mathrm{i}\Omega_W\mathrm{e}^{-\mathrm{i}\omega_1 z/c}\sigma_{gg} + F_{eg}, \tag{30}$$

where ω_1 (ω_2) indicates the frequency of the write control field (write photon field), respectively, and $\bar{g}^2N = \frac{d\gamma_{es}c}{L}$.

B.2. Creating atomic coherences

During the write process we account for possible depletion of the write laser intensity, and hence do not assume $\Omega_{\mathrm{W}}(r,\ t)$ to be constant throughout the sample. As a result of the laser we create coherences between the $|g\rangle - |e\rangle$

transition, which forms the initial state for the write photon field. Here we proceed to find the atomic coherences prepared as a result of our exponential shaped resonant write control field.

For a sufficiently short write control field, the dynamics of the field and the atoms can be described with the dynamics along the $|g\rangle - |e\rangle$ transition. Ignoring the noise terms on σ_{ge} and making the analogy between the classical and quantum fields on the $|g\rangle - |e\rangle$ transition,

$$\begin{aligned} c\partial_z \Omega_{\mathrm{W}}(z,\, t) &= \mathrm{i}g^2 N \sigma_{ge}(z,\, t)\mathrm{e}^{-\mathrm{i}\omega_1 z/c}, \\ \partial_t \sigma_{ge} &= -\gamma_{eg}\sigma_{ge} + \mathrm{i}\Omega_{\mathrm{W}}(z,\, t)\mathrm{e}^{+\mathrm{i}\omega_1 z/c}\sigma_{gg} \\ &\approx -\gamma_{eg}\sigma_{ge} + \mathrm{i}\Omega_{\mathrm{W}}(z,\, t)\mathrm{e}^{+\mathrm{i}\omega_1 z/c}, \end{aligned} \tag{31}$$

where we have assumed that almost all atoms remain in the $|g\rangle$ level.

Let us first assume a write control field with Rabi frequency Ω_{W} that begins at $t = 0$. Taking the Laplace transforms from $t \rightarrow w$, we find

$$\partial_z \Omega_{\mathrm{W}}(z,\, w) = \mathrm{i}\frac{g^2 N}{c}\sigma_{ge}(z,\, w)\mathrm{e}^{-\mathrm{i}\omega_1 z/c}, \tag{32}$$

$$\sigma_{ge}(z,\, w) = \frac{1}{w + \gamma_{eg}}[\mathrm{i}\Omega_{\mathrm{W}}(z,\, w)\mathrm{e}^{\mathrm{i}\omega_1 z/c} + \sigma_{ge}(z,\, t = 0)]. \tag{33}$$

Insert equation (33) into equation (32), and use the initial condition $\sigma_{ge}(z, t = 0) = 0$ to obtain

$$\partial_z \Omega_W(z,\, w) = -\frac{g^2 N}{c}\left(\frac{1}{w + \gamma_{eg}}\right)\Omega_W(z,\, w),$$

yielding

$$\Omega_{\mathrm{W}}(z,\, w) = \mathrm{e}^{-\frac{g^2 N}{c}\left(\frac{1}{w+\gamma_{eg}}\right)z}\Omega_{\mathrm{W}}(z = 0,\, w).$$

Insert this into equation (33) to obtain

$$\sigma_{ge}(z,\, w) = (\mathrm{i}\mathrm{e}^{\mathrm{i}\omega_1 z/c})\left[\frac{1}{w + \gamma_{eg}}\mathrm{e}^{-\frac{g^2 N}{c}\frac{1}{w+\gamma_{eg}}z}\Omega_{\mathrm{W}}(z = 0,\, w)\right].$$

After inverting the Laplace transform, we now shift the limits to consider a write control field with support on negative times, giving

$$\begin{aligned} \sigma_{ge}(z,\, t) = (\mathrm{i}\mathrm{e}^{\mathrm{i}\omega_1 z/c})&\int_{-\infty}^{t} \mathrm{e}^{-\gamma_{eg}(t - t_1'')} \\ &\times J_0\left[2\sqrt{\frac{\gamma_{eg} d}{L}(t - t_1'')z}\right]\Omega_{\mathrm{W}}(z = 0,\, t_1'')\mathrm{d}t_1'', \end{aligned} \tag{34}$$

where $J_n(x)$ indicates the nth Bessel function of the first kind.

Thus, with an exponential write control field $\Omega_{\mathrm{W}}(0,\, t) = \Omega_{\mathrm{W}}^{\max}\mathrm{e}^{t/\tau_{\mathrm{W}}}$ sent up to $t = 0$, we evaluate the atomic coherence at $t = 0$ with the help of $\int_0^\infty \mathrm{e}^{-At}J_0[2\sqrt{Bt}]\mathrm{d}t = \frac{1}{A}\mathrm{e}^{-B/A}$ and finally obtain

$$\sigma_{ge}(z,\, 0) = \mathrm{e}^{\mathrm{i}\omega_1 z/c}\theta_0 \mathrm{e}^{-\frac{\alpha z}{2}}, \tag{35}$$

where $\theta_0 = \mathrm{i}\frac{\Omega_{\max}\tau_{\mathrm{W}}}{1 + \gamma_{eg}\tau_{\mathrm{W}}}$ and $\alpha/2 = d\frac{\gamma_{eg}\tau_{\mathrm{W}}}{1 + \gamma_{eg}\tau_{\mathrm{W}}}\frac{1}{L}$.

B.3. Write photon emission

After the preparation of atomic coherences, we begin to see spontaneous emission from the $|e\rangle$ level. Along with the field propagation equation, the relevant Heisenberg–Langevin equations are

$$\begin{aligned} c\partial_z \mathcal{E}_{\mathrm{w}} &= \mathrm{i}\bar{g}N\mathrm{e}^{-\mathrm{i}\omega_2 z/c}\sigma_{se}(z,\, t), \\ \partial_t \hat{\sigma}_{es} &= -\gamma_{es}\sigma_{se} - \mathrm{i}\bar{g}\mathcal{E}_w \mathrm{e}^{\mathrm{i}\omega_2 z/c}(\sigma_{ee} - \sigma_{ss}) + F_{se}. \end{aligned}$$

Defining $Q^\dagger = \sqrt{N}\mathrm{e}^{-\mathrm{i}\omega_2 z/c}\sigma_{se}$, we will consider the write emission for short detection times. Using (35) we thus replace $\sigma_{ee} - \sigma_{ss}$ with its mean value at position z and $t = 0$ to obtain

$$\begin{aligned} c\partial_z \mathcal{E}_{\mathrm{w}}(z,\, t) &= \mathrm{i}\bar{g}\sqrt{N}Q^\dagger(z,\, t), \\ \partial_t Q^\dagger(z,\, t) &= -\gamma_{es}Q^\dagger(z,\, t) - \mathrm{i}\bar{g}\sqrt{N}|\theta_0|^2\mathrm{e}^{-\alpha z}\mathcal{E}_{\mathrm{w}}(z,\, t) \\ &\quad + F_Q^\dagger(z,\, t). \end{aligned} \tag{36}$$

Performing first the Laplace transform in space ($z \rightarrow s$)

$$\begin{aligned} s\mathcal{E}_{\mathrm{w}}(s,\,t) - \mathcal{E}_{\mathrm{w}}(z=0,\,t) &= A\;Q^{\dagger}(s,\,t),\\ \partial_{\mathrm{t}}Q^{\dagger}(s,\,t) &= -\gamma_{es}Q^{\dagger}(s,\,t) + B\mathcal{E}_{\mathrm{w}}(s+\alpha,\,t)\\ &\quad + F_{Q}^{\dagger}(s,\,t), \end{aligned}$$

and then in time ($t \rightarrow \omega$), we get

$$\begin{aligned} s\mathcal{E}_{\mathrm{w}}(s,\,\omega) - \mathcal{E}_{\mathrm{w}}(z=0,\,\omega) &= A\;Q^{\dagger}(s,\,\omega),\\ Q^{\dagger}(s,\,\omega) &= \frac{1}{\gamma_{es}+\omega}B\mathcal{E}_{\mathrm{w}}(s+\alpha,\,\omega) + F_{Q}^{\dagger}(s,\,\omega) + Q^{\dagger}(s,\,t=0), \end{aligned}$$

where $A = \mathrm{i}\frac{\bar{g}\sqrt{N}}{c}$ and $B = -\mathrm{i}\bar{g}\sqrt{N}\theta_0^2$.

Substituting the second line into the first, we eliminate $Q(s,\omega)$ and are left with a boundary term in Q:

$$\begin{aligned} s\mathcal{E}(s,\,\omega) - \mathcal{E}(z=0,\,\omega) = &\left(\frac{A}{\gamma_{es}+\omega}\right)[B\mathcal{E}(s+\alpha,\,\omega)\\ &+ F_{Q}^{\dagger}(s,\,\omega) + Q^{\dagger}(s,\,t=0)]. \end{aligned}$$

The following formula also holds with a shift from s to $s+\alpha$:

$$\begin{aligned} &(s+\alpha)\mathcal{E}_{\mathrm{w}}(s+\alpha,\,\omega) - \mathcal{E}_{\mathrm{w}}(z=0,\,\omega)\\ &= \left(\frac{A}{\gamma_{es}+\omega}\right)[B\mathcal{E}_{\mathrm{w}}(s+2\alpha,\,\omega) + F_{Q}^{\dagger}(s+\alpha,\,\omega) + Q^{\dagger}(s+\alpha,\,t=0)]. \end{aligned}$$

By substituting $\mathcal{E}_{\mathrm{w}}(s+\alpha,\,\omega)$ into the previous equation we can find $\mathcal{E}(s,\,\omega)$ in terms of $\mathcal{E}_{\mathrm{w}}(s+2\alpha,\,\omega)$, and by taking the substitution into the nth step we have

$$\begin{aligned} \mathcal{E}_{\mathrm{w}}(s,\,\omega) = &K(\omega)^{n}D(n)\mathcal{E}_{\mathrm{w}}(s+n\alpha,\,\omega)\\ &+ \frac{1}{B}\sum_{j=1}^{n}K(\omega)^{j}D(j)F_{Q}^{\dagger}(s+(j-1)\alpha,\,\omega)\\ &+ \frac{1}{B}\sum_{j=1}^{n}K(\omega)^{j}D(j)Q^{\dagger}(s+(j-1)\alpha,\,t'=0)\\ &+ [K(\omega)]^{-1}\sum_{j=1}^{n}[K(\omega)^{j}D(j)]\mathcal{E}_{\mathrm{w}}(z'=0,\,\omega), \end{aligned}$$

where $K(\omega) = \frac{AB}{\gamma_{es}+\omega}$ and $D(n) = \prod_{k=0}^{n-1}\frac{1}{s\;+\;k\alpha}$.

Taking the limit of $n \rightarrow \infty$, the first term disappears, and we proceed to perform the inverse transform $s \rightarrow z$. With a shift in the index j, $\mathcal{L}^{-1}[D(j+1)] = \frac{1}{j!}\left(\frac{1-\mathrm{e}^{-\alpha z}}{\alpha}\right)^{j}$ and the shifting property of the Laplace Transform,

$$\begin{aligned} &\mathcal{E}_{w}(z,\,\omega)\\ &= \frac{1}{B}\sum_{j=0}^{\infty}K(\omega)^{j+1}\int_{0}^{z}\frac{1}{j!}\left(\frac{1-\mathrm{e}^{-\alpha(z-z'')}}{\alpha}\right)^{j}\mathrm{e}^{-j\alpha z''}F_{Q}^{\dagger}(z'',\,\omega)\;\mathrm{d}z''\\ &\quad + \frac{1}{B}\sum_{j=0}^{\infty}K(\omega)^{j+1}\int_{0}^{z}\frac{1}{j!}\left(\frac{1-\mathrm{e}^{-\alpha(z-z'')}}{\alpha}\right)^{j}\mathrm{e}^{-j\alpha z''}Q^{\dagger}(z'',\,t=0)\;\mathrm{d}z''\\ &\quad + \frac{1}{K(\omega)}\sum_{j=0}^{\infty}K(\omega)^{j+1}\frac{1}{j!}\left(\frac{1-\mathrm{e}^{-\alpha(z)}}{\alpha}\right)^{j}\mathcal{E}_{\mathrm{w}}(z'=0,\,\omega)\\ &= \frac{A}{\gamma_{es}+\omega}\int_{0}^{z}\mathrm{e}^{\left[\frac{1}{\gamma_{es}+\omega}M(z,z'')\mathrm{e}^{-\alpha z''}\right]}F_{Q}^{\dagger}(z'',\,\omega)\mathrm{d}z''\\ &\quad + \frac{A}{\gamma_{es}+\omega}\int_{0}^{z}\mathrm{e}^{\left[\frac{1}{\gamma_{es}+\omega}M(z,z'')\mathrm{e}^{-\alpha z''}\right]}Q^{\dagger}(z'',\,t'=0)\mathrm{d}z''\\ &\quad + \mathrm{e}^{\frac{1}{\gamma_{es}+\omega}M(z,0)}\mathcal{E}_{w}(z=0,\,\omega), \end{aligned} \tag{37}$$

where $M(z',\,z'') = \frac{AB}{\alpha}[1-\mathrm{e}^{-\alpha(z'-z'')}]$.

Finally, noting that

$$\mathcal{L}^{-1}\left[\frac{1}{\gamma_{es}+\omega}e^{\frac{A}{\gamma_{es}+\omega}}\right] = e^{-\gamma_{es}t}[\sqrt{At}^{(-1)}I_1(2\sqrt{At}) + I_2(2\sqrt{At})],$$
$$\mathcal{L}^{-1}[e^{\frac{A}{\gamma_{es}+\omega}}] = e^{-\gamma_{es}t}\left[\sqrt{\frac{A}{t}}I_1(2\sqrt{At}) + \delta(t)\right],$$

we get

$$\begin{aligned}\mathcal{E}_w(z,\,t) = A\int_0^z\int_0^t e^{-\gamma_{es}(t-t_1'')}H_1[\alpha,\,z,\,z_1'',\,t,\,t_1'']F_Q^\dagger(z_1'',\,t_1'')\,dt_1''\,dz_1''\\ + A\int_0^z e^{-\gamma_{es}(t)}H_1[\alpha,\,z,\,z_1'',\,t,\,0]Q^\dagger(z_1'',\,0)\,dz_1''\\ + \int_0^t e^{-\gamma_{es}(t-t'')}H_2(\alpha,\,z,\,0,\,t,\,t'')\mathcal{E}_w(0,\,t'')\,dt''\\ + \mathcal{E}_w(0,\,t),\end{aligned} \tag{38}$$

where

$$H_1(\alpha,\,z_1,\,z_2,\,t_1,\,t_2) = I_0[2\sqrt{M(z_1,\,z_2)e^{-\alpha z_2}(t_1-t_2)}],$$
$$H_2(\alpha,\,z_1,\,z_2,\,t_1,\,t_2) = \sqrt{\frac{M(z_1,\,z_2)}{t_1-t_2}}I_1[2\sqrt{M(z_1,\,z_2)e^{-\alpha z_2}(t_1-t_2)}].$$

B.4. Number of write photons

Computing the photon flux requires the commutation relations for Q and a 2-point noise correlation function involving F_Q. In a short time window τ_d where $\sigma_{ee} - \sigma_{ss}$ is not changing, and with the Einstein relations (see Ch 15.5 of [23]), the Langevin equations for system operators can be written

$$\dot{A}_\mu = D_\mu(t) + F_\mu(t). \tag{39}$$

The corresponding memoryless noise correlations for operators μ and ν are such that

$$\langle F_\mu(t')F_\nu(t'')\rangle = 2\langle D_{\mu\nu}\rangle\delta(t'-t''), \tag{40}$$

where

$$2\langle D_{\mu\nu}\rangle = -\langle A_\mu D_\nu\rangle - \langle D_\mu A_\nu\rangle + \frac{d}{dt}\langle A_\mu A_\nu\rangle. \tag{41}$$

Thus, identifying terms in equation (36) with terms in equation (39), we make use of

$$\begin{aligned}[Q(z,\,t),\,Q^\dagger(z',\,t)] &= N[\sigma_{es}(z,\,t),\,\sigma_{se}(z',\,t)]\\ &= L\delta(z-z')|\theta_0|^2e^{-\alpha z'},\end{aligned} \tag{42}$$

then we make use of the fact that $\langle Q^\dagger(z,\,t)Q(z',\,t)\rangle$ right after our preparation of atomic coherences is zero, giving $\langle Q(z,\,t)Q^\dagger(z',\,t)\rangle = L\delta(z-z')|\theta_0|^2e^{-\alpha z'}$.

Then one obtains

$$2\langle D_{Q,Q^\dagger}\rangle = 2\gamma_{es}L|\theta_0|^2e^{-\alpha z}\delta(z-z'), \tag{43}$$

yielding

$$\langle F_Q(z,\,t)F_Q^\dagger(z',\,t')\rangle = 2\gamma_{es}L|\theta_0|^2e^{-\alpha z}\delta(z-z')\delta(t-t'), \tag{44}$$

valid when $\sigma_{ee} - \sigma_{ss}$ is not changing.

This yields a photon flux of

$$\begin{aligned}\frac{c}{L}\langle\mathcal{E}_w^\dagger(L,\,t)\mathcal{E}_w(L,\,t)\rangle = \frac{c}{L}\frac{\bar{g}^2N}{c^2}\int_0^L e^{-2\gamma_{es}t}H_1[\alpha,\,L,\,z_1'',\,t,\,0]^2V|\theta_0|^2e^{-\alpha z_1''}dz_1''\\ + \frac{c}{L}\frac{\bar{g}^2N}{c^2}\int_0^t\int_0^L e^{-2\gamma_{es}(t-t_1'')}H_1[\alpha,\,L,\,z_1'',\,t,\,t_1'']^2\\ \times 2\gamma_{es}L|\theta_0|^2e^{-\alpha z_1''}dz_1''\,dt_1''.\end{aligned}$$

For sufficiently short detection times $\tau_d \ll \frac{1}{2\gamma_{es}}$, the noise contribution (second term) can be ignored, and furthermore when the photon number is much smaller than 1 ($\tau_d \ll \left\{\frac{\bar{g}^2N}{c}|\theta_0|^2\left(\frac{1-e^{-\alpha L}}{\alpha}\right)\right\}^{-1}$) we can consider just the leading term in the series expansion, and observe a constant flux

$$\begin{aligned}
&\frac{c}{L}\langle \mathcal{E}_{\mathrm{w}}^{\dagger}(L,\,\tau_{\mathrm{d}})\mathcal{E}_{\mathrm{w}}(L,\,\tau_{\mathrm{d}})\rangle \\
&=\frac{\bar{g}^2N}{c}|\theta_0|^2\int_0^L (I_0[2\sqrt{M[L,\,z_1'']\mathrm{e}^{-\alpha z_1''}\tau_{\mathrm{d}}}])^2\mathrm{e}^{-\alpha z_1''}\mathrm{d}z_1'' \\
&\approx\frac{\bar{g}^2N}{c}|\theta_0|^2\int_0^L (1+2M[L,\,z_1'']\mathrm{e}^{-\alpha z_1''}\tau_{\mathrm{d}}+O(\tau_{\mathrm{d}}^2))\mathrm{e}^{-\alpha z_1''}\mathrm{d}z_1'' \\
&=\frac{\bar{g}^2N}{c}|\theta_0|^2\frac{1-\mathrm{e}^{-\alpha L}}{\alpha}.
\end{aligned} \tag{45}$$

We therefore obtain a photon number of $\frac{\bar{g}^2N}{c}|\theta_0|^2\frac{1-\mathrm{e}^{-\alpha L}}{\alpha}\tau_{\mathrm{d}}$ within this short detection window. This is precisely the excited atom fraction multiplied by $\bar{d}\gamma_{es}\tau_{\mathrm{d}}$, since the fraction of atoms that were excited after the write pulse is $\frac{1}{L}\int_0^L\langle\sigma_{ee}(z,\,0)\rangle\,\mathrm{d}z=\frac{1}{L}\int_0^L|\theta_0|^2\mathrm{e}^{-\alpha z}\mathrm{d}z=|\theta_0|^2\frac{1-\mathrm{e}^{-\alpha L}}{\alpha L}$.

B.5. Number of prepared spins

We start with the description of the spin operator from equation (30), by defining $S=\sqrt{N}\sigma_{gs}\mathrm{e}^{-\mathrm{i}(\omega_1-\omega_2)z/c}$ and replacing $\sigma_{eg}(z,\,t)$ by its mean value $\theta_0^*\mathrm{e}^{-\alpha z/2}\mathrm{e}^{-\mathrm{i}\omega_1 z/c}$

$$\begin{aligned}
(\partial_{\mathrm{t}}+\gamma_0)\hat{S}^{\dagger}(z,\,t)-F_S^{\dagger}(z,\,t)&=-\mathrm{i}\bar{g}\sqrt{N}\mathrm{e}^{\mathrm{i}k_{\mathrm{w}}\mathrm{r}}\mathcal{E}_{\mathrm{w}}(z,\,t)\sigma_{eg} \\
&=-\mathrm{i}\bar{g}\sqrt{N}\mathcal{E}_{\mathrm{w}}(z,\,t)[\theta_0^*\mathrm{e}^{-\alpha z/2}].
\end{aligned}$$

Take the Laplace transform from $t\rightarrow\omega$ to see

$$(\omega+\gamma_0)S^{\dagger}(z,\,\omega)-S^{\dagger}(z,\,t=0)-F_S^{\dagger}(z,\,\omega)=C(z)\mathcal{E}_w(z,\,\omega),$$

where $C(z)=-\mathrm{i}\bar{g}\sqrt{N}\theta_0^*\mathrm{e}^{-\alpha z/2}$. Then we have

$$S^{\dagger}(z,\,\omega)=\frac{C(z)}{\omega+\gamma_0}\mathcal{E}_{\mathrm{w}}(z,\,\omega)+\frac{1}{\omega+\gamma_0}S^{\dagger}(z,\,t=0)+\frac{1}{\omega+\gamma_0}F_S^{\dagger}(z,\,\omega), \tag{46}$$

and noting that $\mathcal{L}^{-1}\left[\frac{1}{\omega+\gamma_0}\right]=\mathrm{e}^{-\gamma_0 t}$ yields

$$\begin{aligned}
S^{\dagger}(z,\,t)=C(z)&\int_0^t \mathrm{e}^{-\gamma_0(t-t')}\mathcal{E}_w(z,\,t')\mathrm{d}t' \\
&+\mathrm{e}^{-\gamma_0 t}S^{\dagger}(z,\,t=0)+\int_0^t \mathrm{e}^{-\gamma_0(t-t')}F_S^{\dagger}(z,\,t')\mathrm{d}t',
\end{aligned} \tag{47}$$

where the field expression $\mathcal{E}$ from the previous subsection is required. Ignoring terms that do not show up in the normal ordered $\langle S^{\dagger}S\rangle$, we have

$$\begin{aligned}
S^{\dagger}(z,\,t)=C(z)&\int_0^t \mathrm{d}t'\mathrm{e}^{-\gamma_0(t-t')} \\
&\times\left(\int_0^{t'}\mathrm{d}t''\mathrm{e}^{-\gamma_{es}(t'-t'')}H_2(\alpha,\,z,\,0,\,t',\,t'')\mathcal{E}_{\mathrm{w}}(0,\,t'')+\mathcal{E}_{\mathrm{w}}(0,\,t')\right).
\end{aligned} \tag{48}$$

Computing $\langle S^{\dagger}S\rangle$ requires the commutator $[\mathcal{E}_{\mathrm{w}}(z,\,t),\,\mathcal{E}_{\mathrm{w}}^{\dagger}(z',\,t')]=L\delta[z-z'-c(t-t')]$ and yields 4 terms. In the short time window where one can ignore the atomic dephasing $\left(\tau_{\mathrm{d}}\ll\frac{1}{2\gamma_0},\,\frac{1}{2\gamma_{es}}\right)$, and also where the photon number is much smaller than 1 $\left(\tau_{\mathrm{d}}\ll\left\{\frac{\bar{g}^2N}{c}|\theta_0|^2\left(\frac{1-\mathrm{e}^{-\alpha L}}{\alpha}\right)\right\}^{-1}\right)$, only one term dominates (the term independent of H_2). The number of spins is then equivalent to the photon number

$$\frac{1}{L}\int_0^L\langle S^{\dagger}(z,\,\tau_{\mathrm{d}})S(z,\,\tau_{\mathrm{d}})\rangle\,\mathrm{d}z\approx\frac{\bar{g}^2N}{c}|\theta_0|^2\frac{1-\mathrm{e}^{-\alpha L}}{\alpha}\tau_{\mathrm{d}}.$$

Appendix C. Phase matching

By assuming the retrieval process to perform retrieval from the exact same spin wave function $S(z,\,t)$ that has been created by the write pulse, we have assumed the degeneracy of the two metastable states $|g\rangle$ and $|s\rangle$. In general, the metastable states could have different energies which would lead to a read process from $S(z,\,t)\mathrm{e}^{2\mathrm{i}(\omega_e-\omega_s)z/c}$. However, this effect is negligible in the regime $|\omega_e-\omega_s|\frac{L}{c}\ll 1$.

Appendix D. Second order coherence

D.1. Multi-pair two-mode squeezing

To ensure that a single photon source is single mode in all degrees of freedom, one would have to verify that the outgoing emission is not produced in a combination of modes. In the system that we consider, one cause for multi-mode emission are multiple two mode squeezing processes occurring during the initial write process. Thereafter, the subsequent retrieval process yields a read photon in more than one mode. Here, we include a short section to explain how the unconditional autocorrelation measurement ($g^{(2)}(0)$) scales with the number of driven mode pairs [20], and this allows one to verify that no higher-number two mode squeezing processes have occured.

Let us first consider the state created by K vacuum squeezing processes

$$\rho_{\text{multi}} = (1-p)^K \left[\mathrm{e}^{\sqrt{p}\sum_{m=1}^{K} a_m^\dagger b_m^\dagger} |\Omega\rangle \langle\Omega| \mathrm{e}^{\sqrt{p}\sum_{n=1}^{K} a_n b_n} \right], \tag{49}$$

where $|\Omega\rangle$ indicates the vacuum in all modes. Now consider a detector that sees all the K modes, giving a number operator of the form

$$\hat{N}_K = \sum_{c=1}^{K} a_c^\dagger a_c. \tag{50}$$

This yields

$$\mathrm{Tr}\left[\sum_{c,d=1}^{K} a_c^\dagger a_d^\dagger a_c a_d \rho_{\text{multi}} \right] = \left(\frac{p}{1-p} \right)^2 (K^2 + K), \tag{51}$$

$$\mathrm{Tr}\left[\sum_{c=1}^{K} a_c^\dagger a_c \rho_{\text{multi}} \right] = \frac{p}{1-p} K, \tag{52}$$

giving the unconditional autocorrelation of the a modes

$$\begin{aligned} g^{(2)}_{\text{multi}} &= \frac{\left\langle \sum_{c,d=1}^{K} a_c^\dagger a_d^\dagger a_c a_d \right\rangle}{\left\langle \sum_{c=1}^{K} a_c^\dagger a_c \right\rangle^2} \\ &= 1 + \frac{1}{K}, \end{aligned} \tag{53}$$

which leads us to check if our photon field is indeed consistent with that coming from a single-pair two-mode squeezing process.

We thus compute the unconditional autocorrelation function of the read photon field at time t

$$g^2_{\text{read}} = \frac{\langle \mathcal{E}_r^\dagger(0,\, t) \mathcal{E}_r^\dagger(0,\, t) \mathcal{E}_r(0,\, t) \mathcal{E}_r(0,\, t) \rangle}{\langle \mathcal{E}_r^\dagger(0,\, t) \mathcal{E}_r(0,\, t) \rangle^2},$$

In the regime we consider, where we have a short detection time and a fast readout, developing the numerator of the $g^{(2)}$ function leads to the term

$$\begin{aligned} &\langle \mathcal{E}_{\text{w}}(0,\, t_a) \mathcal{E}_{\text{w}}(0,\, t_b) \mathcal{E}_{\text{w}}^\dagger(0,\, t_c) \mathcal{E}_{\text{w}}^\dagger(0,\, t_{\text{d}}) \rangle \\ &= \langle \mathcal{E}_{\text{w}}(0,\, t_a) \left[\mathcal{E}_{\text{w}}^\dagger(0,\, t_c) \mathcal{E}_{\text{w}}(0,\, t_b) + \frac{L}{c} \delta(t_b - t_c) \right] \mathcal{E}_{\text{w}}(0,\, t_{\text{d}}) \rangle \\ &= \left(\frac{L}{c} \right)^2 \delta(t_a - t_c) \delta(t_b - t_{\text{d}}) + \left(\frac{L}{c} \right)^2 \delta(t_a - t_{\text{d}}) \delta(t_b - t_c), \end{aligned}$$

which yields

$$g^2_{\text{read}} = \frac{2 \langle \mathcal{E}_r^\dagger(0,\, t) \mathcal{E}_r(0,\, t) \rangle^2}{\langle \mathcal{E}_r^\dagger(0,\, t) \mathcal{E}_r(0,\, t) \rangle^2} = 2$$

as it should, since we assume a mono-mode emission ($K = 1$). Here we have used equation (25) and the leading term of equation (48).

ORCID iDs

Melvyn Ho https://orcid.org/0000-0002-2459-1306

References

[1] Eisaman M D, Fan J, Migdall A and Polyakov S V 2011 *Rev. Sci. Instrum.* **82** 071101
[2] Sangouard N and Zbinden H 2012 *J. Mod. Opt.* **59** 1458
[3] Duan L-M, Lukin M D, Cirac J I and Zoller P 2001 *Nature (London)* **414** 413
[4] Sangouard N, Simon C, de Riedmatten H and Gisin N 2011 *Rev. Mod. Phys.* **83** 33
[5] Simon C *et al* 2010 *Eur. Phys. J.* D **58** 1
[6] Bussières F, Sangouard N, Afzelius M, de Riedmatten H, Simon C and Tittel W 2013 *J. Mod. Opt.* **60** 1519
[7] Heshami K, England D G, Humphreys P C, Bustard P J, Acosta V M, Nunn J and Sussman B J 2016 *J. Mod. Opt.* **63** 2005
[8] Radnaev A G, Dudin Y O, Zhao R, Jen H H, Jenkins S D, Kuzmich A and Kennedy T A B 2010 *Nat. Phys.* **6** 894
[9] Yang S J, Wang X-J, Bao X-H and Pan J-W 2016 *Nat. Photonics* **10** 381
[10] Farrera P, Heinze G, Albrecht B, Ho M, Chávez M, Teo C, Sangouard N and de Riedmatten H 2016 *Nat. Comm.* **7** 13556
[11] Simon J, Tanji H, Thompson J K and Vuletić V 2007 *Phys. Rev. Lett.* **98** 183601
[12] Bimbard E, Boddeda R, Vitrant N, Grankin A, Parigi V, Stanojevic J, Ourjoumtsev A and Grangier P 2014 *Phys. Rev. Lett.* **112** 033601
[13] Cho Y-W, Campbell G T, Everett J L, Bernu J, Higginbottom D B, Cao M T, Geng J, Robins N P, Lam P K and Buchler B C 2016 *Optica* **3** 1
[14] Gorshkov A V, André A, Fleischhauer M, Sørensen A S and Lukin M D 2007 *Phys. Rev. Lett.* **98** 123601
[15] Gorshkov A V, André A, Lukin M D and Sørensen A S 2007 *Phys. Rev.* A **76** 033805
[16] Mendes M S, Saldanha P L, Tabosa J W R and Felinto D 2013 *New J. Phys.* **15** 075030
[17] Hammerer K, Sørensen A S and Polzik E S 2010 *Rev. Mod. Phys.* **82** 1041
[18] Gradshteyn I S and Rhyzik I M 2007 *Table of Integrals, Series and Products* (Amsterdam: Elsevier)
[19] Vivoli V, Sangouard N, Afzelius M and Gisin N 2013 *New J. Phys.* **15** 095012
[20] Sekatski P, Sangouard N, Bussières F, Clausen C, Gisin N and Zbinden H 2012 *J. Phys. B: At. Mol. Opt. Phys.* **45** 124016
[21] Golla A, Chalopin B, Bader M, Harder I, Mantel K, Maiwald R, Lindlein N, Sondermann M and Leuchs G 2012 *Eur. Phys. J.* D **66** 190
[22] Dao H L, Aljunid S A, Maslennikov G and Kurtsiefer C 2012 *Rev. Sci. Instrum.* **83** 083104
[23] Meystre P and Sargent M III 1999 *Elements of Quantum Optics* (New York: Springer)

CHAPTER 2

OPTOMECHANICAL DEVICES FOR QUANTUM REPEATERS

In the original DLCZ architecture for quantum repeaters, atomic ensembles are used as quantum memories, where delocalised single atomic excitations can be heralded and then read out. We presented a way to control the waveforms of the retrieved photons in the previous chapter so that quantum repeaters can be implemented with heterogenous resources. However, the central frequency response of atomic ensembles remain largely fixed by the energy level properties of the chosen atomic species. In contrast, one can use different kinds of nodes, and engineer the design of photonic crystals [40, 41] or mechanical resonators [42, 43] instead, so that they can efficiently couple to light while tailoring their central frequency with great flexibility. One can thus envision optomechanical devices being used in future quantum repeaters, as long as they are also capable of first creating correlated excitations between the resonator and a first photon mode, followed by a retrieval process converting the excitation into a second photon mode.

One can first consider a mechanical oscillator in a cavity, operating within the resolved sideband regime and weak coupling limit. Sending a blue-detuned laser pulse into the resonator results in a two-mode squeezing interaction, creating correlated excitations between the resonator and a first emitted photon mode. A subsequent red-detuned laser pulse results in a beamsplitter-type interaction, performing a state transfer from the resonator mode to a second emitted photon mode. Quantum correlations that are detected between the two photonic modes are a sign of optomechanical entanglement, meaning correlations between the first photons and the mechanical phonons. In fact, it is possible for these photonic

correlations to yield a Bell inequality violation with displacement-aided photon counting measurements, but such a violation requires stringent global detection efficiencies and a manageable number of excitations in the resonator for the detection of nonlocality and hence the conclusion of optomechanical entanglement [44]. If, however, one is able to guarantee a detailed description of the measurement devices, one can form an entanglement witness instead. This requires assumptions at the level of the measurements, but can lead to less severe requirements on the global detection efficiency.

In order to verify that a chosen optomechanical oscillator is a capable quantum memory producing two-mode squeezed states with a controllable delay, we design an entanglement witness with displacement-aided photon counting measurements, tailored for two-mode squeezed photonic states [45]. Let us point out that this witness does not require any prior knowlege of the state to be assessed, or any assumptions on the dimensionality of the Hilbert space in which it resides. We find that the witness detects entanglement for low efficiencies, and is robust to initial thermal excitations in the resonator. Since the setup we consider is the same as that of [44], a successful witness of entanglement with our proposal also represents an initial step towards a fully device-independent characterisation of optomechanical entanglement using a Bell test.

Paper C

Witnessing optomechanical entanglement with photon counting

Melvyn Ho, Enky Oudot, Jean-Daniel Bancal and Nicolas Sangouard

Physical Review Letters **121**, 023602 (2018)

Witnessing Optomechanical Entanglement with Photon Counting

Melvyn Ho, Enky Oudot, Jean-Daniel Bancal, and Nicolas Sangouard
Quantum Optics Theory Group, University of Basel, Klingelbergstrasse 82, 4056 Basel, Switzerland

(Received 8 April 2018; published 11 July 2018)

The ability to coherently control mechanical systems with optical fields has made great strides over the past decade, and now includes the use of photon counting techniques to detect the nonclassical nature of mechanical states. These techniques may soon be used to perform an optomechanical Bell test, hence highlighting the potential of cavity optomechanics for device-independent quantum information processing. Here, we propose a witness which reveals optomechanical entanglement without any constraint on the global detection efficiencies in a setup allowing one to test a Bell inequality. While our witness relies on a well-defined description and correct experimental calibration of the measurements, it does not need a detailed knowledge of the functioning of the optomechanical system. A feasibility study including dominant sources of noise and loss shows that it can readily be used to reveal optomechanical entanglement in present-day experiments with photonic crystal nanobeam resonators.

DOI: 10.1103/PhysRevLett.121.023602

Introduction.—Bell tests have initially been proposed to show that correlations between the results of measurements performed on two separated systems cannot be reproduced by classical strategies [1]. They have been used to show the limit of classical physics as a complete description of small systems involving two atoms [2,3] or two photons [4,5]. This naturally raises the question of a Bell inequality violation with larger systems. Concrete proposals have been made recently along this line to realise Bell tests with cavity opto- and electromechanical systems [6–8].

Cavity optomechanics is at the core of intense research where the cavity field is used to control the motion of a mechanical system via radiation pressure. While initial efforts have focused on the cooling of mechanical oscillators down to the ground state [9–11], impressive results including the detection of electro- [12] and optomechanical [13,14] nonclassical correlations and entanglement between two mechanical systems [15,16] are now suggesting that cavity optomechanics could serve as a building block of future quantum networks [17] for the processing and storage of quantum information [18,19]. If one is to show that cavity optomechanics can form the cornerstone of future quantum networks, it is crucial to prove that it is qualified for all possible uses of such networks. This means that the qualification must be device independent [20], that is, it cannot rely on a physical description of the actual implementation. A particular model using seemingly harmless assumptions, on the underlying Hilbert space dimension for instance, can completely corrupt the security guarantees that are offered by quantum networks for secure communications over long distances [21,22]. Device-independent schemes have been derived to certify all the building blocks of quantum networks that can be used to create, store, or process quantum information [23]. They could be directly implemented from the Bell tests proposed in Refs. [6,7]. Optomechanical Bell tests are thus not only of fundamental interest but are resources to certify the usefulness of optomechanical systems for long distance quantum communication with device-independent security guarantees.

The violation of a Bell inequality as proposed in Refs. [6–8] is, however, not trivial. Reference [6] uses a cavity optomechanical system in the resolved sideband regime where the mechanical frequency is larger than the cavity decay rate. Once cooled, the mechanical system is excited by laser light resonant with the blue sideband; see Fig. 1. Photons of the laser can decay into phonon-photon pairs, the photon being resonant with the cavity frequency and the phonon corresponding to a single excitation of the vibrational mode of the mechanical system. Energy conservation ensures that for each phononic excitation of the mechanical state, the cavity mode gets populated with a photonic excitation. These quantum correlations between phonon and photon numbers are strong enough to violate a Bell inequality [6,7]. The way to show this consists first in mapping the phononic excitations to cavity photons using laser light driving the red optomechanical sideband. This leads to a two-mode photonic state, where each mode can subsequently be detected with photon counting techniques preceded by displacement operations in phase space. By changing the amplitude and phase of the local displacements, the Bell-Clauser-Horne-Shimony-Holt (Bell-CHSH) [24] inequality can be violated as long as the global detection efficiency is higher than 67%. While several experiments have been realized combining cavity optomechanics in the revolved-sideband regime and photon counting [13–15,25], the requirement on the efficiency remains very challenging to meet.

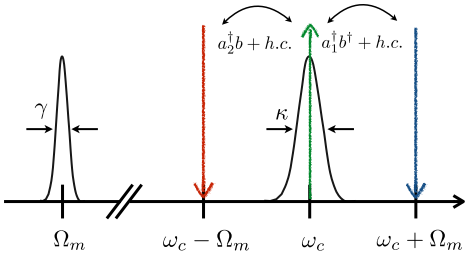

FIG. 1. A cavity optomechanical system is made with a cavity with frequency ω_c and a mechanical oscillator with frequency Ω_m. κ, and γ are the cavity and mechanical decay rates, respectively. We consider the resolved sideband regime where $\Omega_m \gg \kappa$. Starting with a cooled mechanical system, the cavity optomechanical system is first driven by a laser resonant with the blue sideband. Photon-phonon pairs are created by means of an effective squeezing operation $a_1^\dagger b^\dagger + \text{H.c.}$, the bosonic operators a_1 and b corresponding to the cavity photons and mechanical phonons. The quantum nature of the correlations between the cavity photon number and the phonon number can be revealed by applying a laser resonant with the red sideband. This effectively maps the phononic state to a photonic state through a beam splitter interaction $a_2^\dagger b + \text{H.c.}$ The resulting photonic state involving two temporal modes a_1 and a_2 is detected with a photon detector supplemented with a displacement operation in phase space.

Here we propose the first step of an entire research program aiming to violate a Bell inequality with optomechanical systems, that is, we propose a witness for revealing optomechanical entanglement in the same scenario. In opposition to Bell tests (see Ref. [26], Sec. A), our witness is not device independent but assumes a detailed description and correct experimental calibration of measurements. Additional measurements are also taken locally to get information about the photon number distribution. This allows us to relax the requirement on the detection efficiency, even without any assumptions about the measured state. A feasibility study shows that our witness can readily be used to reveal optomechanical entanglement in present-day experiments with photonic crystal nanobeam resonators.

Temporal evolution of the cavity field and mechanical system.—Let us recall the physics of optomechanical systems in the resolved sideband and weak coupling regime, which has been presented, at least partially, in various Refs. [6,19,29–31]. We consider the optical and mechanical modes of an optomechanical cavity with frequencies ω_c and Ω_m, respectively. The bosonic operators associated to the optical mode are called a and $a^\dagger$ while we use b and $b^\dagger$ for the mechanical mode. g_0 denotes the bare optomechanical coupling rate, κ and γ the cavity and mechanical decay rates. The cavity optomechanical system is laser driven on the lower or upper mechanical sideband with corresponding frequencies $\omega_\pm = \omega_c \pm \Omega_m$. The laser powers are labeled $P_\pm$, respectively. The full Hamiltonian includes the uncoupled cavity and mechanical systems $\mathcal{H}_0 = \hbar\omega_c a^\dagger a + \hbar\Omega_m b^\dagger b$, the optomechanical coupling $-\hbar g_0 a^\dagger a(b^\dagger + b)$, and the coupling between the cavity mode and the driving laser $\hbar(s_\pm^* e^{i\omega_\pm t} a + s_\pm e^{-i\omega_\pm t} a^\dagger)$ with $|s_\pm| = \sqrt{\kappa P_\pm/\hbar\omega_\pm}$. In the interaction picture with respect to $\mathcal{H}_0$ and focusing on the weak coupling $g_0 \ll \kappa$ and resolved-sideband $\kappa \ll \Omega_m$ regimes, the temporal evolution is given by a set of effective Langevin equations [19]

$$\frac{da}{dt} = \frac{i}{\hbar}[\mathcal{H}_\pm, a] - \frac{\kappa}{2}a + \sqrt{\kappa}a_{\text{in}}, \qquad \frac{db}{dt} = \frac{i}{\hbar}[\mathcal{H}_\pm, b], \quad (1)$$

with $\mathcal{H}_+ = -\hbar g_0\sqrt{n_+}(a^\dagger b^\dagger + \text{H.c.})$ and $\mathcal{H}_- = -\hbar g_0\sqrt{n_-}(a^\dagger b + \text{H.c.})$ for a blue and red detuned driving laser, respectively. $n_\pm = (|s_\pm|^2)/(\Omega_m^2 + \kappa^2/4)$ is the intracavity photon number. a_{in} is the noise entering the cavity. The mechanical decay and corresponding thermal noise are neglected, that is, we focus on timescales smaller than the thermal decoherence time of the mechanical system $(\hbar\Omega_m/k_B T_{\text{bath}}\gamma)$, where $k_B T_{\text{bath}}$ is the Boltzmann energy.

Phonon-photon correlations in the resolved sideband regime.—Let us first focus on the initial step where a laser drives the upper sideband. We use the subscript 1 for the cavity field operators corresponding to this initial step. We proceed with an adiabatic elimination of the cavity mode $(da_1/dt) = 0$ that is, we consider a temporal evolution which is long compared to κ^{-1}. Together with the input and ouput relation, that is, $a_{1,\text{out}} = -a_{1,\text{in}} + \sqrt{\kappa}a_1$, we get

$$a_{1,\text{out}} = a_{1,\text{in}} + i\sqrt{2\tilde{g}_+}b^\dagger, \quad \frac{db_1}{dt} = \tilde{g}_+ b + i\sqrt{2\tilde{g}_+}a_{1,\text{in}}^\dagger, \quad (2)$$

where $\tilde{g}_+ = (2g_0^2 n_+/\kappa)$. Integrating the previous equations and introducing the temporal modes $A_{1,(\text{in/out})}(t) = \sqrt{(2\tilde{g}_+/\pm 1 \mp e^{\mp 2\tilde{g}_+ t})}\int_0^t dt' e^{\mp\tilde{g}_+ t'} a_{1,(\text{in/out})}(t')$ [29] leads to $A_{1,\text{out}}(t) = e^{\tilde{g}_+ t}A_{1,\text{in}}(t) + i\sqrt{e^{2\tilde{g}_+ t} - 1}b^\dagger(0)$, $b(t) = e^{\tilde{g}_+ t}b(0) + i\sqrt{e^{2\tilde{g}_+ t} - 1}A_{1,\text{in}}^\dagger(t)$. These two solutions can be written as $A_{1,\text{out}}(t) = U_1^\dagger(t)A_{1,\text{in}}U_1(t)$ and $b(t) = U_1^\dagger(t)b(0)U_1(t)$ where the propagator $U_1(t)$ is given by

$$U_1(t) = e^{i\sqrt{1-e^{-2\tilde{g}_+ t}}A_{1,\text{in}}^\dagger b^\dagger} e^{-\tilde{g}_+ t(A_{1,\text{in}}^\dagger A_{1,\text{in}} + b^\dagger b + 1)} e^{i\sqrt{1-e^{-2\tilde{g}_+ t}}A_{1,\text{in}} b}. \quad (3)$$

When $U_1(t)$ is applied on the vacuum, phonon-photon pairs are created where the phonon number equals the photon number, each of them following a thermal distribution with mean excitation number $e^{2\tilde{g}_+ t} - 1$. These correlations between the phonon and photon numbers are strong enough to violate a Bell inequality, cf. below.

Phonon-photon correlations as the basis for a Bell inequality violation.—Consider the case where a laser drives the lower sideband. We use the subscript 2 for the cavity field operators corresponding to this second step.

Following the line of thought developed in the previous paragraph while introducing $\tilde{g}_- = (2g_0^2 n_-/\kappa)$, we can show that the cavity field and photon operators evolve according to the propagator [6,19]

$$U_2(t) = e^{i\sqrt{e^{2\tilde{g}_- t}-1}A_{2,\mathrm{in}}b^\dagger} e^{-\tilde{g}_- t(A_{2,\mathrm{in}}^\dagger A_{2,\mathrm{in}} - b^\dagger b)} e^{i\sqrt{e^{2\tilde{g}_- t}-1}A_{2,\mathrm{in}}^\dagger b}. \quad (4)$$

This corresponds to a beam splitter-type evolution, performing a conversion between the phononic and photonic modes with probability $1 - e^{-2\tilde{g}_- t}$. In the limit $\tilde{g}_- t \to \infty$, the phononic mode is perfectly mapped to the photonic mode $A_{2,\mathrm{out}}$ and the phonon-photon correlations created in the first step are mapped to two temporal photonic modes $A_{1,\mathrm{out}}$ and $A_{2,\mathrm{out}}$. If both the cavity and mechanical system are in the vacuum before the laser drive, these two photonic temporal modes are described by a vacuum squeezed state $U_2(t)^{\tilde{g}_- t\to\infty} U_1(T_1)|0\rangle = e^{-\tilde{g}_+ T_1} e^{-\sqrt{1-e^{-2\tilde{g}_+ T_1}} A_{1,\mathrm{out}}^\dagger A_{2,\mathrm{out}}^\dagger}|00\rangle$. References [32–34] have shown that such a state violates the Bell-CHSH inequality when it is measured with photon detection preceded by a displacement operation in phase space, the phase and amplitude being used to change the measurement setting. Reference [6] showed that a minimum detection efficiency of ~67% is necessary to observe a violation of the Bell-CHSH inequality. This minimum detection efficiency even increases if the mechanical system is not in its ground state initially [6]. These efficiencies include all the loss from the cavity to the detector and are thus challenging to obtain in practice. We show in the following sections a way around this requirement which consists in replacing the Bell-CHSH inequality by a witness inequality, which assumes a physical description and correct experimental calibration of the measurement devices.

Photon counting preceded by a displacement operation.—We focus on the setup described before, with which a Bell inequality is tested using photon detections preceded by a displacement operation $D(\alpha)$. Before presenting our entanglement witness, we first comment on such a measurement. We consider the realistic case where the photon detector does not resolve the photon number, that is, only two measurement results can be produced at each run. The first result corresponds to "no-detection" and is modelled by a projection on the vacuum $|0\rangle\langle 0|$. The second possible result is a conclusive detection corresponding to the projection into the orthogonal subspace, that is, $\mathbb{1} - |0\rangle\langle 0|$. If we attribute the outcome $+1$ to a no-detection and -1 to a conclusive detection, the observable including the displacement operation is given by $\sigma_\alpha = D(\alpha)^\dagger(2|0\rangle\langle 0| - \mathbb{1})D(\alpha)$. In the qubit subspace $\{|0\rangle, |1\rangle\}$, σ_0 corresponds exactly to the Pauli matrix σ_z, that is, the outcome $+1$ (-1) is associated to a projection into the state $|0\rangle$ $(|1\rangle)$. When α increases, the positive-operator valued measure (POVM) elements associated to outcomes ± 1 get closer to projections in the x-y plane of the Bloch sphere having $|0\rangle$ and $|1\rangle$ as north and south poles, respectively [35]. For $\alpha = 1$, these POVM elements are projections along nonunit vectors pointing in the x direction, while for $\alpha = i$, they are noisy projections along the y direction. This means that photon detection supplemented by a displacement operation performs noisy measurements in the qubit space $\{|0\rangle, |1\rangle\}$ whose direction in the Bloch sphere can be chosen by controlling the amplitude and phase of the displacement.

Witnessing phonon-photon correlations in a qubit subspace.—In order to clarify on how to witness entanglement in two-mode squeezed vacuum using local observables σ_α, we consider the state projection in the qubit subspace $1/\sqrt{1+|\epsilon|^2}(|00\rangle + \epsilon|11\rangle)$. The sum of relevant coherence terms $|00\rangle\langle 11| + |11\rangle\langle 00|$ can be measured using the ideal observable $M_{\mathrm{ideal}} = (1/2\pi)\int(\cos\varphi\sigma_x + \sin\varphi\sigma_y)\otimes(\cos\varphi\sigma_x - \sin\varphi\sigma_y)d\varphi$. Since separable states are (i) non-negative states and (ii) they stay non-negative under partial transposition [36,37], these coherence terms are upper bounded by $2\min\{\sqrt{p(0,0)p(1,1)}, \sqrt{p(0,1)p(1,0)}\}$ for two-qubit separable states. $p(i,j)$ is the probability for having i photons in mode A_1 and j photons in A_2. Any state ρ such that $\mathrm{Tr}(M_{\mathrm{ideal}}\rho) > 2\min\{\sqrt{p(0,0)p(1,1)}, \sqrt{p(0,1)p(1,0)}\}$ is thus entangled. Since $p(0,1) = p(1,0) = 0$ and $\mathrm{Tr}(M_{\mathrm{ideal}}\rho) = 2\mathrm{Re}(\epsilon)/(1+|\epsilon|^2)$ for a state of the form $1/\sqrt{1+|\epsilon|^2}(|00\rangle + \epsilon|11\rangle)$, the witness observable M_{ideal} has the potential to detect entanglement in two-mode squeezed vacuum, in the experimentally relevant regime where the squeezing is small $2\tilde{g}_+ T_1 \ll 1$, that is, when the two-mode squeezed vacuum is well approximated by its projection in the qubit subspace. This suggests that a relevant witness observable for our purpose is

$$M(\alpha,\beta) = \int_0^{2\pi} \frac{d\phi}{2\pi} \mathbf{U}_\phi^\dagger(\sigma_\alpha \otimes \sigma_\beta)\mathbf{U}_\phi, \quad (5)$$

where the unitary $\mathbf{U}_\phi = e^{i\phi A_1^\dagger A_1} \otimes e^{-i\phi A_2^\dagger A_2}$ is used to randomize the phase of displacements through the averaging over ϕ. Note that in Eq. (5), the amplitude of displacements is a free parameter. Further note that we are interested in revealing entanglement at the level of the detection. The nonunit efficiency of the detector can be

TABLE I. The witness observable here proposed is $M(\alpha,\beta)$ (see Eq. (5). The maximum value it takes on separable states is bounded by $S^\star(\alpha,\beta)$ (see [26] Eq. (9)), that is, $\max_{\rho_{\mathrm{sep}}}\mathrm{Tr}(M(\alpha,\beta)\rho_{\mathrm{sep}}) \le S^\star(\alpha,\beta)$. The observed value in an actual experiment is Q. $Q - S^\star \le 0$ thus holds for all separable state and a violation of this inequality certifies entanglement.

Witness observable	Maximum value for separable states	Observed value	Witness Inequality
$M(\alpha,\beta)$	$\le S^\star(\alpha,\beta)$	$Q(\alpha,\beta)$	$Q - S^\star \le 0$

seen as a loss operating on the state; i.e., the beam splitter modeling the detector inefficiency acts before the displacement operation whose amplitude is changed accordingly; see Ref. [26] Sec. B. This allows us to derive a witness observable with unit efficiency detection and to include the detector efficiency at the end; see Ref. [26] Sec. C.

Witnessing phonon-photon correlations without dimensionality restriction.—Using the property that separable states stay positive under partial transposition, we show in Ref. [26] Sec. C that the maximum mean value $M(\alpha,\beta)$ can take if the measured state is separable is such that

$$\max_{\rho_{\mathrm{sep}}}[M(\alpha,\beta)\rho_{\mathrm{sep}}] \leq S^{\star}(\alpha,\beta), \tag{6}$$

where $S^{\star}(\alpha,\beta)$ depends on some joint probabilities $p(i,j)$ for having i photons in mode A_1 and j photons in A_2 and the marginal probabilities $p(n_{A_1}\geq 2)$ and $p(n_{A_2}\geq 2)$ to have strictly more than one photon in mode A_1 and A_2, respectively. These probabilities are bounded in two steps in practice. In the first step, the probability $P(\pm 1 \pm 1|00)$ and $P(\pm 1 \mp 1)|00)$ of having ± 1 for the outcomes of the detection of mode A_1 and A_2 without displacement ($\alpha=\beta=0$) are measured. They provide the following upper bounds $p(0,0)\leq P(+1+1|0,0)$, $p(0,1)\leq P(+1-1|0,0)$, $p(1,0)\leq P(-1+1|0,0)$ and $p(1,1)\leq P(-1-1|0,0)$. Second, two detectors after a 50/50 beam splitter are used to measure the probability to get a twofold coincidence $P_{\mathrm{c}}(A_{1/2})$ after the beam splitter for both mode A_1 and A_2. These coincidence probabilities provide the upper bounds on the missing elements, that is, $p(2,1)\leq p(n_{A_1}\geq 2)\leq 2P_{\mathrm{c}}(A_1)$ and $p(1,2)\leq p(n_{A_2}\geq 2)\leq 2P_{\mathrm{c}}(A_2)$. This results in a bound $S^{\star}(\alpha,\beta)$ whose value depends on the local displacement amplitudes α and β. Finally, the mean value $Q(\alpha,\beta)$ of $M(\alpha,\beta)$ is measured by evaluating $P(+1+1|\alpha,\beta)$, $P(+1|\alpha)$ and $P(+1|\beta)$, that is

$$Q(\alpha,\beta)=1-2P(+1|\alpha)-2P(+1|\beta)+4P(+1+1|\alpha,\beta). \tag{7}$$

If there is a value for the couple α, β such that $Q(\alpha,\beta)-S^{\star}(\alpha,\beta)>0$, we deduce that the photonic modes A_1 and A_2 are entangled. Since the state describing A_2 is obtained from a local operation on the phononic state, $Q(\alpha,\beta)-S^{\star}(\alpha,\beta)>0$ also certifies photon-phonon entanglement. See Table I for a clarification of the quantities involved.

Results.—We focus on the statistics that would be collected in modes A_1 and A_2 if the upper sideband is laser driven during the time interval T_1 and the lower sideband is subsequently driven for a duration T_2. The value $Q-S^{\star}$ that would be obtained in this case when optimizing the arguments of local displacements α, β and the amount of initial squeezing $\bar{g}_{+}T_1$ is shown in Fig. 2 as a function of the phonon-photon conversion efficiency $T=1-e^{-2\bar{g}_{-}T_2}$ for various overall detection efficiency η; see Ref. [26], Sec. D for more details. Figure 2 shows a very favorable robustness of our witness to inefficiencies. We stress that the efficiency η represents the global detection efficiency, including all the loss from the cavity optomechanical system to the detector (except the phonon-photon conversion efficiency for mode A_2 specified by T). We here assumed that the mechanical system is prepared in its ground state. In the more realistic case where the initial mechanical cooling leads to a mechanical thermal state with nonzero mean occupation number n_0, the results presented in Fig. 2 for $\eta=0.3$, for example, are essentially unchanged as long as $n_0\leq 0.1$ and substantial differences between Q and $S^{\star}$ can still be observed for $n_0\sim 1$; see Ref. [26], Sec. D. Note that in case where the marginal probabilities $p(n_{A_1}\geq 2)$ and $p(n_{A_2}\geq 2)$ are negligible, the observed quantum correlations are ultimately limited by single phonon coherence time, which could be upper bounded by recording $Q-S^{\star}$ for various delays between the pulses resonant with the upper and lower sidebands.

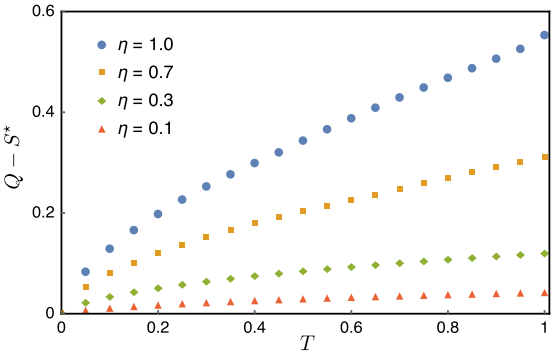

FIG. 2. Difference $Q-S^{\star}$ between the mean value of our witness observable $M(\alpha,\beta)$ that would be observed between the optical modes A_1 and A_2 and the maximum value that would be obtained with a separable state as a function of the phonon-photon conversion efficiency $T=1-e^{-2\bar{g}_{-}T_2}$ for various overall detection efficiencies η, optimized over displacement choices α, β and the amount of initial squeezing $\bar{g}_{+}T_1$ which is kept small. $Q-S^{\star}>0$ witnesses entanglement.

Feasibility study.—To illustrate the feasibility, we focus on a photonic crystal nanobeam resonator [11,38,39] which distinguishes itself by a high mechanical frequency $\Omega_m/2\pi=5.25$ GHz [14]. Together with the cavity decay rate $\kappa/2\pi=846$ MHz [14] and the optomechanical coupling rate $g_0/2\pi=869$ kHz [14], this resonator is placed in the deep resolved sideband and weak coupling regimes. To control the initial number of excitations, we consider the use of a dilution refrigerator, which can bring the mean phonon number down to $n_0\sim 0.2$. Furthermore, to prevent decoherence of the phonon state we also consider pulse durations much smaller than the typical decoherence time of the oscillator, which is of the order of 10 μs [38,40]. Considering a global detection efficiency $\eta=10\%$, an initial mean phonon number of $n_0=0.2$ and state-swap

efficiency of $T = 30\%$ which can be realized using a pulse laser resonant with the red sideband with a duration of $T_2 = 50$ ns and intracavity photon number $n_- \approx 318$, we expect to conclude about the presence of entanglement (violation of the inequality $Q - S^\star \leq 0$ by 3 standard deviations) within 750 000 experimental runs, see Ref. [26], Sec. E. This involves the creation of a phonon-photon state using a blue-detuned pulse of duration $T_1 = 50$ ns and $n_+ \approx 298$, and the choice of displacement amplitudes $\alpha = -\beta = 2.63$. Given the experiments reported in Refs. [14,15], we conclude that our scheme appears feasible with currently available technologies.

Conclusion.—We have presented a witness tailored for the detection of optomechanical entanglement using photon countings. Our proposal is based on the measurement of single and twofold coincidence counts. It requires basic phase stabilizations and is robust to loss, see Ref. [26], Sec. F. This makes us confident that it can be used in present day experiments with photonic crystal nanobeam resonators to show directly optomechanical entanglement. Following Ref. [7], it also applies straightforwardly to electromechanical systems where it could be used to demonstrate electromechanical entanglement with non-Gaussian resources. Beyond opto- and electromechanics, our witness could find applications in nanophotonics to measure the coherence time of single phonons in any Raman-active vibrational modes using two-color pump-probe Raman scattering measurements [41]. It could also be used to detect atom-photon entanglement directly in spontaneous Raman protocols, e.g., to certify the proper functioning of photon pair sources relevant for long-distance quantum communications [42,43].

We thank C. Galland and B. Gouraud for enlightening discussions. This work was supported by the Swiss National Science Foundation (SNSF), through the Grants No. PP00P2-150579 and No. PP00P2-179109. We also acknowledge the Army Research Laboratory Center for Distributed Quantum Information via the project SciNet.

[1] J. S. Bell, Physics **1**, 195 (1964).
[2] B. Hensen *et al.* Nature (London) **526**, 682 (2015).
[3] W. Rosenfeld, D. Burchardt, R. Garthoff, K. Redeker, N. Ortegel, M. Rau, and H. Weinfurter, Phys. Rev. Lett. **119**, 010402 (2017).
[4] M. Giustina *et al.* Phys. Rev. Lett. **115**, 250401 (2015).
[5] L. K. Shalm *et al.* Phys. Rev. Lett. **115**, 250402 (2015).
[6] V. C. Vivoli, T. Barnea, C. Galland, and N. Sangouard, Phys. Rev. Lett. **116**, 070405 (2016).
[7] S. G. Hofer, K. W. Lehnert, and K. Hammerer, Phys. Rev. Lett. **116**, 070406 (2016).
[8] M. Asjad, J. Manninen, E. Selenius, R. Ojajarvi, P. Kuusela, and F. Massel, arXiv:1803.00331.
[9] A. D. O'Connell, M. Hofheinz, M. Ansmann, R. C. Bialczak, M. Lenander, E. Lucero, M. Neeley, D. Sank, H. Wang, M. Weides, J. Wenner, J. M. Martinis, and A. N. Cleland, Nature (London) **464**, 697 (2010).
[10] J. D. Teufel, T. Donner, D. Li, J. W. Harlow, M. S. Allman, K. Cicak, A. J. Sirois, J. D. Whittaker, K. W. Lehnert, and R. W. Simmonds, Nature (London) **475**, 359 (2011).
[11] J. Chan, T. P. M. Alegre, A. H. Safavi-Naeini, J. T. Hill, A. Krause, S. Groblacher, M. Aspelmeyer, and O. Painter, Nature (London) **478**, 89 (2011).
[12] T. A. Palomaki, J. D. Teufel, R. W. Simmonds, and K. W. Lehnert, Science **342**, 710 (2013).
[13] R. Riedinger, S. Hong, R. A. Norte, J. A. Slater, J. Shang, A. G. Krause, V. Anant, M. Aspelmeyer, and S. Groblacher, Nature (London) **530**, 313 (2016).
[14] S. Hong, R. Riedinger, I. Marinkovic, A. Wallucks, S. G. Hofer, R. A. Norte, M. Aspelmeyer, and S. Groblacher, Science **358**, 203 (2017).
[15] R. Riedinger, A. Wallucks, I. Marinkovic, C. Loschnauer, M. Aspelmeyer, S. Hong, and S. Groblacher, Nature (London) **556**, 473 (2018).
[16] C. F. Ockeloen-Korppi, E. Damskagg, J.-M. Pirkkalainen, A. A. Clerk, F. Massel, M. J. Woolley, and M. A. Sillanpaa, Nature (London) **556**, 478 (2018).
[17] H. J. Kimble, Nature (London) **453**, 1023 (2008).
[18] K. Borkje, A. Nunnenkamp, and S. M. Girvin, Phys. Rev. Lett. **107**, 123601 (2011).
[19] C. Galland, N. Sangouard, N. Piro, N. Gisin, and T. J. Kippenberg, Phys. Rev. Lett. **112**, 143602 (2014).
[20] V. Scarani, Acta Phys. Slovaca **62**, 347 (2012).
[21] A. Acin, N. Gisin, and L. Masanes, Phys. Rev. Lett. **97**, 120405 (2006).
[22] L. Lydersen, C. Wiechers, C. Wittmann, D. Elser, J. Skaar, and V. Makarov, Nat. Photonics **4**, 686 (2010).
[23] P. Sekatski, J.-D. Bancal, S. Wagner, and N. Sangouard, arXiv: 1802.02170.
[24] J. F. Clauser, M. A. Horne, A. Shimony, and R. A. Holt, Phys. Rev. Lett. **23**, 880 (1969).
[25] J. D. Cohen, S. M. Meenehan, G. S. MacCabe, S. Groblacher, A. H. Safavi-Naeini, F. Marsili, M. D. Shaw, and O. Painter, Nature (London) **520**, 522 (2015).
[26] See Supplemental Material at http://link.aps.org/supplemental/10.1103/PhysRevLett.121.023602 for further details, which includes Refs. [27,28]. Section A explains the connection between Bell tests and device independent conclusions, and how our witness yields a state independent conclusion. Sections B–E explain technical details for our calculations and statistical analysis. Section F has a summary on how our witness can be implemented.
[27] R. Schmied, J.-D. Bancal, B. Allard, M. Fadel, V. Scarani, P. Treutlein, and N. Sangouard, Science **352**, 441 (2016).
[28] N. Brunner, D. Cavalcanti, S. Pironio, V. Scarani, and S. Wehner, Rev. Mod. Phys. **86**, 419 (2014).
[29] S. G. Hofer, W. Wieczorek, M. Aspelmeyer, and K. Hammerer, Phys. Rev. A **84**, 052327 (2011).
[30] M. R. Vanner, M. Aspelmeyer, and M. S. Kim, Phys. Rev. Lett. **110**, 010504 (2013).
[31] M. Aspelmeyer, S. Groeblacher, K. Hammerer, and N. Kiesel, J. Opt. Soc. Am. B **27**, A189 (2010).
[32] A. Kuzmich, I. A. Walmsley, and L. Mandel, Phys. Rev. Lett. **85**, 1349 (2000).

[33] S.-W. Lee, H. Jeong, and D. Jaksch, Phys. Rev. A **80**, 022104 (2009).
[34] J. B. Brask and R. Chaves, Phys. Rev. A **86**, 010103(R) (2012).
[35] V. Caprara Vivoli, P. Sekatski, J.-D. Bancal, C. C. W. Lim, A. Martin, R. T. Thew, H. Zbinden, N. Gisin, and N. Sangouard, New J. Phys. **17**, 023023 (2015).
[36] A. Peres, Phys. Rev. Lett. **77**, 1413 (1996).
[37] M. Horodecki, P. Horodecki, and R. Horodecki, Phys. Lett. A **223**, 1 (1996).
[38] J. Chan, A. H. Safavi-Naeini, J. T. Hill, S. Meenehan, and O. Painter, Appl. Phys. Lett. **101**, 081115 (2012).
[39] E. Kuramochi, H. Taniyama, T. Tanabe, K. Kawasaki, Y.-G. Roh, and M. Notomi, Opt. Express **18**, 15859 (2010).
[40] X. Sun, X. Zhang, C. Schuck, and H. X. Tang, Sci. Rep. **3**, 1436 (2013).
[41] M. D. Anderson, S. T. Velez, K. Seibold, H. Flayac, V. Savona, N. Sangouard, and C. Galland, Phys. Rev. Lett. **120**, 233601 (2018).
[42] L.-M. Duan, M. D. Lukin, J. I. Cirac, and P. Zoller, Nature (London) **414**, 413 (2001).
[43] N. Sangouard, C. Simon, H. de Riedmatten, and N. Gisin, Rev. Mod. Phys. **83**, 33 (2011).

Supplemental Material : Witnessing Opto-Mechanical Entanglement with Photon-Counting

Melvyn Ho,[1] Enky Oudot,[1] Jean-Daniel Bancal,[1] and Nicolas Sangouard[1]
[1] *Quantum Optics Theory Group, University of Basel, Klingelbergstrasse 82, 4056 Basel, Switzerland*
(Dated: June 14, 2018)

A-BELL TESTS AND DEVICE-INDEPENDENT APPROACHES TO QUANTUM INFORMATION

The purpose of this first section is to clarify on Bell tests and on the meaning of device-independent approaches to quantum information. For simplicity, let us consider the simplest Bell test with two parties, each having a measurement device with two possible questions and two possible results for each question. At each run, each partie receives a particle. He/she chooses a question and records the result. The experiment is then repeated so that the parties can estimate the probability distribution of results given the questions. In practice, the questions correspond to measurement settings and the results to clicks on detectors. But there is no need to know the internal functioning of the particle source and measurement devices. No physical model of these devices is needed. A Bell inequality is simply an inequality that is satisfied by probability distributions coming from a local causal theory such as classical theory. A violation of such an inequality thus shows the limit of classical physics as complete description of the physical reality. A loophole-free Bell inequality violation has been reported in experiments with two photons or two atoms and proposals have been made for a loophole-free Bell test with mechanical devices, see e.g. [1].

Within the quantum framework, i.e. if one assumes that the source and the measurements admit a quantum description, a Bell inequality violation witnesses non-separability, that is, the measured particles are described by a non-separable state. In particular, a Bell inequality witnesses a strong form of non-separability that is called Bell correlation [2]. Interestingly, the conclusion about the presence of non-classical correlations between the measured particles hold independently of the details and imperfections of the source and measurements. No assumption is needed about the Hilbert space dimension or the proper calibration of measurements [3]. This refers to a device-independent certification of non-separable states.

Note that a device-independent certification is challenging as it relies on a proper Bell inequality violation, without the detection loophole. This is only possible if the overall detection efficiency is high, typically $\sim 67\%$ for the proposal of Ref. [1]. Here, we propose a witness for revealing opto-mechanical entanglement in the same scenario of Ref. [1]. In opposition to a fully device-independent certification, our witness is based on a detailed description and correct experimental calibration of measurements, that is, our witness relies on photon counting preceded by displacement operation with well defined amplitudes, c.f. Eq. 5 of the main text. Together with measurements on the photon numbers in each mode, this allows us to relax the requirement on the detection efficiency, even without any assumptions about the Hilbert space dimension of the measured state. Our witness is not fully device-independent but can be seen as a state-independent certification of entanglement.

While the violation of a Bell inequality reveals Bell-correlations, that is, correlations that are strong enough to violate a Bell inequality, our witness detect entanglement, which is a weaker form of quantum correlations. Indeed, there are entangled states which do not violate a Bell inequality but there is no Bell-correlated state that is separable [4]. We emphasize, however, that the same experimental setup can be used to test a Bell inequality and a violation of the Bell-CHSH inequality in particular can be observed if the overall detection efficiency is higher than $\sim 67\%$ hence witnessing Bell correlations in a fully-device independent way.

Finally, it is worth mentioning that the detailed experimental descriptions of the optomechanical system available in the main text and in the following sections of the Supplemental Material do not prevent a state-independent certification of quantum correlations. They are given to compute the expected values of our witness observables and to conclude about the feasibility of our proposal with existing experiments. Once Q and $S^\star$ will be measured in an actual experiment, it will be possible to conclude about the presence of opto-mechanical entanglement without assumption on the detailed functioning of the opto-mechanical device or about the Hilbert space dimension. This corresponds to a state-independent certification of opto-mechanical entanglement, that is, a first step towards a fully-device independent certifications of Bell-correlations between light and a mechanical system.

B-MODELLING DETECTORS WITH NON-UNIT EFFICIENCIES

The proposed entanglement witness relies on measurements that are realized with non-photon resolving detectors preceded by displacement operations in phase space. As explained in the main text, we assign the outcome $+1$ to a no-detection and -1 to a conclusive detection. Given a state ρ in the mode corresponding to the bosonic operators A_1 and $A_1^\dagger$, the probability to get the outcome $+1$ using a displacement with argument α is given by

$$P(+1|\alpha) = \mathrm{Tr}\big(D(\alpha)^\dagger|0\rangle\langle 0|D(\alpha)\rho\big)\,. \tag{1}$$

So far, we assumed that the detector has unit efficiency. To model the detector inefficiency, a beamsplitter with transmission $\eta = \cos^2\theta$ can be introduced, that is

$$P(+1|\alpha) = \mathrm{Tr}\Big(D(\alpha)^\dagger U_\theta^\dagger|\bar{0}\rangle\langle\bar{0}|U_\theta D(\alpha)\rho\Big)\,.$$

with $U_{A_1c} = e^{\theta(A_1^\dagger c - A_1 c^\dagger)}$, the auxiliary mode described by c and $c^\dagger$ being initially empty. The state $|\bar{0}\rangle$ corresponds to the projection onto the vacuum for both A_1 and c. Commuting the beamsplitter and displacement operation leads to

$$P(+1|\alpha) = \mathrm{Tr}\Big(D(\sqrt{\eta}\alpha)^\dagger|0\rangle\langle 0|D(\sqrt{\eta}\alpha)U_\theta\rho\otimes|0\rangle\langle 0|U_\theta^\dagger\Big)\,.$$

This means that we can model the detection inefficiency as loss operating on the state that is measured if the amplitude of the displacement operation is changed accordingly. Hence, we consider detectors with unit efficiencies to derive our entanglement witness, and only replace the displacement amplitudes $\alpha \to \sqrt{\eta}\alpha$, $\beta \to \sqrt{\eta}\beta$ at the end to account for the non-unit detection efficiency. Nonetheless, the data collected in the proposed experiment can violate a Bell inequality, hence revealing Bell-correlations, as soon as the global detection efficiency is higher than $\sim 67\%$.

C-MAXIMUM VALUE OF THE WITNESS OBSERVABLE FOR SEPARABLE STATES

Our aim is to bound the value of the witness observable

$$M(\alpha,\beta) = \int_0^{2\pi}\frac{d\phi}{2\pi}\mathbf{U}_\phi^\dagger(\mathfrak{o}_\alpha\otimes\mathfrak{o}_\beta)\mathbf{U}_\phi \tag{2}$$

with

$$\mathbf{U}_\phi = U_\phi^{A_1}\otimes U_{-\phi}^{A_2} = e^{i\phi A_1^\dagger A_1}\otimes e^{-i\phi A_2^\dagger A_2}$$

when applied on separable states. We first use the fact that the trace is cyclic. Hence, the phase averaging can be applied on the state, that is

$$\begin{aligned}\mathrm{Tr}(M(\alpha,\beta)\rho) &= \mathrm{Tr}\left(\int_0^{2\pi}\frac{d\phi}{2\pi}(\mathfrak{o}_\alpha\otimes\mathfrak{o}_\beta)\mathbf{U}_\phi\rho\mathbf{U}_\phi^\dagger\right)\\ &= \int_0^{2\pi}\frac{d\phi}{2\pi}\mathrm{Tr}\Big((\mathfrak{o}_\alpha\otimes\mathfrak{o}_\beta)\mathbf{U}_\phi\rho\mathbf{U}_\phi^\dagger\Big)\,,\end{aligned}$$

where the last equality holds by linearity of the trace. Next, we recognise that the expectation value can be obtained from the partial transposed quantities if ρ is separable, that is, for $\rho^{\mathrm{sep}} = p_i\sum_i\rho_{A_1}^i\otimes\rho_{A_2}^i$, we have

$$\begin{aligned}\mathrm{Tr}(M(\alpha,\beta)\rho^{\mathrm{sep}}) = \textstyle\int_0^{2\pi}\frac{d\phi}{2\pi}\sum_i p_i\mathrm{Tr}\Big(\mathfrak{o}_\alpha^T(U_\phi^{A_1}\rho_{A_1}^i U_\phi^{A_1\dagger})^T\Big)\\ \times\mathrm{Tr}\Big(\mathfrak{o}_\beta U_{-\phi}^{A_2}\rho_{A_2}^i U_{-\phi}^{A_2\dagger}\Big)\end{aligned} \tag{3}$$

where T indicates the transpose in the photon number basis. This can be shown in the following way

$$\begin{aligned}&\mathrm{Tr}\Big((\mathfrak{o}_\alpha\otimes\mathfrak{o}_\beta)\mathbf{U}_\phi\rho^{\mathrm{sep}}\mathbf{U}_\phi^\dagger\Big)\\ &= \mathrm{Tr}\left((\mathfrak{o}_\alpha\otimes\mathfrak{o}_\beta)\mathbf{U}_\phi\sum_i p_i\rho_{A_2}^i\otimes\rho_{A_1}^i\mathbf{U}_\phi^\dagger\right)\\ &= \sum_i p_i\mathrm{Tr}\Big(\mathfrak{o}_\alpha U_\phi^{A_1}\rho_{A_1}^i U_\phi^{A_1\dagger}\Big)\mathrm{Tr}\Big(\mathfrak{o}_\beta U_{-\phi}^{A_2}\rho_{A_2}^i U_{-\phi}^{A_2\dagger}\Big)\\ &= \sum_i p_i\mathrm{Tr}\Big(\mathfrak{o}_\alpha^T(U_\phi^{A_1}\rho_{A_1}^i U_\phi^{A_1\dagger})^T\Big)\mathrm{Tr}\Big(\mathfrak{o}_\beta U_{-\phi}^{A_2}\rho_{A_2}^i U_{-\phi}^{A_2\dagger}\Big)\,.\end{aligned}$$

The previous expression can be further simplified using the properties of the transpose, that is

$$\begin{aligned}&\mathrm{Tr}\Big((\mathfrak{o}_\alpha\otimes\mathfrak{o}_\beta)\mathbf{U}_\phi\rho^{\mathrm{sep}}\mathbf{U}_\phi^\dagger\Big)\\ &= \sum_i p_i\mathrm{Tr}\Big(\mathfrak{o}_\alpha^T(U_\phi^{A_1\dagger})^T\rho_{A_1}^{i,T}(U_\phi^{A_1})^T\Big)\mathrm{Tr}\Big(\mathfrak{o}_\beta U_{-\phi}^{A_2}\rho_{A_2}^i U_{-\phi}^{A_2\dagger}\Big)\\ &= \sum_i p_i\mathrm{Tr}\Big(\mathfrak{o}_\alpha^T U_{-\phi}^{A_1}\rho_{A_1}^{i,T}U_{-\phi}^{A_1\dagger}\Big)\mathrm{Tr}\Big(\mathfrak{o}_\beta U_{-\phi}^{A_2}\rho_{A_2}^i U_{-\phi}^{A_2\dagger}\Big)\,.\end{aligned}$$

Further note that $\mathfrak{o}_\alpha^T = D(\alpha^*)^\dagger\,(2|0\rangle\langle 0| - \mathbb{1})\,D(\alpha^*) = \mathfrak{o}_{\alpha^*}$. Hence,

$$\begin{aligned}&\mathrm{Tr}\Big((\mathfrak{o}_\alpha\otimes\mathfrak{o}_\beta)\mathbf{U}_\phi\rho^{\mathrm{sep}}\mathbf{U}_\phi^\dagger\Big)\\ &= \sum_i p_i\mathrm{Tr}\Big(\mathfrak{o}_{\alpha^*}U_{-\phi}^{A_1}\rho_{A_1}^{i,T}U_{-\phi}^{A_1\dagger}\Big)\mathrm{Tr}\Big(\mathfrak{o}_\beta U_{-\phi}^{A_2}\rho_{A_2}^i U_{-\phi}^{A_2\dagger}\Big)\\ &= \mathrm{Tr}\Big((\mathfrak{o}_{\alpha^*}\otimes\mathfrak{o}_\beta)(U_{-\phi}^{A_1}\otimes U_{-\phi}^{A_2})\rho^{\mathrm{sep},T_{A_1}}(U_{-\phi}^{A_1\dagger}\otimes U_{-\phi}^{A_2\dagger})\Big)\,.\end{aligned}$$

Therefore

$$\mathrm{Tr}(M(\alpha,\beta)\rho^{\mathrm{sep}}) = \mathrm{Tr}\Big((\mathfrak{o}_{\alpha^*}\otimes\mathfrak{o}_\beta)\rho_{\mathrm{rand}}^{\mathrm{sep},T_{A_1}}\Big) \tag{4}$$

where

$$\rho_{\mathrm{rand}}^{\mathrm{sep},T_{A_1}} = \int_0^{2\pi}\frac{d\phi}{2\pi}(U_{-\phi}^{A_1}\otimes U_{-\phi}^{A_2})\rho^{\mathrm{sep},T_{A_1}}(U_{-\phi}^{A_1\dagger}\otimes U_{-\phi}^{A_2\dagger}).$$

Interestingly, $\rho_{\rm rand}^{{\rm sep},T_{A_1}}$ has a simple structure due to the phase randomization. It can be written as

$$\rho_{\rm rand}^{{\rm sep},T_{A_1}} = \left[\begin{array}{cccc|cccc} \checkmark & & & & & & & \\ & \checkmark & \checkmark & & & & & \\ & \checkmark & \checkmark & & & & & \\ & & & \checkmark & \checkmark & \checkmark & & \\ \hline & & & \checkmark & . & . & . & . \\ & & & \checkmark & . & . & . & . \\ & & & & . & . & . & . \end{array}\right] \tag{5}$$

in the basis $\{|00\rangle, |01\rangle, |10\rangle, |11\rangle, |02\rangle, |20\rangle ...\}$. The checkmarks indicate non-zero terms. The upper block on the left corresponds to the projection in the qubit subspace where modes A_1 and A_2 are filled with at most one photon each. Similarly, the lower block on the right corresponds to the projection on a subspace where at least one mode is filled with at least two photons. The anti-diagonal blocks correspond to coherences between these two subspaces. Considering the contributions from each of these blocks separately, we obtain

$$\begin{aligned} {\rm Tr}(M(\alpha,\beta)\rho^{\rm sep}) &= {\rm Tr}\Big((\varpi_{\alpha^*}\otimes\varpi_\beta)\rho_{\rm rand}^{{\rm sep},T_{A_1},n_{A_1}\leq 1\cap n_{A_2}\leq 1}\Big) \\ &+ 2\times{\rm Re}[\langle 11|(\varpi_{\alpha^*}\otimes\varpi_\beta)|02\rangle\langle 02|\rho_{\rm rand}^{{\rm sep},T_{A_1}}|11\rangle] \\ &+ 2\times{\rm Re}[\langle 11|(\varpi_{\alpha^*}\otimes\varpi_\beta)|20\rangle\langle 20|\rho_{\rm rand}^{{\rm sep},T_{A_1}}|11\rangle] \\ &+ {\rm Tr}\Big((\varpi_{\alpha^*}\otimes\varpi_\beta)\rho_{\rm rand}^{{\rm sep},T_{A_1},n_{A_1}\geq 2\cup n_{A_2}\geq 2}\Big) \end{aligned} \tag{6}$$

where $\rho_{\rm rand}^{{\rm sep},T_{A_1},n_{A_1}\leq 1\cap n_{A_2}\leq 1}$ corresponds to the projection in the qubit subspace and $\rho_{\rm rand}^{{\rm sep},T_{A_1},n_{A_1}\geq 2\cup n_{A_2}\geq 2}$ is the state projection in the subspace with two photons or more in at least one of the modes.

Eq. (6) allows us to bound the value of the witness observable in the case where the measured state is separable. The reasoning is the following: Let $p(i,j)$ be the probability of having i photons in A_1 and j photons in A_2 which is a diagonal element of the measured state in the Fock basis. If this state is separable, we have $p(i,j) = \langle i,j|\rho^{\rm sep}|i,j\rangle = \langle i,j|\rho_{\rm rand}^{{\rm sep},T_{A_1}}|i,j\rangle$. Furthermore $|\langle i,j+1|\rho_{\rm rand}^{{\rm sep},T_{A_1}}|i+1,j\rangle| = |\langle i+1,j+1|\rho^{\rm sep}|i,j\rangle| \leq \min\{\sqrt{p(i,j)p(i+1,j+1)}, \sqrt{p(i,j+1)p(i+1,j)}\}$ since both $\rho^{\rm sep}$ and its partial transpose are positive. Similarly, we have $|\langle i+1,j|\rho_{\rm rand}^{{\rm sep},T_{A_1}}|i,j+1\rangle| = |\langle i,j|\rho^{\rm sep}|i+1,j+1\rangle| \leq \min\{\sqrt{p(i,j)p(i+1,j+1)}, \sqrt{p(i+1,j)p(i,j+1)}\}$. This means that the value of the first term in Eq. (6) is bounded by

$$\begin{aligned} &{\rm Tr}\Big((\varpi_{\alpha^*}\otimes\varpi_\beta)\rho_{\rm rand}^{{\rm sep},T_{A_1},n_{A_1}\leq 1\cap n_{A_2}\leq 1}\Big) \\ &= \sum_{i,j=0}^{1}\langle ij|\varpi_{\alpha^*}\otimes\varpi_\beta|ij\rangle p(i,j) \\ &\quad +2\times{\rm Re}[\langle 01|\varpi_{\alpha^*}\otimes\varpi_\beta|10\rangle\langle 00|\rho^{\rm sep}|11\rangle] \\ &\leq \sum_{i,j=0}^{1}\langle ij|\varpi_{\alpha^*}\otimes\varpi_\beta|ij\rangle p(i,j) \\ &\quad +2|\langle 01|\varpi_{\alpha^*}\otimes\varpi_\beta|10\rangle\langle 00|\rho^{\rm sep}|11\rangle| \\ &= \sum_{i,j=0}^{1}\langle ij|\varpi_{\alpha^*}\otimes\varpi_\beta|ij\rangle p(i,j) \\ &\quad +2|\langle 01|\varpi_{\alpha^*}\otimes\varpi_\beta|10\rangle||\langle 00|\rho^{\rm sep}|11\rangle| \\ &\leq \sum_{i,j=0}^{1}\langle ij|\varpi_{\alpha}\otimes\varpi_\beta|ij\rangle p(i,j) \\ &\quad +2|\langle 01|\varpi_{\alpha}\otimes\varpi_\beta|10\rangle| \\ &\qquad \times\min\{\sqrt{p(0,0)p(1,1)}, \sqrt{p(0,1)p(1,0)}\} \end{aligned}$$

where in the last 2 lines, α and β can be considered as real numbers without loss of generality. Similarly, the coherences in the second and third terms are bounded by

$$\begin{aligned} &2\times{\rm Re}[\langle 11|\varpi_{\alpha^*}\otimes\varpi_\beta|02\rangle\langle 02|\rho_{\rm rand}^{{\rm sep},T_{A_1}}|11\rangle] \\ &\leq 2|\langle 11|\varpi_{\alpha}\otimes\varpi_\beta|02\rangle| \\ &\quad\times\min\{\sqrt{p(1,2)p(0,1)}, \sqrt{p(0,2)p(1,1)}\} \end{aligned}$$

and

$$\begin{aligned} &2\times{\rm Re}[\langle 11|\varpi_{\alpha^*}\otimes\varpi_\beta|20\rangle\langle 20|\rho_{\rm rand}^{{\rm sep},T_{A_1}}|11\rangle] \\ &\leq 2|\langle 11|\varpi_{\alpha}\otimes\varpi_\beta|20\rangle| \\ &\quad\times\min\{\sqrt{p(1,0)p(2,1)}, \sqrt{p(2,0)p(1,1)}\}. \end{aligned}$$

As for the last term, we use the fact $\rho_{\rm rand}^{{\rm sep},T_{A_1}}$ is a physical state, so that its projection into the subspace where there is at least two photons in at least one mode is also a physical state with a norm given by ${\rm Tr}\Big(\rho_{\rm rand}^{{\rm sep},T_{A_1},n_{A_1}\geq 2\cup n_{A_2}\geq 2}\Big) = p(n_{A_1}\geq 2\cup n_{A_2}\geq 2)$. The maximum eigenvalue of the observable $(\varpi_{\alpha^*}\otimes\varpi_\beta)$ being one, we conclude that

$$\begin{aligned} &{\rm Tr}\Big((\varpi_{\alpha^*}\otimes\varpi_\beta)\rho_{\rm rand}^{{\rm sep},T_{A_1},n_{A_1}\geq 2\cup n_{A_2}\geq 2}\Big) \\ &\leq p(n_{A_1}\geq 2) + p(n_{A_2}\geq 2). \end{aligned} \tag{7}$$

Hence, a bound on the maximum mean value $S^\star(\alpha,\beta)$ that $M(\alpha,\beta)$ can take if the measured state is separable

$$\max_{\rho_{\rm sep}}({\rm Tr}(M(\alpha,\beta)\rho_{\rm sep})) \leq S^\star(\alpha,\beta) \tag{8}$$

can be obtained by upper bounding some joint probabilities $p(i,j)$ for having i photons in mode A_1 and j

photons in A_2 and the marginal probabilities $p(n_{A_1} \geq 2)$ and $p(n_{A_2} \geq 2)$ to have strictly more than one photon in mode A_1 and A_2 respectively.

These probabilities can be bounded experimentally in two steps. In the first step, the probabilities $P(\pm 1 \pm 1|00)$ and $P(\mp 1 \mp 1|00)$ of having outcomes ± 1 for the measurement of mode A_1 and A_2 without displacement ($\alpha = \beta = 0$) are determined. They provide the following upper bounds

$$p(0,0) \leq P(+1+1|0,0), \quad p(0,1) \leq P(+1-1|0,0),$$
$$p(1,0) \leq P(-1+1|0,0), \quad p(1,1) \leq P(-1-1|0,0).$$

Second, a measurement similar to an autocorrelation measurement using two detectors after a 50/50 beamsplitter is used to measure the probability to get a twofold coincidence $P_{\rm c}(A_{1/2})$ after the beamsplitter for both mode A_1 and A_2. These coincidence probabilities provide the upper bounds on the missing elements, that is,

$$p(2,1) \leq p(n_{A_1} \geq 2) \leq 2P_{\rm c}(A_1)$$
$$p(1,2) \leq p(n_{A_2} \geq 2) \leq 2P_{\rm c}(A_2).$$

Once the detection efficiency is included, one gets the following upper bound

$$\begin{aligned}
&S^\star(\alpha,\beta)\\
&= \langle 0|\sigma_{\sqrt{\eta}\alpha}|0\rangle\langle 0|\sigma_{\sqrt{\eta}\beta}|0\rangle P(+1+1|0,0)\\
&+ \langle 0|\sigma_{\sqrt{\eta}\alpha}|0\rangle\langle 1|\sigma_{\sqrt{\eta}\beta}|1\rangle P(+1-1|0,0)\\
&+ \langle 1|\sigma_{\sqrt{\eta}\alpha}|1\rangle\langle 0|\sigma_{\sqrt{\eta}\beta}|0\rangle P(-1+1|0,0)\\
&+ \langle 1|\sigma_{\sqrt{\eta}\alpha}|1\rangle\langle 1|\sigma_{\sqrt{\eta}\beta}|1\rangle P(-1-1|0,0)\\
&+ 2|\langle 0|\sigma_{\sqrt{\eta}\alpha}|1\rangle\langle 1|\sigma_{\sqrt{\eta}\beta}|0\rangle|\\
&\quad \times \min\{\sqrt{P(+1+1|0,0)P(-1-1|0,0)},\\
&\qquad \sqrt{P(+1-1|0,0)P(-1+1|0,0)}\}\\
&+ 2\sqrt{2}|\langle 1|\sigma_{\sqrt{\eta}\alpha}|0\rangle\langle 1|\sigma_{\sqrt{\eta}\beta}|2\rangle|\\
&\quad \times \min\{\sqrt{P_c(A_2)P(+1-1|0,0)},\\
&\qquad \sqrt{P_c(A_2)P(-1-1|0,0)}\}\\
&+ 2\sqrt{2}|\langle 1|\sigma_{\sqrt{\eta}\alpha}|2\rangle\langle 1|\sigma_{\sqrt{\eta}\beta}|0\rangle|\\
&\quad \times \min\{\sqrt{P_c(A_1)P(-1+1|0,0)},\\
&\qquad \sqrt{P_c(A_1)P(-1-1|0,0)}\}\\
&+ 2P_c(A_1) + 2P_c(A_2),
\end{aligned} \tag{9}$$

where

$$\langle 0|\sigma_{\sqrt{\eta}\alpha}|0\rangle = -1 + 2e^{-(\sqrt{\eta}\alpha)^2}$$
$$\langle 1|\sigma_{\sqrt{\eta}\alpha}|1\rangle = -1 + 2(\sqrt{\eta}\alpha)^2 e^{-(\sqrt{\eta}\alpha)^2}$$
$$\langle 0|\sigma_{\sqrt{\eta}\alpha}|1\rangle = -2(\sqrt{\eta}\alpha) e^{-(\sqrt{\eta}\alpha)^2}$$
$$\langle 0|\sigma_{\sqrt{\eta}\alpha}|2\rangle = \sqrt{2}(\sqrt{\eta}\alpha)^2 e^{-(\sqrt{\eta}\alpha)^2}$$
$$\langle 1|\sigma_{\sqrt{\eta}\alpha}|2\rangle = -\sqrt{2}(\sqrt{\eta}\alpha)^3 e^{-(\sqrt{\eta}\alpha)^2}$$

In practice, the separable bound is obtained by inserting directly the measured probabilities $P(\pm 1 \pm 1|0,0)$, $P(\mp 1 \pm 1|0,0)$, $P_{\rm c}(A_1)$ and $P_{\rm c}(A_2)$ into the previous expression. Note that there is no need to know the amplitude of the displacement and the detector efficiency separately as only the knowledge of the product $\sqrt{\eta}\alpha$ is needed. This is convenient as $\alpha^2\eta$ can be directly obtained from the click rate on the detector.

Finally, the mean value $Q(\alpha,\beta)$ of $M(\alpha,\beta)$ is measured. If there is a value for the couple α,β such that $Q(\alpha,\beta) - S^\star(\alpha,\beta) > 0$, we deduce that the assumption on separability does not hold, that is, the photonic modes A_1 and A_2 are entangled. Since the state describing A_2 is obtained from a local operation on the phononic state, $Q(\alpha,\beta) - S^\star(\alpha,\beta) > 0$ also certifies entanglement between the photon mode A_1 and the phonon mechanical mode.

D-ESTIMATION OF THE EXPERIMENTAL VALUE OF THE WITNESS OBSERVABLE

We here estimate the mean value of $M(\alpha,\beta)$ that can be obtained in practice, that is, we estimate the value of $Q(\alpha,\beta)$ using a realistic model of the proposed experiment. We consider the case where the mechanical oscillator is not exactly prepared in its ground state at the beginning of the experiment but has a main thermal excitation n_0. The corresponding state can be written as a mixture of coherent states $|\gamma\rangle$, that is

$$\rho_b = \frac{1}{\pi n_0}\int d^2\gamma\ e^{-|\gamma|^2/n_0}|\gamma\rangle\langle\gamma|. \tag{10}$$

We then consider that the blue-detuned excitation is on during a time interval T_1 such that the probability that at least one photon-phonon pair is created is given by $p = 1 - e^{-2\tilde{g}_+ T_1}$. The red-detuned excitation is then switched on during a time interval T_2 such that the phonon-photon conversion efficiency is given by $T = 1 - e^{-2\tilde{g}_- T_2}$. The detection efficiency is η for both mode A_1 and A_2. Following the procedure presented in Ref. [1], we find

$$P(+1+1|\alpha,\beta)$$
$$=\frac{1-p}{1+n_0\eta T-p(-1+\eta+n_0\eta)(-1+\eta T)}\times e^{-\left[\frac{\eta|\alpha|^2[(1+p(-1+\eta T)+n_0\eta T)]+\eta|\beta|^2[(1+p(-1+\eta+n_0\eta))]+\eta^2(\alpha\beta+\alpha^*\beta^*)(1+n_0)\sqrt{pT}}{1+n_0\eta T-p(-1+\eta+n_0\eta)(-1+\eta T)}\right]}, \quad (11)$$

$$P(+1|\alpha)=(1-p)\frac{e^{-\frac{\eta|\alpha|^2(1-p)}{p(\eta+\eta n_0-1)+1}}}{p(\eta+\eta n_0-1)+1}, \quad (12)$$

$$P(+1|\beta)=(1-p)\frac{e^{-\frac{\eta|\beta|^2(1-p)}{\eta T(n_0+p)-p+1}}}{\eta T(n_0+p)-p+1}. \quad (13)$$

These expressions allows us to deduce the expected mean value for the witness observable $Q(\alpha,\beta)$ using

$$Q(\alpha,\beta)=1-2P(+1|\alpha)-2P(+1|\beta)+4P(+1+1|\alpha,\beta).$$

This observed value $Q(\alpha,\beta)$ must then be compared to the maximum value $S^\star(\alpha,\beta)$ for all separable states to assess the presence of entanglement. To estimate $S^\star(\alpha,\beta)$, we still need to estimate the probabilities of coincidence counts after a 50/50 beamsplitter on each mode. For example, sending mode A_1 into a 50-50 beamsplitter yields two output modes a_1 and a_1' with photon number probabilities

$$\begin{aligned}&P(n_{a_1}=m,n_{a_1'}=0)\\ =&2^{-m}(1-p)\frac{[p(1+n_0)\eta]^m}{[1-p(1-\eta-n_0\eta)]^{m+1}}\\ =&P(n_{a_1}=0,n_{a_1'}=m),\end{aligned}$$

which then allows us to obtain the probabilities for coincidence counts on mode A_1,

$$\begin{aligned}P_c(A_1)=&1-P(n_{a_1}=0,n_{a_1'}=0)\\ &-\sum_{m=1}^{\infty}P(n_{a_1}=m,n_{a_1'}=0)\\ &-\sum_{m=1}^{\infty}P(n_{a_1}=0,n_{a_1'}=m)\\ =&1-\frac{1-p}{1-p(1-\eta-n_0\eta)}\\ &-2\left[\frac{(1+n_0)(1-p)\eta p}{(2-p(2-\eta-\eta n_0))(1+p(-1+\eta+n_0\eta))}\right].\end{aligned}$$

Similarly for mode A_2, the probability for coincidence counts is given by

$$\begin{aligned}&P_c(A_2)\\ &=1-\frac{1-p}{1-p+(n_0+p)T\eta}\\ &-2\left[\frac{(1-p)(n_0+p)T\eta}{(2+n_0T\eta+p(-2+T\eta))(1+n_0T\eta+p(-1+T\eta))}\right].\end{aligned}$$

These probabilities allow us to estimate the value of $S^\star(\alpha,\beta)$ from Eq. (9) and thus to deduce $Q(\alpha,\beta)-S^\star(\alpha,\beta)$. The result is shown in Fig. 2 of the Main Text as a function of the conversion efficiency T for various detection efficiency in the case where the mechanical system is initially in its ground state $n_0=0$. Fig. 1 shows $Q(\alpha,\beta)-S^\star(\alpha,\beta)$ for various values of initial thermal excitations in the resonator n_0.

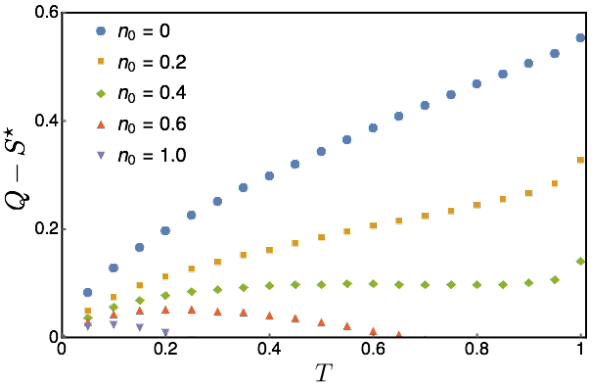

FIG. 1. Optimal values of the witness observable Q with respect to the separable bound $S^\star$ for unit detection efficiency ($\eta=1$) as a function of the phonon-photon conversion efficiency $T=1-e^{-2\bar{g}_-T_2}$ for various values of the mechanical thermal noise n_0. The difference $Q-S^\star$ is optimised over the displacement amplitudes α,β and the amount of initial squeezing $\bar{g}_+T_1$.

It is important to mention that the same values for $Q-S^\star$ are obtained in the case where η corresponds to the efficiency with which the photons are generated and transmitted until the displacement operation and are subsequently detected with unit efficiency detectors, although with different displacement amplitudes. This is clear mathematically since the same statistics are obtained with loss operating before or after the displacement operations provided that the displacement amplitude is changed accordingly, c.f. section B. The results presented in Fig. 2 of the main text can thus be seen as the expected value of the observable witness with respect to the separable bound for various overall detection efficiencies, including all the loss from the generation to the detection of photons.

E-STATISTICAL ANALYSIS

What we have calculated so far for expected values of $Q - S^\star$ are asymptotic values. These values are derived from probabilities computed using the Born rule, and are guaranteed to be the observed quantities only in the situation where the number of experimental runs tends to infinity.

The number of runs available, however, are limited in practice. This would lead to a scenario where, due to statistical fluctuations, an experiment that reveals $Q - S^\star > 0$ in the asymptotic case might not reveal this entanglement with limited runs. To overcome this, we require sufficient runs for an estimator $\overline{Q(\alpha,\beta) - S^\star(\alpha,\beta)}$, so that its variance will be low as compared to its asymptotic value $Q(\alpha,\beta) - S^\star(\alpha,\beta)$. This guarantees that a significant violation is likely to be experimentally observed. Once such a violation is observed, a similar calculation could be made to guarantee that the observed statistics are not compatible with an entangled state, i.e. bounding the possible p-value.

We now present how we form an appropriate estimator for our witness. As an initial example, an event with probability $P(m)$ can be estimated with N runs, using a sample estimator $\overline{P(m)}$

$$\overline{P(m)} = \frac{1}{N}\sum_i^N x_i \quad , \; x_i \begin{cases} +1 & \text{if the } i\text{-th run shows 'm'} \\ 0 & \text{otherwise} \end{cases},$$

This is a consistent estimator, as the expectation value of the sample gives the quantity to be estimated

$$\begin{aligned} \mathbb{E}\Big(\overline{P(m)}\Big) &= \mathbb{E}\Big(\frac{1}{N}\sum_i^N x_i\Big) \\ &= \frac{1}{N}\sum_i^N \mathbb{E}(x_i) \\ &= P(m). \end{aligned} \tag{14}$$

The variance of the sample estimator with N runs can be found to scale with $\frac{1}{N}$, since noting that $x_i^2 = x_i$, we have

$$\begin{aligned} \mathbb{E}\Big([\overline{P(m)}]^2\Big) &= \mathbb{E}\Big(\frac{1}{N^2}\sum_{i,j}^N x_i x_j\Big) \\ &= \frac{1}{N^2}\mathbb{E}\Big(\sum_{i=j} x_i x_j + \sum_{i\neq j} x_i x_j\Big) \\ &= \frac{1}{N^2}\Big[\sum_{i=j}\mathbb{E}(x_i x_j) + \sum_{i\neq j}\mathbb{E}(x_i x_j)\Big] \\ &= \frac{1}{N^2}\Big[\sum_i^N \mathbb{E}(x_i^2) + \sum_i^N \mathbb{E}(x_i)\sum_{j\neq i}\mathbb{E}(x_j)\Big] \\ &= \frac{1}{N^2}\Big[NP(m) + N(N-1)P(m)^2\Big], \end{aligned} \tag{15}$$

and we compute

$$\begin{aligned} \mathrm{Var}\Big(\overline{P(m)}\Big) &= \mathbb{E}\Big(\Big[\overline{P(m)}\Big]^2\Big) - \mathbb{E}\Big(\overline{P(m)}\Big)^2 \\ &= \frac{1}{N}P(m)\big[1 - P(m)\big], \end{aligned} \tag{16}$$

allowing us to assess the variance of $P(m)$ as a function of the probability $P(m)$ and the number of runs. If the variance of the sample estimator is small using N runs, one can be confident that in those N runs the sample estimator gives a value close to its expectation value.

Let us now move on to more complicated combinations of estimators, starting with linear combinations. The variance of linear combinations of probabilities of different events can be easily computed if the runs are uncorrelated. For example, if we estimate $P(m)$ from a sample of N_1 runs, and $P(n)$ from a sample of separate N_2 runs, then

$$\mathrm{Var}\Big(\alpha\overline{P(m)} + \beta\overline{P(n)}\Big) = \alpha^2\mathrm{Var}\Big(\overline{P(m)}\Big) + \beta^2\mathrm{Var}\Big(\overline{P(n)}\Big) \tag{17}$$

by the well known variance addition formula for uncorrelated data.

Other examples include the product of two probabilities, such as $P(m)P(n)$. One could use a natural choice for the estimator, where probabilities $P(m)(P(n))$ are assessed with $N_A(N_B)$ runs over separate data, such that

$$\overline{P(m)P(n)} = \frac{1}{N_A}\sum_i^{N_A} x_i \frac{1}{N_B}\sum_j^{N_B} y_j, \tag{18}$$

where y_i is assigned to indicate runs showing 'n', similar to the case for $P(m)$. One can easily see that our estimator is consistent, giving $\mathbb{E}\Big(\overline{P(m)P(n)}\Big) = P(m)P(n)$. One can also get the variance of this chosen estimator as an explicit function of $P(m), P(n), N_A$ and N_B.

Considering now the quantites in $S^\star$, however, we have terms involving the square root of products of two probabilities. Choosing a natural choice for the estimator as we did before does not give us the analytical functions for the variance we would like, since if for $\sqrt{P(m)P(n)}$ we use the estimator

$$\overline{\sqrt{P(m)P(n)}} = \sqrt{\frac{1}{N_A}\sum_i^{N_A} x_i \frac{1}{N_B}\sum_j^{N_B} y_j}, \tag{19}$$

then we obtain

$$\mathbb{E}\Big(\Big[\overline{\sqrt{P(m)P(n)}}\Big]^2\Big) = P(m)P(n) \tag{20}$$

but

$$\begin{aligned}\mathbb{E}\Big(\overline{\sqrt{P(m)P(n)}}\Big) =&\mathbb{E}\left(\sqrt{\frac{1}{N_A}\sum_i^{N_A} x_i \frac{1}{N_B}\sum_j^{N_B} y_j}\right)\\ \leq&\sqrt{\mathbb{E}\Big(\frac{1}{N_A}\sum_i^{N_A} x_i \frac{1}{N_B}\sum_j^{N_B} y_j\Big)}\\ =&\sqrt{P(m)P(n)}, \end{aligned} \tag{21}$$

leading only to the trivial bound $\mathrm{Var}\Big(\overline{\sqrt{P(m)P(n)}}\Big) \geq 0$. We thus do not consider such estimators directly in our variance assessment for nonlinear terms.

We instead consider a linearisation on the nonlinear quantities in $S^\star(\alpha,\beta)$ by finding the tangent surface at a point. We recall that for a 2-dimensional function $f(x,y)$, the tangent surface at the point (x_0,y_0) is given by

$$\begin{aligned}&f_{linear}\\ =&f(x_0,y_0)+f_x(x_0,y_0)(x-x_0)+f_y(x_0,y_0)(y-y_0),\end{aligned}$$

where the partial derivatives of $f(x,y)$ to $x(y)$ are $f_{x(y)}(x,y)$ respectively.

With this, we can find the tangent surface to each of the square root terms and obtain linear combinations of probabilities. For example, for $z = \sqrt{P(+1+1|0,0)\ P(-1-1|0,0)}$ at the point (A,B), we have

$$\begin{aligned} z &= \sqrt{P(+1+1|0,0)\ P(-1-1|0,0)}\\ &\leq \frac{1}{2}\left[\sqrt{\frac{B}{A}}P(+1+1|0,0)+\sqrt{\frac{A}{B}}P(-1-1|0,0)\right]\\ &= z_{\text{linear}}.\end{aligned}$$

In this case it is important to note that the resulting linear combination of probabilities forms an upper bound due to the concavity of the square root function, overestimating z in a conservative manner. We stress that any surface z_{linear} with nonzero A and B is a valid upper bound on z. Since we overestimate quantities that are in $S^\star(\alpha,\beta)$, this does not lead to a false conclusion of entanglement. To assess the value of z_{linear}, we can now use individual estimators $\overline{P(+1+1|0,0)}$ and $\overline{P(-1-1|0,0)}$ that converge to $P(+1+1|0,0)$ and $P(-1-1|0,0)$ respectively, so that

$$\overline{z_{linear}} = \frac{1}{2}\left[\sqrt{\frac{B}{A}}\overline{P(+1+1|0,0)}+\sqrt{\frac{A}{B}}\overline{P(-1-1|0,0)}\right],$$

and whose variance we can easily compute assuming separate runs in the estimation for each term.

At this point, A and B can independently take any nonzero value from 0 to 1, and still give valid linearised upper bounds. To select more optimal values for A and B in such a linearised estimator, one can perform an initial calibration experiment. Given these values, one can then form a valid, but close to optimal z_{linear}. We first point out with an infinite number of runs for the calibration, an accurate calibration is possible, yielding $A = P(+1+1|0,0)_{\text{cal}} \to P(+1+1|0,0)$ and $B = P(-1-1|0,0)_{\text{cal}} \to P(-1-1|0,0)$. Furthermore, consistent estimators asymptotically converge to the quantum values, giving $\overline{P(+1+1|0,0)} \to P(+1+1|0,0)$ and $\overline{P(-1-1|0,0)} \to P(-1-1|0,0)$. Therefore in the case where $P(+1+1|0,0)$ and $P(-1-1|0,0)$ are nonzero, the asymptotic $z_{\text{linear}} = z$.

We thus create an estimator $\overline{Q(\alpha,\beta) - S^\star_{\text{linear}}(\alpha,\beta)}$ in this best case scenario, made up of a linear combination of individual estimators so that we can easily assess its variance

$$\begin{aligned}&\overline{Q(\alpha,\beta)-S^\star(\alpha,\beta)} \leq \overline{Q(\alpha,\beta)-S^\star_{\text{linear}}(\alpha,\beta)}\\ =&\overline{P(+1+1|\alpha,\beta)}+\overline{P(+1-1|\alpha,\beta)}\\ +&\overline{P(-1+1|\alpha,\beta)}+\overline{P(-1-1|\alpha,\beta)}\\ -&\langle 0|\sigma_{\sqrt{\eta}\alpha}|0\rangle\langle 0|\sigma_{\sqrt{\eta}\beta}|0\rangle\overline{P(+1+1|0,0)}\\ -&\langle 0|\sigma_{\sqrt{\eta}\alpha}|0\rangle\langle 1|\sigma_{\sqrt{\eta}\beta}|1\rangle\overline{P(+1-1|0,0)}\\ -&\langle 1|\sigma_{\sqrt{\eta}\alpha}|1\rangle\langle 0|\sigma_{\sqrt{\eta}\beta}|0\rangle\overline{P(-1+1|0,0)}\\ -&\langle 1|\sigma_{\sqrt{\eta}\alpha}|1\rangle\langle 1|\sigma_{\sqrt{\eta}\beta}|1\rangle\overline{P(-1-1|0,0)}\\ -&|\langle 0|\sigma_{\sqrt{\eta}\alpha}|1\rangle\langle 1|\sigma_{\sqrt{\eta}\beta}|0\rangle|\\ \times&\min\Big[k_1\ \overline{P(+1+1|0,0)}+k_1^{-1}\overline{P(-1-1|0,0)},\\ &\quad k_2\ \overline{P(+1-1|0,0)}+k_2^{-1}\overline{P(-1+1|0,0)}\Big]\\ -&\sqrt{2}|\langle 1|\sigma_{\sqrt{\eta}\alpha}|0\rangle\langle 1|\sigma_{\sqrt{\eta}\beta}|2\rangle|\\ \times&\min\Big[k_3\ \overline{P_c(A_2)}+k_3^{-1}\overline{P(+1-1|0,0)},\\ &\quad k_4\ \overline{P_c(A_2)}+k_4^{-1}\overline{P(-1-1|0,0)}\Big]\\ -&\sqrt{2}|\langle 1|\sigma_{\sqrt{\eta}\alpha}|2\rangle\langle 1|\sigma_{\sqrt{\eta}\beta}|0\rangle|\\ \times&\min\Big[k_5\ \overline{P_c(A_1)}+k_5^{-1}\overline{P(-1+1|0,0)},\\ &\quad k_6\ \overline{P_c(A_1)}+k_6^{-1}\overline{P(-1-1|0,0)}\Big]\\ -&2\Big[\overline{P_c(A_1)}+\overline{P_c(A_2)}\Big],\end{aligned} \tag{22}$$

where[1] $k_1 = \sqrt{\frac{P(-1-1|0,0)_{\text{cal}}}{P(+1+1|0,0)_{\text{cal}}}}$, $k_2 = \sqrt{\frac{P(-1+1|0,0)_{\text{cal}}}{P(+1-1|0,0)_{\text{cal}}}}$, $k_3 = \sqrt{\frac{P(+1-1|0,0)_{\text{cal}}}{P_c(A_2)_{\text{cal}}}}$, $k_4 = \sqrt{\frac{P(-1-1|0,0)_{\text{cal}}}{P_c(A_2)_{\text{cal}}}}$, $k_5 = \sqrt{\frac{P(-1+1|0,0)_{\text{cal}}}{P_c(A_1)_{\text{cal}}}}$ and $k_6 = \sqrt{\frac{P(-1-1|0,0)_{\text{cal}}}{P_c(A_1)_{\text{cal}}}}$.

[1] If one has some knowledge of the state parameters, one might even compute the expected asymptotic values to use as the calibration parameters. The use of this knowledge does not affect the validity of the entanglement conclusion from the actual experiment, as it only varies the overestimation of each term of the witness.

With a budget of N_{total} runs, we can now minimise the variance of $\overline{Q(\alpha,\beta) - S^{\star}_{\text{linear}}(\alpha,\beta)}$ over possible distributions of N_{total} runs across each estimator term within. For our purposes, we will consider a number of runs N_{total} sufficient for revealing entanglement if the variance for an accurately calibrated $\overline{Q(\alpha,\beta) - S^{\star}_{\text{linear}}(\alpha,\beta)}$ is such that

$$\sqrt{\text{Var}\left(\overline{Q(\alpha,\beta) - S^{\star}_{\text{linear}}(\alpha,\beta)}\right)} \leq \frac{1}{3}\left[Q(\alpha,\beta) - S^{\star}(\alpha,\beta)\right]. \quad (23)$$

In the case discussed in the Main Text, where one has an overall detection efficiency $\eta = 10\%$, an initial mechanical excitation $n_0 = 0.2$ and a state-swap efficiency of $T = 30\%$, we find that $N_{\text{total}} = 7.5 \times 10^5$ runs are sufficient to violate our witness inequality by three standard deviations. For a more conservative value $n_0 = 1$ of the initial mechanical excitation, we find that $N_{\text{total}} = 3.2 \times 10^6$. Given that 7 billions of runs have been reported in Ref. [5], we conclude that our proposal appears feasible with currently available setups.

F-IMPLEMENTATION

We present in Fig. 2 a possible way to implement our proposal. Pulses which are created at the cavity frequency ω_c, are split before being sent into Mach-Zehnder interferometers. The pulses in the first interferometer are used to drive the opto-mechanical system, that is, the frequency in the short and long arm is shifted so as to be resonant with the relevant optomechanical sidebands implementing the two-mode squeezing and phonon-photon state transfer operations respectively. Each arm of the second interferometer is equipped with phase and amplitude modulators to set the the phase and amplitude of displacement operations. The latter is indeed implemented by combining the state to be displaced and a coherent state into a partially reflecting beamsplitter. The modulators are here to guarantee that both states are indistinguishable in all degrees of freedom, differing only with regards to their photon number distribution.

We point out that this scheme imposes minimal requirements on the phase stability. As can be seen in Fig. 2, the only phase stability requirement is that the relative path length fluctuations in each of the interferometers A and B are small with respect to the wavelength. Phase stability in the larger interferometer that separates the initial laser pulses towards interferometers A and B is not required. Furthermore, for the detection of outcomes, at most twofold coincidences are required.

Finally, let us list the steps one should take to certify optomechanical entanglement.

1. Evaluate $S^{\star}(\alpha,\beta)$ by first recording the events 'click' and 'no-click' without displacement (measurement scheme (a)) to obtain the probabilities $P(\pm1,\pm1|0,0)$ and $P(\pm1,\mp1|0,0)$; and then introducing a beamsplitter and recording the coincidences (measurement scheme (b)) to obtain $P_c(A_1)$ and $P_c(A_2)$.

2. Evaluate $Q(\alpha,\beta)$ by recording the events 'click' and 'no-click' with settings α and β, to obtain $P(\pm1,\pm1|\alpha,\beta)$ and $P(\pm1,\mp1|\alpha,\beta)$.

3. Conclude entanglement if there is a couple (α,β) such that $Q(\alpha,\beta) - S^{\star}(\alpha,\beta) > 0$.

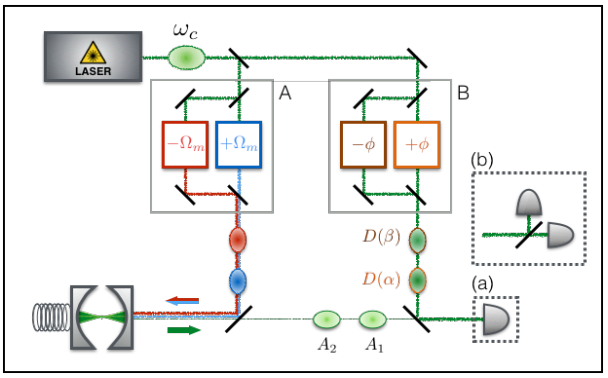

FIG. 2. Schematic of a possible setup. A laser set to the resonant frequency of the cavity is sent onto a beamsplitter where the beam is diverted towards interferometers A and B. Interferometer A is set up such that the pulse on the shorter/longer path is respectively detuned by plus/minus the mechanical frequency. The blue and red detuned pulses then enter the cavity and result in optical modes A_1 and A_2 which we detect for the witness. Interferometer B separates the incoming light into two paths, each modified so as to obtain the amplitude and phase of the respective displacement operation. Light leaving interferometer B then combines with the light from the cavity in order to realise the displacement operations before the photon detection. The two methods of detection required are shown in (a) using a single detector capable of measuring both A_1 and A_2, and in (b) with two detectors after a beamsplitter to measure coincidences.

[1] V. Caprara Vivoli, T. Barnea, C. Galland, and N. Sangouard, Phys. Rev. Lett. **116**, 070405 (2016)
[2] R. Schmied *et al.* Science **352**, 441 (2016)
[3] V. Scarani, Acta Physica Slovaca **62**, 347 (2012)
[4] N. Brunner, D. Cavalcanti, S. Pironio, V. Scarani and S. Wehner, Rev. Mod. Phys. **86**, 419 (2014)
[5] S. Hong *et al.*, Science **358**, 203 (2017)

CHAPTER 3

CERTIFYING QUANTUM REPEATERS

Upon the success of quantum repeater protocols, one expects to have an entangled state across two remote locations. For the case of the DLCZ architecture, this entangled state takes the form of two atomic ensembles which share a single excitation. Performing retrieval upon the remote atomic ensembles yields a path-entangled state, that is, two optical modes sharing a single photon. To show that the quantum repeater system is functioning as expected, one can first verify that this distributed photonic state is indeed entangled.

To perform entanglement verification upon this photonic state, one option is to involve the addition of another chain of repeaters altogether, which can become logistically prohibitive [34]. An alternative solution is to do a partial state tomography, where coherence terms are measured by interfering the two optical modes [46]. This method is not suited for the framework of quantum repeaters, since after the repeater protocol, the two entangled atomic ensembles could possibly be thousands of kilometers apart. Finally, a full tomography can be performed by local homodyne measurements [47], but this requires assumptions on the dimension of the underlying Hilbert space. Finding a simple method for verification while making minimal assumptions on the tested state would allow for a convenient but quantitative assessment on the functioning of the network.

To tackle this problem, we have designed a witness of single-photon entanglement based on the CHSH inequality, using phase-averaged homodyne measurements with a sign binning for the outcomes [48]. Homodyne measurements do not allow for a violation of the CHSH inequality, even in the ideal case where a

single photon is perfectly delocalised into two modes, but can nonetheless be used to form an entanglement witness, similar in spirit to the previous chapter. Our witness here is based on the CHSH inequality, but relies on a detailed description of well calibrated measurements. While knowledge of the measurements are necessary, any resulting conclusion of entanglement does not require assumptions on the tested state.

In a subsequent work [49], we perform a refinement on the witness used in Ref. [48] with a systematic and complete way to use available information on all local photon probabilities. This allows us to detect entanglement for all nonzero efficiencies.

Paper D

Witnessing trustworthy single-photon entanglement with local homodyne measurements

Olivier Morin, Jean-Daniel Bancal, Melvyn Ho, Pavel Sekatski, Virginia D'Auria, Nicolas Gisin, Julien Laurat and Nicolas Sangouard

Physical Review Letters **110**, 030401 (2013)

Witnessing Trustworthy Single-Photon Entanglement with Local Homodyne Measurements

Olivier Morin,[1] Jean-Daniel Bancal,[2] Melvyn Ho,[3] Pavel Sekatski,[2] Virginia D'Auria,[4] Nicolas Gisin,[2] Julien Laurat,[1] and Nicolas Sangouard[2]

[1]*Laboratoire Kastler Brossel, Université Pierre et Marie Curie, Ecole Normale Supérieure, CNRS, 4 Place Jussieu, 75252 Paris Cedex 05, France*

[2]*Group of Applied Physics, University of Geneva, CH-1211 Geneva 4, Switzerland*

[3]*Centre for Quantum Technologies, National University of Singapore, 3 Science Drive 2, Singapore 117543*

[4]*Laboratoire de Physique de la Matière Condensée, CNRS UMR 7336, Université de Nice-Sophia Antipolis, Parc Valrose, 06108 Nice Cedex 2, France*

(Received 2 July 2012; published 25 March 2013)

Single-photon entangled states, i.e., states describing two optical paths sharing a single photon, constitute the simplest form of entanglement. Yet they provide a valuable resource in quantum information science. Specifically, they lie at the heart of quantum networks, as they can be used for quantum teleportation, swapped, and purified with linear optics. The main drawback of such entanglement is the difficulty in measuring it. Here, we present and experimentally test an entanglement witness allowing one to say whether a given state is path entangled and also that entanglement lies in the subspace, where the optical paths are each filled with one photon at most, i.e., refers to single-photon entanglement. It uses local homodyning only and relies on no assumption about the Hilbert space dimension of the measured system. Our work provides a simple and trustworthy method for verifying the proper functioning of future quantum networks.

DOI: 10.1103/PhysRevLett.110.130401 PACS numbers: 03.65.Ud, 42.50.Dv

Motivations.—Quantum networks [1] provide broad capabilities, ranging from long distance quantum communication at large scales [2,3], to the simulation of quantum many-body systems [4] in tabletop implementations. Remarkable progresses have been made in practice [5–7] and experimental capabilities are now advancing into a domain of rudimentary functionality for quantum nodes connected by quantum channels [8–11]. Surprisingly, the task of checking that a newly implemented quantum network performs well remains nontrivial.

In the past decade, a great number of architectures based on atomic ensembles and linear optics have been proposed [12]. We now know that quantum networks based on single-photon entanglement [13], i.e., entangled states of the form

$$\frac{1}{\sqrt{2}}(|1\rangle_A|0\rangle_B + |0\rangle_A|1\rangle_B), \tag{1}$$

where A and B are two spatial modes sharing a delocalized photon, are very attractive: They require significantly fewer resources than the other architectures and are less sensitive to memory and photon detector inefficiencies [12]. Furthermore, they are efficient when combined with temporal multiplexing [14]. However, such networks have a major drawback: The detection of single-photon entangled states is very challenging. One cannot resort, for example, to violating a Bell inequality given solely photon-counting techniques.

Hitherto, there are three prescribed methods to detect single-photon entanglement. The first one converts two copies of a single-photon entangled state into one copy of two-particle entanglement. Starting from entanglement $(|1\rangle_{A_1}|0\rangle_{B_1} + |0\rangle_{A_1}|1\rangle_{B_1}) \otimes (|1\rangle_{A_2}|0\rangle_{B_2} + |0\rangle_{A_2}|1\rangle_{B_2})$ between the modes A_1 and B_1 and between A_2 and B_2, it basically consists of a postselective projection onto the subspace with one excitation in each location, yielding $|1\rangle_{A_1}|1\rangle_{B_2} + |1\rangle_{A_2}|1\rangle_{B_1}$ [3]. The latter is analogous to conventional polarization or time-bin entanglement, and any witness suited for such entanglement can thus be used to postselectively detect single-photon entanglement. Nevertheless, this approach is not fully satisfying conceptually because it relies on postselection. Furthermore, for practical implementation, the need to create two copies requires twice the number of resources at each node.

The second method is based on partial quantum state tomography. Specifically, one reconstructs a reduced density matrix that corresponds to a projection of the full density matrix into a subspace with at most one photon locally. The presence of entanglement is then inferred from an entanglement measure computed from the reduced density matrix [15]. Specifically, this tomographic approach requires the knowledge of probabilities p_{mn} of having m photons in mode A and n in mode B, where $m, n \in \{0, 1\}$, and the visibility V of the single-photon interference pattern obtained by combining the modes A and B into a beam splitter. Although it has triggered highly successful experiments [15–18], the approach presented in Ref. [15] cannot be directly used in large-scale networks when one needs to check the entanglement between far away locations, since the knowledge of V relies on a joint measurement of A and B modes.

The last method uses local homodyne detections and provides, *a priori*, a full tomography of the state that can subsequently be used to measure the entanglement [19,20]. However, the tomographic approach requires a number of measurements, which increase with the dimension of the state being measured [21]. In practice, one could be tempted to make an assumption on the regularity of the measured Wigner function to reduce the number of measurements or, equivalently, on the dimension of the system's Hilbert space, especially when focusing on single-photon entanglement. But this would amount to making an assumption about the system that we want to characterize. One can also estimate the dimension of the state from measurements, but it is not clearly established how errors on this estimation can affect the conclusion about the presence of entanglement. More generally, the exponential increase of required measurements with the number of measured subsystems makes the tomography not suited to decide on the presence of entanglement in quantum networks [22], contrary to entanglement witnesses [23].

Principle.—Here, we propose a simple approach to witness single-photon entanglement which relies on local measurements only and needs neither postselection nor assumption on the tested state. The basic principle is drawn in Fig. 1. Two distant observers, Alice and Bob, share a quantum state. To check whether it is entangled, each of them randomly chooses a measurement among two quadratures, $\{X, P\}$ for Alice and $\{X+P, X-P\}$ for Bob. At each run, they obtain a real number. They then process the results to get binary outcomes using a sign binning; i.e., they attribute the result -1 if the result is negative and $+1$ otherwise. By repeating the experiment several times, Alice and Bob can compute the conditional probabilities $p(a, b|x, y)$, where $a, b \in \{-1, +1\}$, $x \in \{X, P\}$, and $y \in \{X+P, X-P\}$. Substituting these probabilities by their values into the Clauser-Horne-Shimony-Holt (CHSH) [24] polynomial

$$S = E_{X,X+P} + E_{X,X-P} + E_{P,X+P} - E_{P,X-P}, \qquad (2)$$

where $E_{x,y} = \sum_{a,b=\{-1,+1\}} p(a = b|x, y) - p(a \neq b|x, y)$, they obtain a real number S.

The value of S can easily be obtained under the assumption that Alice and Bob each have a qubit. Indeed, in the Fock basis $\{|0\rangle, |1\rangle\}$, the measurement of the X quadrature

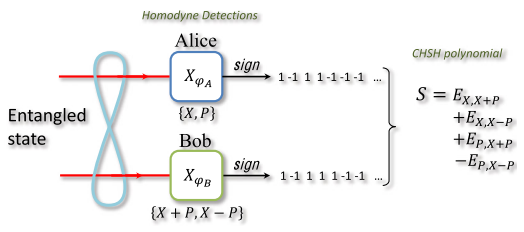

FIG. 1 (color online). Principle of the proposed entanglement witness.

with sign binning is equivalent to a noisy σ_x measurement [25,26], $\int_{-\infty}^{0} dx|x\rangle\langle x| - \int_{0}^{\infty} dx|x\rangle\langle x| = \sqrt{\frac{2}{\pi}}\sigma_x$ and, similarly, the P quadrature corresponds to σ_y with the same noise. For the setting choice $\{X, P\}$ and $\{X+P, X-P\}$, the state (1) thus yields to $S = 2\sqrt{2} \times \frac{2}{\pi} \approx 1.8$. Furthermore, the maximum value that can be obtained with a separable state belonging to the subspace $\{|0\rangle, |1\rangle\}^{\otimes 2}$ is $S_{\text{sep}} = \sqrt{2} \times \frac{2}{\pi} \approx 0.9$ [27]. Since S is smaller than 2, the proposed CHSH-like test does not highlight the nonlocal characteristic of a single photon delocalized among two modes, but it does provide an attractive entanglement witness: If the measured CHSH value is larger than S_{sep}, Alice and Bob can conclude that they share an entangled state.

This holds for qubits only. In practice, however, the state describing the modes A and B includes multiphoton components and does not reduce to a two-qubit state. We show below how the entanglement witness can be extended to the case of arbitrary dimensional bipartite states. First, we show how Alice and Bob can accurately estimate the probability that their state lies out of a two-qubit space $\{|0\rangle, |1\rangle\}^{\otimes 2}$. We then demonstrate that this probability can be used to upper bound the maximal CHSH value that can be obtained with separable states.

Bounding the Hilbert space dimension.—Let us consider the case where Alice and Bob do not have qubits but quantum states of arbitrary dimension. First, they need to bound the probability that at least one of their modes is populated with more than one photon $p(n_A \geq 2 \cup n_B \geq 2)$. This can be realized without assumption on the Hilbert space dimension by first determining the probabilities $p(n_A = j)$ $(p(n_B = j))$ of having j photons in Alice's (Bob's) mode, using local homodyning with phase-averaged local oscillators through a direct integration of the obtained data with a pattern function [28]. The joint probability $p(n_A \geq 2 \cup n_B \geq 2) = p(n_A \geq 2) + p(n_B \geq 2) - p(n_A \geq 2 \cap n_B \geq 2)$ can then be bounded by the parameter $p^\star$, defined as follows

$$p^\star = 2 - \left(\sum_{j=0}^{1} p(n_A = j) + p(n_B = j) \right). \qquad (3)$$

We now show how the knowledge of $p^\star$ can be used to construct an operational witness for single-photon entanglement.

Evaluating the maximal CHSH value with separable states.—Consider the general case, where $p^\star \neq 0$, i.e. $p(n_A \geq 2 \cup n_B \geq 2) \neq 0$ *a priori*. The state of Alice and Bob can be described by the density matrix

$$\rho = \begin{pmatrix} \rho_{n_A \leq 1 \cap n_B \leq 1} & \rho_{\text{coh}} \\ \rho_{\text{coh}}^\dagger & \rho_{n_A \geq 2 \cup n_B \geq 2} \end{pmatrix}, \qquad (4)$$

where $\rho_{n_A \leq 1 \cap n_B \leq 1}$ denotes the 4×4 block with, at most, one photon per mode, $\rho_{n_A \geq 2 \cup n_B \geq 2}$ refers to the block where at least one of the two modes contains at least two photons,

and ρ_{coh} is associated with the coherence between these two blocks. Since $\rho_{n_A\geq 2\cup n_B\geq 2}$ possibly spans a Hilbert space of infinite dimension, there could be an infinite number of coherence terms. However, a few of them give a nonzero contribution to the CHSH polynomial if a phase-averaged homodyne detection is used at each location. Specifically, consider the case where Alice and Bob perform the measurements $X_{\varphi_A} = \cos\varphi_A X + \sin\varphi_A P$ and $X_{\varphi_B} = \cos\varphi_B X + \sin\varphi_B P$, respectively, where φ_A and φ_B are random variables such that $\langle e^{ik\varphi_{A,B}}\rangle = 0$, $k \in \mathbb{N}^\star$ but the phase difference $\varphi_A - \varphi_B = \Delta\varphi$ is fixed. This requires classical but not quantum communication and, hence, can only decrease the entanglement that Alice and Bob potentially share. In particular, if Alice can choose a measurement among the two quadratures $\{X_{\varphi_A^1}, X_{\varphi_A^2}\}$ and if Bob's choice reduces to one of the quadratures $\{X_{\varphi_B^1}, X_{\varphi_B^2}\}$ such that $\varphi_A^1 - \varphi_B^1 = -\frac{\pi}{4}$, $\varphi_A^1 - \varphi_B^2 = \frac{\pi}{4}$, $\varphi_A^2 - \varphi_B^1 = \frac{\pi}{4}$ and $\varphi_A^2 - \varphi_B^2 = \frac{3\pi}{4}$, we show in the Supplemental Material [29] that the CHSH polynomial corresponding to the state (4) is bounded by

$$S^{\max} = \frac{16}{\sqrt{2}\pi}\Re[\langle 01|\rho_{n_A\leq 1\cap n_B\leq 1}|10\rangle] + \frac{8}{\pi}(\Re[\langle 20|\rho_{\text{coh}}|11\rangle] + \Re[\langle 02|\rho_{\text{coh}}|11\rangle]) + 2\sqrt{2}p(n_A \geq 2 \cup n_B \geq 2), \quad (5)$$

where $\Re$ denotes the real part. For a given value of $p(n_A \geq 2 \cup n_B \geq 2)$, $S^{\max}$ can be directly maximized over the set of physical states ($\rho \in \{|0\rangle, |1\rangle, |2\rangle\}^{\otimes 2}$, $\text{tr}(\rho) \leq 1$, $\rho \geq 0$) that satisfy the observed photon number distributions, i.e., $p_{00} + p_{10} + p_{01} + p_{11} = 1 - p(n_A \geq 2 \cup n_B \geq 2)$ and that are separable in the $\{|0\rangle, |1\rangle\}^{\otimes 2}$ subspace, i.e., for which the projection into this subspace remains positive under partial transposition (PPT) [30,31]. Figure 2 shows the result of this optimization $S_{\text{sep}}^{\max}$.

Witnessing single-photon entanglement.—This provides a truly state-independent witness [32] of entanglement. First, the protagonists determine the local photon-number distributions from which they deduce an upper bound $p^\star$ on the joint probability $p(n_A \geq 2 \cup n_B \geq 2)$. Second, they deduce $S_{\text{sep}}^{\max}(p^\star)$ from Fig. 2 (see the Supplemental Material [29]). Third, they measure the CHSH value S_{obs} by randomly choosing measurements among $\{X_{\varphi_A^1}, X_{\varphi_A^2}\}$ and $\{X_{\varphi_B^1}, X_{\varphi_B^2}\}$, respectively, and by subsequently computing the CHSH polynomial through Eq. (2). If $S_{\text{obs}} > S_{\text{sep}}^{\max}(p^\star)$, Alice and Bob know that the projection of their state into the subspace $\{|0\rangle, |1\rangle\}^{\otimes 2}$ has a negative partial transpose; i.e., they can safely conclude that the state is entangled and that the entanglement resides in the subspace with at most one photon locally.

Importantly, a tighter bound can be obtained if $S^{\max}$ is maximized over the set of states with a positive partial transpose not only satisfying $p_{00} + p_{10} + p_{01} + p_{11} = 1 - p(n_A \geq 2 \cup n_B \geq 2)$ but also reproducing the locally measured probabilities $p(n_A = j)$ ($p(n_B = j)$) for having $j = 0, 1$ photon in Alice's (Bob's) mode. These additional constraints have been taken into account for the computation of the separable bounds related to the experiment presented below (see the Supplemental Material [29]).

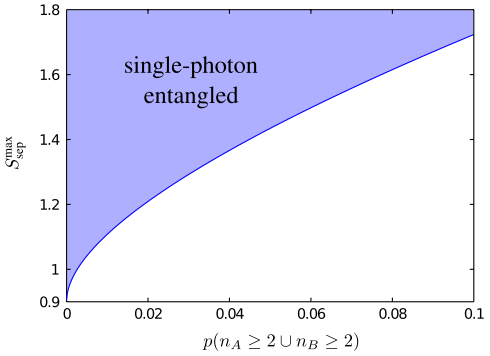

FIG. 2 (color online). Separable bound $S_{\text{sep}}^{\max}$ as a function of the probability that at least one of the two protagonists gets more than one photon $p(n_A \geq 2 \cup n_B \geq 2)$. The blue curve allows one to know the maximum value of the CHSH polynomial $S_{\text{sep}}^{\max}$ that a state separable in the $\{|0\rangle, |1\rangle\}^{\otimes 2}$ subspace can reach. If $S_{\text{obs}} > S_{\text{sep}}^{\max}$, one can conclude that the projection of the state in the subspace with zero and one photon locally is entangled.

Proof-of-principle experiment.—We start off with a heralded single photon generated by a conditional preparation technique operated on a two-mode squeezed vacuum emitted by a type-II optical parametric oscillator [33]. Without correction for detection loss, the overall fidelity reaches 70%. Single-photon entanglement is obtained by sending

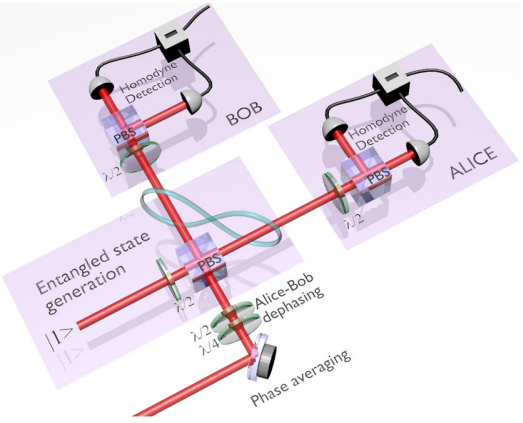

FIG. 3 (color online). Experimental setup. A tunable single-photon entangled state is created by sending a heralded single photon on a tunable beam splitter based on a polarizing beam splitter (PBS) and a half-wave plate ($\lambda/2$). The proposed witness is then tested with two independent homodyne detections (Alice and Bob). The local oscillator is superposed to each mode via the first PBS. Its global phase is swept with a piezoelectric actuator. The relative phase $\Delta\varphi$ is set with a combination of birefringent plates.

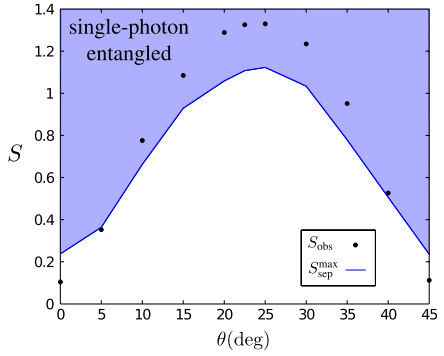

FIG. 4 (color online). Observed CHSH values S_{obs} (the size of points accounts for statistical errors) and separable bound S_{sep}^{max} as a function of beam-splitter angle θ. When $S_{obs} > S_{sep}^{max}$, one can conclude that the measured state is entangled.

the created photon into a beam splitter [34]. Specifically, by controlling the angle θ of a half-wave plate relative to the axis of a polarizing beam splitter (PBS), we create a tunable single-photon entangled state $\cos(2\theta)|0\rangle_A|1\rangle_B + \sin(2\theta)|1\rangle_A|0\rangle_B$ between the two output modes of the PBS, as sketched in Fig. 3.

The local oscillators that Alice and Bob need to reveal entanglement are obtained by impinging a bright beam on the second input of the PBS: one polarization mode is used as the quantum channel, and the orthogonal one conveys the local oscillator. It is worth mentioning that this technique can be implemented over long distances as realized in field implementation of quantum key distribution [35]. The relative phase between Alice's and Bob's local oscillators $\Delta\varphi$ is fixed by choosing an appropriate elliptical polarization of the bright beam just before the PBS [36]. In practice, the setting difference is calibrated by observing the dephasing of interference fringes (the quantum state is replaced here by a coherent state). A global phase averaging is obtained by sweeping a piezoelectric transducer located on the path of the bright beam before the PBS.

For each heralding event, Alice and Bob each obtain a real valued outcome, which is extracted from homodyne photocurrents. Accumulating 200 000 events for each quadrature relative measurements, they deduce the value of the CHSH polynomial S_{obs}. The same homodyne measurements also provide the local photon number distributions which are used to compute the separable bound S_{sep}^{max}. We emphasize that the separable bound is here obtained by maximizing the CHSH value over the set of separable states that fulfill the locally measured photon-number occupation probabilities $p(n_A = j)$ and $p(n_B = j)$ for having $j = 0, 1$ photon in Alice and Bob's mode, respectively. Furthermore, it takes several errors into account, for example, errors related to the quadrature measurement imperfections were considered (see the Supplemental Material [29]). The procedure is repeated for various angles θ ranging from 0 to 45°. Figure 4 shows the main result, i.e., the observed CHSH values and the separable bounds as a function of θ. One sees that they both reach maximal values around $\theta = 22.5°$, where Alice and Bob ideally share a maximally entangled state. The small deviation between the observed value $S_{obs}(\theta = 22.5°) \approx 1.33$ and the CHSH value that would be obtained with a maximally entangled state (1.8) demonstrates that the overall source and detection efficiencies are very high. Furthermore, the observed CHSH values are almost all larger than the separable bounds when dealing with entangled states ($\theta \neq 0°, 45°$). This shows the great robustness of the proposed witness.

Conclusion.—We have presented and experimentally tested a witness for single-photon entanglement that does not need postselection, uses local measurements only, and does not rely on assumptions about the dimension of the measured state. Note that our witness can be easily adapted to detect few-photon entanglement without additional complications. We believe that it will naturally find applications in long-distance quantum communication, allowing users to check whether two remote nodes of a given quantum network are entangled. One important challenge in this context is to reveal the entanglement shared by a large number of parties. Finding Bell inequalities that could be used as witnesses for multipartite single-photon entanglement is work for the future.

We thank Mikael Afzelius, Cyril Branciard, Félix Bussières, Claude Fabre, Ci Wen Lim, Valério Scarani, Rob Thew, and Nuala Timoney for helpful discussions. We acknowledge support from the ERA-NET CHIST-ERA under the QScale project, the EU project Qessence, the Swiss NCCR-QSIT, and the National Research Fund and the Ministry of Education, Singapore. J. L. is a member of the Institut Universitaire de France. O. M. and J.-D. B. contributed equally to this work.

[1] H. J. Kimble, Nature (London) **453**, 1023 (2008).
[2] H.-J. Briegel, W. Dür, J. I. Cirac, and P. Zoller, Phys. Rev. Lett. **81**, 5932 (1998).
[3] L.-M. Duan, M. D. Lukin, J. I. Cirac, and P. Zoller, Nature (London) **414**, 413 (2001).
[4] D. Illuminati, Nat. Phys. **2**, 803 (2006).
[5] Efficiently light storages have been reported in M. P. Hedges, J. J. Longdell, Y. Li, and M. J. Sellars, Nature (London) **465**, 1052 (2010); M. Hosseini, B. M. Sparkes, G. Campbell, P. K. Lam, and B. C. Buchler, Nat. Commun. **2**, 174 (2011).
[6] Long storage times have been reported in J. J. Longdell, E. Fraval, M. J. Sellars, and N. B. Manson, Phys. Rev. Lett. **95**, 063601 (2005); R. Zhang, S. R. Garner, and L. V. Hau, Phys. Rev. Lett. **103**, 233602 (2009); F. Yang, T. Mandel, C. Lutz, Z.-S. Yuan, and J.-W. Pan, Phys. Rev. A **83**, 063420 (2011); A. G. Radnaev, Y. O. Dudin, R. Zhao, H. H. Jen, S. D. Jenkins, A. Kuzmich, and T. A. B. Kennedy, Nat. Phys. **6**, 894 (2010).

[7] Entanglement between atomic ensembles has been reported in B. Julsgaard, A. Kozhekin, and E. S. Polsik, Nature (London) **413**, 400 (2001); J. Simon, H. Tanji, S. Ghosh, and V. Vuletić, Nat. Phys. **3**, 765 (2007), and in Refs. [15–18].
[8] C. W. Chou, J. Laurat, H. Deng, K. S. Choi, H. de Riedmatten, D. Felinto, and H. J. Kimble, Science **316**, 1316 (2007).
[9] Z.-S. Yuan, Y.-A. Chen, B. Zhao, S. Chen, J. Schmiedmayer, and J.-W. Pan, Nature (London) **454**, 1098 (2008).
[10] D. L. Moehring, P. Maunz, S. Olmschenk, K. C. Younge, D. N. Matsukevich, L.-M. Duan, and C. Monroe, Nature (London) **449**, 68 (2007).
[11] S. Ritter, C. Nölleke, C. Hahn, A. Reiserer, A. Neuzner, M. Uphoff, M. Mücke, E. Figueroa, J. Bochmann, and G. Rempe, Nature (London) **484**, 195 (2012).
[12] N. Sangouard, C. Simon, H. De Riedmatten, and N. Gisin, Rev. Mod. Phys. **83**, 33 (2011).
[13] S. J. van Enk, Phys. Rev. A **72**, 064306 (2005).
[14] C. Simon, H. de Riedmatten, M. Afzelius, N. Sangouard, H. Zbinden, and N. Gisin, Phys. Rev. Lett. **98**, 190503 (2007).
[15] C. W. Chou, H. de Riedmatten, D. Felinto, S. V. Polyakov, S. J. van Enk, and H. J. Kimble, Nature (London) **438**, 828 (2005).
[16] K. S. Choi, H. Deng, J. Laurat, and H. J. Kimble, Nature (London) **452**, 67 (2008).
[17] I. Usmani, C. Clausen, F. Bussières, N. Sangouard, M. Afzelius, and N. Gisin, Nat. Photonics **6**, 234 (2012).
[18] K. C. Lee *et al.*, Science **334**, 1253 (2011).
[19] S. A. Babichev, J. Appel, and A. I. Lvovsky, Phys. Rev. Lett. **92**, 193601 (2004).
[20] Note that in Ref. [19], in addition to a tomographic approach, a Bell test is presented which can be used for witnessing single-photon entanglement. The latter relies on the rejection of some of the acquired data. In comparison, our witness does not need postselection.
[21] For a state with dimension d, $d+1$ measurements are needed; see for example U. Leonhardt and M. Munroe, Phys. Rev. A **54**, 3682 (1996).
[22] The number of measurements that are needed to reconstruct a state of dimension d shared by n parties (nodes) is given by $(d+1)^n = e^{n\log(d+1)}$.
[23] O. Guhne and G. Toth, Phys. Rep. **474**, 1 (2009).
[24] J. F. Clauser, M. Horne, A. Shimony, and R. A. Holt, Phys. Rev. Lett. **23**, 880 (1969).
[25] M. T. Quintino, M. Araújo, D. Cavalcanti, M. F. Santos, and M. T. Cunha, J. Phys. A **45**, 215308 (2012).
[26] N. Sangouard, J.-D. Bancal, N. Gisin, W. Rosenfeld, P. Sekatski, M. Weber, and H. Weinfurter, Phys. Rev. A **84**, 052122 (2011).
[27] S. M. Roy, Phys. Rev. Lett. **94**, 010402 (2005).
[28] M. Munroe, D. Boggavarapu, M. E. Anderson, and M. G. Raymer, Phys. Rev. A **52**, R924 (1995).
[29] See Supplemental Material at http://link.aps.org/supplemental/10.1103/PhysRevLett.110.130401 for details.
[30] A. Peres, Phys. Rev. Lett. **77**, 1413 (1996).
[31] M. Horodecki, P. Horodecki, and R. Horodecki, Phys. Lett. A **223**, 1 (1996).
[32] The witness does not require one to know the way in which the state was created nor its dimensionality. However, it requires that Alice and Bob's devices perform the desired measurements. In particular, for the proposed witness, measurements are assumed to be homodyne measurements defined in the single optical mode of a local oscillator.
[33] O. Morin, V. D'Auria, C. Fabre, and J. Laurat, Opt. Lett. **37**, 3738 (2012).
[34] Note that it is sufficient for the input state to be nonclassical with respect to the P representation to create entanglement at a beam splitter, as shown, e.g., in J. K Asboth, J. Calsamiglia, and H. Ritsch, Phys. Rev. Lett. **94**, 173602 (2005).
[35] S. Fossier, E. Diamanti, T. Debuisschert, A. Villing, R. Tualle-Brouri, and P. Grangier, New J. Phys. **11**, 045023 (2009).
[36] J. Laurat, T. Coudreau, G. Keller, N. Treps, and C. Fabre, Phys. Rev. A **71**, 022313 (2005).

Witnessing trustworthy single-photon entanglement with local homodyne measurements : Supplementary Material

Olivier Morin*,[1] Jean-Daniel Bancal*,[2] Melvyn Ho,[3] Pavel Sekatski,[2] Virginia D'Auria,[4] Nicolas Gisin,[2] Julien Laurat,[1] and Nicolas Sangouard[2]

[1]*Laboratoire Kastler Brossel, Université Pierre et Marie Curie, Ecole Normale Supérieure, CNRS, 4 place Jussieu, 75252 Paris Cedex 05, France*
[2]*Group of Applied Physics, University of Geneva, CH-1211 Geneva 4, Switzerland*
[3]*Centre for Quantum Technologies, National University of Singapore, 3 Science Drive 2, Singapore 117543*
[4]*Laboratoire de Physique de la Matière Condensée, CNRS UMR 7336, Université de Nice - Sophia Antipolis, Parc Valrose, 06108 Nice Cedex 2, France*

(Dated: January 9, 2013)

I. WITNESSING SINGLE-PHOTON ENTANGLEMENT IN QUDIT SPACES: THEORY

As mentioned in the main text, if Alice & Bob can guarantee that they perform measurements on qubits, they can demonstrate entanglement by simply performing a Bell-like test by randomly choosing a setting among two quadratures, $\{X, P\}$ for Alice and $\{X+P, X-P\}$ for Bob. If the resulting CHSH value is larger than 0.9, they can safely conclude that their state is entangled. In practice, however, it is challenging to show that the systems one is measuring are well described by qubits. Below, we detail the procedure to follow in the general case where Alice & Bob have qudits.

A. CHSH polynomial for phase averaged homodyning

Let

$$\rho = \sum_{ijkl} c_{ijkl} |ij\rangle\langle kl|$$

be the state that Alice & Bob share, $|ij\rangle$ describing the state with i photons in Alice's mode and j photons in Bob's one. Consider that the phase of local oscillators that are required for homodyning, is averaged, i.e. Alice & Bob perform the measurements

$$X_{\varphi_A^\ell} = \cos\varphi_A^\ell X + \sin\varphi_A^\ell P,$$
$$X_{\varphi_B^{\bar\ell}} = \cos\varphi_B^{\bar\ell} X + \sin\varphi_B^{\bar\ell} P$$

respectively, with φ_A^ℓ and $\varphi_B^{\bar\ell}$ random variables satisfying $\langle e^{i\varphi_A^\ell}\rangle = \langle e^{i\varphi_B^{\bar\ell}}\rangle = 0$. Further consider that the phase difference $\Delta\varphi^{\ell\bar\ell} = \varphi_A^\ell - \varphi_B^{\bar\ell}$ to be tunable such that Alice can choose a measurement among the two quadatures $\{X_{\varphi_A^1}, X_{\varphi_A^2}\}$ relative to Bob's choice $\{X_{\varphi_B^1}, X_{\varphi_B^2}\}$. (This can only underestimate the entanglement in average because this can be realized by local operations and classical communications. Namely, they could each apply a random phase shift to a shared local oscillator such that the phase difference is fixed, subsequently choose a quadrature measurement locally and ignore the information about the individual phase shifts). At each run, Alice & Bob obtain each a real number. They then process the results to get binary outcomes using a sign binning, i.e. they assign the result -1 if the real number is negative and $+1$ otherwise. By repeating this procedure many times, they can access the probability that both get $+1$ for instance, knowing that they chose $X_{\varphi_A^\ell}$ and $X_{\varphi_B^{\bar\ell}}$

$$\begin{aligned} p(+1,+1|X_{\varphi_A^\ell}, X_{\varphi_B^{\bar\ell}}) &= \sum_{ijkl} \langle e^{i\varphi_B^{\bar\ell}(i+j-(k+l))}\rangle c_{ijkl} \\ &\quad \times e^{i\Delta\varphi^{\ell\bar\ell}(i-k)} \int_0^\infty dx \phi_i(x)\phi_k(x) \\ &\quad \times \int_0^\infty dy \phi_j(y)\phi_l(y) \end{aligned}$$

where $\phi_i(x) = \langle x|i\rangle$. One sees that the off-diagonal elements $|ij\rangle\langle kl|$ with different numbers of photons ($i + j \neq k + l$) do not contribute to the probabilities $p(a, b|X_{\varphi_A^\ell}, X_{\varphi_B^{\bar\ell}})$, with $a, b = \{-1, +1\}$. Furthermore, since for all n and m having the same parity,

$$\int_0^\infty dy \phi_n(y)\phi_m(y) = \int_{-\infty}^0 dy \phi_n(y)\phi_m(y) = \frac{1}{2}\delta_{n,m}$$

the terms c_{ijkl} for which either i-k or j-l is an odd number, have a zero contribution to the correlator

$$\begin{aligned} E_{X_{\varphi_A^\ell}, X_{\varphi_B^{\bar\ell}}} = \textstyle\sum_{a,b=\{-1,+1\}} & p(a=b|X_{\varphi_A^\ell}, X_{\varphi_B^{\bar\ell}}) \\ & - p(a\neq b|X_{\varphi_A^\ell}, X_{\varphi_B^{\bar\ell}}). \end{aligned}$$

Finally, one easily checks that the remaining c_{ijkl} terms satisfying

$$i + j = k + l, \tag{1}$$
$$|i - k| = 1 \mod 2, \tag{2}$$
$$|j - l| = 1 \mod 2, \tag{3}$$

* These authors contributed equally to this work.

yield

$$\begin{aligned} E_{X_{\varphi_A^\ell},X_{\varphi_B^{\bar{\ell}}}} &= 4\sum_{ijkl} c_{ijkl} \\ &\times \int_0^\infty dx\phi_i(x)\phi_k(x)e^{i\Delta\varphi^{\ell\bar{\ell}}(i-k)} \\ &\times \int_0^\infty dy\phi_j(y)\phi_l(y). \end{aligned}$$

Specifically, if $\Delta\varphi^{11} = -\frac{\pi}{4}$, $\Delta\varphi^{12} = \frac{\pi}{4}$, $\Delta\varphi^{21} = \frac{\pi}{4}$ and $\Delta\varphi^{22} = \frac{3\pi}{4}$, the value of the CHSH polynomial

$$S = E_{X_{\varphi_A^1},X_{\varphi_B^1}} + E_{X_{\varphi_A^1},X_{\varphi_B^2}} + E_{X_{\varphi_A^2},X_{\varphi_B^1}} - E_{X_{\varphi_A^2},X_{\varphi_B^2}}$$

is given by

$$\begin{aligned} S = \; & 16\sum_{ijkl} c_{ijkl}\cos\left((i-k)\,\frac{\pi}{4}\right) \\ & \times \int_0^\infty dx\phi_i(x)\phi_k(x)\,.\int_0^\infty dy\phi_j(y)\phi_l(y). \quad (4) \end{aligned}$$

B. Optimizing the CHSH value over the set of separable states

Without loss of generality, Alice & Bob's state can be written as

$$\rho = \begin{pmatrix} \rho_{n_A\leq 1\cap n_B\leq 1} & \rho_{\rm coh} \\ \rho_{\rm coh}^\dagger & \rho_{n_A\geq 2\cup n_B\geq 2} \end{pmatrix} \quad (5)$$

where $\rho_{n_A\leq 1\cap n_B\leq 1}$ denotes the block with at most one photon per mode, $\rho_{n_A\geq 2\cup n_B\geq 2}$ refers to the block where at least one of the two modes is populated with more than one photon and $\rho_{\rm coh}$ is associated to the coherence between these two blocks. Taking the constraints (1),(2) and (3) into account and using the formula (4), the corresponding CHSH polynomial reduces to

$$\begin{aligned} S \; &= \frac{16}{\sqrt{2}\pi}\Re\Big[\langle 01|\rho_{n_A\leq 1\cap n_B\leq 1}|10\rangle\Big] \quad (6) \\ &+\frac{8}{\pi}\left(\Re\Big[\langle 20|\rho_{\rm coh}|11\rangle\Big] + \Re\Big[\langle 02|\rho_{\rm coh}|11\rangle\Big]\right) \\ &+S_{\rho_{n_A\geq 2\cup n_B\geq 2}} \end{aligned}$$

where $\Re$ denotes the real part and $S_{\rho_{n_A\geq 2\cup n_B\geq 2}}$ is associated to the CHSH value obtained from $\rho_{n_A\geq 2\cup n_B\geq 2}$. The goal is now to optimize S over the set of separable states. Let $p(n_A \geq 2 \cup n_B \geq 2)$ be the probability that at least one of the two protogonists has more than one photon, i.e.

$$\text{tr}\;\rho_{\rm n_A\geq 2\cup n_B\geq 2} = {\rm p(n_A\geq 2\cup n_B\geq 2)}. \quad (7)$$

Since $\rho_{n_A\geq 2\cup n_B\geq 2}$ cannot be obtained by local projections, it may maximally contribute to CHSH, i.e. $S_{\rho_{n_A\geq 2\cup n_B\geq 2}} \leq 2\sqrt{2}\times p(n_A \geq 2 \cup n_B \geq 2)$. S is thus upper bounded by

$$\begin{aligned} S \leq \; & S^{\max}(p(n_A\geq 2\cup n_B\geq 2)) \quad (8) \\ &= \frac{16}{\sqrt{2}\pi}\Re\Big[\langle 01|\rho_{n_A\leq 1\cap n_B\leq 1}|10\rangle\Big] \\ &+\frac{8}{\pi}\left(\Re\Big[\langle 20|\rho_{\rm coh}|11\rangle\Big] + \Re\Big[\langle 02|\rho_{\rm coh}|11\rangle\Big]\right) \\ &+2\sqrt{2}\times p(n_A\geq 2\cup n_B\geq 2). \end{aligned}$$

Needless to say, separable states are physical states. They are thus represented by positive matrices with a trace (tr) equal to one. Furthermore, the Peres-Horodecki criterion [1, 2] states that for any separable state $\rho_{\rm sep}$, its partial transpose $\rho_{\rm sep}^{T_b}$ has non-negative eigenvalues. The optimization of $S^{\max}$ over the set of separable states in the subspace with at most one photon locally is thus a problem that can be summarized as follows

$$\begin{aligned} \max_{\rho\in\{|0\rangle,|1\rangle,|2\rangle\}^{\otimes 2}} \; & : \; S^{\max}(p(n_A\geq 2\cup n_B\geq 2)) \quad (9) \\ \text{s. t.} \; & : \; \rho \geq 0 \\ & \quad \text{tr}(\rho) \leq 1 \\ & \quad \left(\prod_{0/1}\rho\prod_{0/1}\right)^{T_b} \geq 0 \\ & \quad \sum_{i,j=0}^{1} p_{ij} = 1 - p(n_A\geq 2\cup n_B\geq 2). \end{aligned}$$

The constraint $\text{tr}(\rho) \leq 1$ comes from the fact that the optimization is performed over finite dimension (9×9) matrices that can either represent a physical state or that can be obtained by local projections of states spanning Hilbert spaces with a larger dimension. $\prod_{0/1}$ stands for the projection into the subspace with at most one photon locally. Eq. (9) is a linear optimization with semidefinite positive constraints which can be efficiently solved numerically [3]. The result of the optimization $S_{\rm sep}^{\max}$ is shown in Fig. 2 (main text) as a function of $p(n_A \geq 2 \cup n_B \geq 2)$. It is also given in Fig. 1 (dashed line). If a physical state that satisfies the last condition leads to a S value larger than $S_{\rm sep}^{\max}$, one concludes that the partial transpose has at least one negative eigenvalue and hence, the state is entangled and entanglement lies in the subspace with zero and one photon locally, i.e. refers to single-photon entanglement.

It is worth mentioning that if the observed CHSH value is not higher than the separable bound obtained through the optimization presented in Eqs. (9), one can still conclude about the presence of entanglement. Indeed, the optimization can be performed over the set of separable states, but not only the ones that are separable in the subspace with at most one photon locally. The constrain $\left(\prod_{0/1}\rho\prod_{0/1}\right)^{T_b} \geq 0$ simply

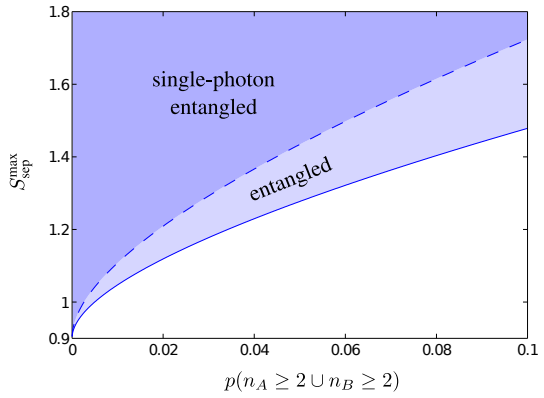

FIG. 1: Separable bound $S^{\max}_{\rm sep}$ as a function of the probability that at least one of the two protagonists gets more than one photon $p(n_A \geq 2 \cup n_B \geq 2)$. The dashed curve allows one to know the maximum value of the CHSH polynomial $S^{\max}_{\rm sep}$ that a state that is separable in the $\{|0\rangle, |1\rangle\}^{\otimes 2}$ subspace can reach. If the observed CHSH value $S_{\rm obs} > S^{\max}_{\rm sep}$, one can conclude that the projection of the state in the subspace with zero and one photon locally is entangled. The full curve give the maximum value that a separable state can reach. If the the oberved CHSH value is higher than the latter, one can conclude about entanglement but without saying where the entanglement lies.

needs to be replaced by $\rho^{T_b} \geq 0$. This leads to the second separable bound (full curve) presented in Fig. 1. If the observed CHSH value is larger than the bound obtained in this manner, one can conclude about the presence of entanglement but we cannot say in which subspace entanglement lies.

Note also that the optimization (9) does not take the individually measured probabilities $p(n_A = j)$ ($p(n_B = j)$) for having j photons in Alice's (Bob's) mode into account. These probabilities add constraints reducing the size of the set of separable states over which $S^{\max}$ is optimized and thus, provide a tighter bound $S^{\max}_{\rm sep}$. We use them for the calculation of the separable bounds related to the experiment (see the optimization (14)).

C. General procedure to follow for witnessing single-photon entanglement

Below, we present the procedure to follow in order to conclude about the presence of entanglement with the proposed witness.

- Firstly, the local photon number distributions $p(n_a = 0), p(n_b = 0), p(n_a = 1), p(n_b = 1)$ are accessed using local phase-averaged quantum state tomography.
- The joint probability $p(n_a \geq 2 \cup n_b \geq 2)$ defined by

$$p(n_a \geq 2) + p(n_b \geq 2) - p(n_a \geq 2 \cap n_b \geq 2)$$

is then upper bounded by

$$\begin{aligned} p^\star = \; & 2 - p(n_a = 0) - p(n_a = 1) \\ & - p(n_b = 0) - p(n_b = 1). \end{aligned}$$

- Thirdly, $p^\star$ is used to obtain the separable bound $S^{\max}_{\rm sep}(p^\star)$ deduced from the following optimization

$$\begin{aligned} \max_{\rho \in \{|0\rangle,|1\rangle,|2\rangle\}^{\otimes 2}} \; & : \; S^{\max}(p^\star) \\ \text{s. t.} \; & : \; \rho \geq 0 \\ & \quad \mathrm{tr}(\rho) \leq 1 \\ & \quad \left(\prod_{0/1} \rho \prod_{0/1} \right)^{T_b} \geq 0 \\ & \quad \sum_{i,j=0}^{1} p_{ij} \geq 1 - p^\star. \end{aligned} \tag{10}$$

Alternatively, $S^{\max}_{\rm sep}(p^\star)$ can simply be obtained from Fig. 2 (main text) because $S^{\max}_{sep}$ is a monotonically increasing function of $p(n_a \geq 2 \cup n_b \geq 2)$. Both methods provide an upper bound on $S^{\max}_{sep}(p(n_a \geq 2 \cup n_b \geq 2)) \leq S^{\max}_{sep}(p^\star)$.

- Fourthly, the CHSH value is measured. In principle, this is done by proposing Alice and Bob to randomly choose measurements among $\{X_{\varphi^1_A}, X_{\varphi^2_A}\}$ and $\{X_{\varphi^1_B}, X_{\varphi^2_B}\}$ respectively and to subsequently compute the CHSH polynomial. However, since $E_{X_{\varphi^1_A}, X_{\varphi^1_B}} = -E_{X_{\varphi^2_A}, X_{\varphi^2_B}}$ and $E_{X_{\varphi^1_A}, X_{\varphi^2_B}} = E_{X_{\varphi^2_A}, X_{\varphi^1_B}}$, S_{obs} can be obtained in practice from the measurements of two correlators only

$$S_{obs} = 2E_{X_{\varphi^1_A}, X_{\varphi^1_B}} + 2E_{X_{\varphi^1_A}, X_{\varphi^2_B}}. \tag{11}$$

- Finally, S_{obs} and $S^{\max}_{sep}(p^\star)$ are compared. If $S_{obs} > S^{\max}_{sep}(p^\star)$ (which implies that $S_{obs} > S^{\max}_{sep}(p(n_a \geq 2 \cup n_b \geq 2))$), one concludes that the measured state is entangled at the single-photon level. Otherwise, we cannot form a conclusion, the state can either be separable or entangled.

II. EXPERIMENTAL DETAILS

A. Heralded creation of single-photon entanglement

A continuous-wave frequency-doubled Nd:YAG laser (Diabolo, Innolight) pumps a triply-resonant type-II phase-matched optical parametric amplifier based on a KTP crystal to generate below threshold, a two-mode squeezed state [4]. The created modes are orthogonally

polarized and are deterministically separated at the output of the amplifier. One of the two modes is send to a single-photon detector (superconducting single-photon detector, with a quantum efficiency of 7% at 1064nm) after filtering of the non-degenerate modes. A detection event ideally heralds the generation of a single-photon state on the twin mode. The heralding rate is around 30 kHz. (See [5] for more details about the source). By controlling the polarization of the heralded photon via a half-wave plate and by subsequently sending it into a polarizing beam splitter (PBS), one gets a versatile source producing states of the form

$$|\psi(\theta)\rangle_{AB} = \cos(2\theta)|0\rangle_A|1\rangle_B + \sin(2\theta)|1\rangle_A|0\rangle_B \qquad (12)$$

where θ is the angle of the half-wave plate relative to the axis of the PBS. For $\theta = 0°$, the created state is separable, whereas for $\theta = 22.5°$ it becomes maximally entangled. This source is thus particularly well suited to test the proposed entanglement witness.

B. Homodyning

Each spatial mode is then detected using an independent homodyne detection. The required local oscillators are obtained by impinging a bright beam into the second input of the PBS. The phase of Alice's local oscillator is controlled relative to Bob's one by choosing appropriately the polarization of the bright beam just before the PBS [6]. To meet the witness requirements, a phase averaging is realized by sweeping a piezoelectric transducer located on the path of the bright beam before the PBS. The overall efficiency of each homodyne detection is 85%, including the quantum efficiency of the photodiodes (Fermionics 500), mode overlap and electronic noise [7].

C. Data acquisition

For each heralding event, Alice and Bob perform a quadrature measurement and the corresponding result is extracted from homodyne photocurrents. 200000 events are accumulated for each relative phase $\Delta\varphi_{AB}^{11} = \frac{\pi}{4}$ and $\Delta\varphi_{AB}^{12} = -\frac{\pi}{4}$. S_{obs} is then deduced from Eq. (11). The same results are also used to compute the local photon number distributions by phase-averaged quantum state tomography using the method given in [8]. We remind that this method does not require assumptions on the the dimension of the measured state. Table 2 shows the results for various angles θ. Alternatively, a MaxLike algorithm [9] can be used to access the local photon number distribution, albeit with a truncation of the Fock space.

D. Error estimations

Several kind of errors should be taken into account.

Firstly, statistical errors affect the measured value of the CHSH polynomial S_{obs}. These errors are estimated in a standard way by using the central limit theorem. They are basically very small (see Table 2) because they were deduced from 200000 results.
Secondly, the accuracy with which the relative phase $\Delta\varphi_{AB}^{\ell\bar{\ell}}$ between Alice & Bob's measurements is estimated to be 2°. This means that when Alice and Bob choose measurement settings, e.g. corresponding ideally to the quadratures $X_{\varphi_A^1}$-$X_{\varphi_B^1}$, the relative phase $\Delta\varphi_{AB}^{11}$ is not exactly equal to $\frac{\pi}{4}$ as it should be, but $\Delta\varphi_{AB}^{11} = \frac{\pi}{4} + \epsilon^{11}$ where $-1° \leq \epsilon^{11} \leq 1°$. This error is taken into account into the separability bound.
Thirdly, errors also affect the local photon-number probability distributions, which are estimated using the phase-averaged homodyne measurements [8]. Evaluating these errors is a not trivial task. We use the following method for estimating the overall error. The tomography that we use to access the local photon number distributions leaves us with the diagonal elements of an estimated density matrix ρ_{estimate}. Using this matrix, we simulate the quadrature data, then reconstruct the diagonal elements of a simulated density matrix ρ_{simul}. The approach is repeated 200 times, always from the same initial state ρ_{estimate}. This generates a random set of 200 data points for each local probability $p(n_A = 0), p(n_B = 0), p(n_A = 1), p(n_B = 1)\ldots$ and the corresponding standard deviation provides the desired error $\delta p(n_A = 0), \delta p(n_B = 0), \delta p(n_A = 1), \delta p(n_B = 1)\ldots$

We now show how the errors on the measurement angles $\epsilon^{\ell\bar{\ell}}$ and on the local photon-number probability distributions $\delta p(n_A = i), \delta p(n_B = j)$ have been taken into account in the calculation of the separable bound $S_{sep}^{\max}$. Since, in practice, it is necessary to measure two correlators only, the separable bound can be calculated under the assumption that the measurements that have been performed are such that

$$\Delta\varphi_{AB}^{11} = -\frac{\pi}{4} + \epsilon^{11}, \Delta\varphi_{AB}^{22} = \frac{3\pi}{4} + \epsilon^{11},$$
$$\Delta\varphi_{AB}^{12} = \Delta\varphi_{AB}^{21} = \frac{\pi}{4} + \epsilon^{12},$$

i.e. that the errors are the same for $\Delta\varphi_{AB}^{11}$ and $\Delta\varphi_{AB}^{22}$ and for $\Delta\varphi_{AB}^{12}$ and $\Delta\varphi_{AB}^{21}$. These erroneous measurement angles yield to an upper bound $S^{\max}$ (which replaces the one in Eq. (8)) given by

$$\begin{aligned} S \leq\ & S^{\max}(p(n_A \geq 2 \cup n_B \geq 2), \epsilon^{11}, \epsilon^{12}) \\ &= \frac{4}{\pi}\left(\Re\Big[\langle 10|\rho|01\rangle\Big] \times C - \Im\Big[\langle 10|\rho|01\rangle\Big] \times D\right) \\ &+ \frac{4}{\sqrt{2}\pi}\Re\Big[\langle 20|\rho|11\rangle + \langle 11|\rho|02\rangle\Big] \times C \\ &- \frac{4}{\sqrt{2}\pi}\Im\Big[\langle 20|\rho|11\rangle + \langle 11|\rho|02\rangle\Big] \times D \\ &+ 2\sqrt{2} \times p(n_A \geq 2 \cup n_B \geq 2) \end{aligned} \qquad (13)$$

angle	Alice p_0	error	Alice p_1	error	Alice p>1	error	Bob p_0	error	Bob p_1	error	Bob p>1	error	p*	error	S_{obs}	error	S_{sep}^{max}
0	**99.8**	0.1	**0.2**	0.1	**0.01**	0.01	**30.6**	0.2	**65.4**	0.3	**3.94**	0.19	**3.9**	0.262	**0.104**	0.001	0.235
5	**98.9**	0.2	**1.1**	0.2	**0.06**	0.04	**30.6**	0.2	**65.5**	0.3	**3.84**	0.20	**3.9**	0.258	**0.353**	0.003	0.355
10	**92.9**	0.2	**7.0**	0.2	**0.10**	0.06	**36.9**	0.2	**60.4**	0.3	**2.70**	0.18	**2.8**	0.274	**0.776**	0.004	0.643
15	**83.6**	0.2	**16.1**	0.2	**0.32**	0.10	**45.6**	0.2	**52.1**	0.3	**2.28**	0.17	**2.6**	0.294	**1.085**	0.004	0.893
20	**72.3**	0.2	**27.2**	0.3	**0.54**	0.13	**55.5**	0.2	**43.2**	0.3	**1.26**	0.17	**1.8**	0.314	**1.289**	0.004	1.017
22.5	**65.0**	0.2	**34.0**	0.3	**0.95**	0.16	**63.1**	0.2	**35.8**	0.3	**1.06**	0.16	**2.0**	0.338	**1.326**	0.004	1.060
25	**59.4**	0.2	**39.3**	0.3	**1.33**	0.17	**67.3**	0.2	**31.8**	0.3	**0.90**	0.13	**2.2**	0.312	**1.330**	0.004	1.072
30	**48.3**	0.2	**49.6**	0.3	**2.17**	0.17	**78.2**	0.2	**21.3**	0.2	**0.47**	0.10	**2.6**	0.292	**1.235**	0.004	0.989
35	**38.8**	0.2	**58.4**	0.3	**2.77**	0.18	**89.5**	0.2	**10.5**	0.2	**0.05**	0.06	**2.8**	0.283	**0.951**	0.004	0.755
40	**32.2**	0.2	**64.2**	0.3	**3.66**	0.20	**96.9**	0.2	**3.1**	0.2	**0.05**	0.04	**3.7**	0.265	**0.527**	0.003	0.493
45	**30.1**	0.2	**66.3**	0.3	**3.59**	0.19	**99.7**	0.1	**0.2**	0.1	**0.02**	0.01	**3.6**	0.224	**0.112**	0.001	0.233

FIG. 2: Results of local measurements versus the angle of the half-wave plate relative to the axis of the PBS. The table on the left gives the photon number distribution in Alice's location. (p_0, p_1, $p > 1$ denote the probability that zero $p(n_A = 0)$, one $p(n_A = 1)$ and more than one photon $p(n_A \geq 2)$ occupy Alice's mode. The second table gives Bob's results. The two last tables give an upper bound on the probability that at least one of the two protagonists gets more than one photon $p(n_A \geq 2 \cup n_B \geq 2)$ and the observed CHSH value S_{obs}.)

where $\Im$ denotes the imaginary part and

$$C = 2\left(\cos(\epsilon^{11} - \frac{\pi}{4}) + \cos(\epsilon^{12} + \frac{\pi}{4})\right),$$
$$D = 2\left(\sin(\epsilon^{11} - \frac{\pi}{4}) + \sin(\epsilon^{12} + \frac{\pi}{4})\right).$$

$S^{\max}$ can now be optimized over the set of separable states, as before. If one takes into account the local photon number probability distribution and the errors as well, one ends up with the following optimization problem

$$\begin{aligned}
max \ : \ & S^{\max}(p^\star, \epsilon^{11}, \epsilon^{12}) \qquad (14)\\
s.t. \ : \ & \rho \geq 0\\
& \mathrm{tr}(\rho) \leq 1\\
& \left(\prod_{0/1} \rho \prod_{0/1}\right)^{T_b} \geq 0\\
& -1^\circ \leq \epsilon^{11}, \epsilon^{12} \leq +1^\circ\\
& p_{00} + p_{10} + p_{01} + p_{11} \geq 1 - p^\star - \delta p^\star\\
& p_{00} + p_{01} + p_{02} \leq p(n_A = 0) + \delta p(n_A = 0)\\
& p_{10} + p_{11} + p_{12} \leq p(n_A = 1) + \delta p(n_A = 1)\\
& p_{20} + p_{21} + p_{22} \leq p(n_A > 1) + \delta p(n_A > 1)\\
& p_{00} + p_{10} + p_{20} \leq p(n_B = 0) + \delta p(n_B = 0)\\
& p_{01} + p_{11} + p_{21} \leq p(n_B = 1) + \delta p(n_B = 1)\\
& p_{02} + p_{12} + p_{22} \leq p(n_B > 1) + \delta p(n_B > 1)
\end{aligned}$$

In addition to errors, we emphasize that the previous optimization uses the knowledge of each local photon number probability $p(n_A = 0)$, $p(n_A = 1)\ldots$ This provides a tighter separable bound as compared to the optimization summarized in Eq. (10).

Note that the optimization (14) is non-linear in ϵ^{11} and ϵ_{12}. Hence, the result cannot be obtained with standard semidefinite solvers. However, one can convince oneself that the maximum value of $S^{\max}_{sep}(p^\star, \epsilon^{11}, \epsilon^{12})$ is obtained for the extremal choice $\epsilon^{11} = 1^\circ$, $\epsilon^{12} = -1^\circ$. This can be understood intuitively since this choice brings the settings closer to each other and thus, helps in increasing the CHSH value. Note that the linearity of the optimization is recovered once the values of $\{\epsilon^{11}, \epsilon^{12}\}$ are fixed. The results of the optimization for $\epsilon^{11} = 1^\circ$ and $\epsilon^{12} = -1^\circ$ are shown in Fig. 4 (main text).

[1] A. Peres, Phys. Rev. Lett. **77**, 1413 (1996).

[2] M. Horodecki, P. Horodecki, R. Horodecki, Phys. Lett. A **223**, 1 (1996).

[3] S. Boyd and L. Vandenberghe, *Convex optimization* Cambridge University Press (2004).

[4] J. Laurat, T. Coudreau, G. Keller, N. Treps, C. Fabre, Phys. Rev. A **70**, 042315 (2004).

[5] O. Morin, V. D'Auria, C. Fabre, J. Laurat, Opt. Lett. **37**,

3738 (2012).
[6] J. Laurat, T. Coudreau, G. Keller, N. Treps, C. Fabre, Phys. Rev. A **71**, 022313 (2005).
[7] R. Kumar, E. Barrios, A. MacRae, E. Cairns, E.H. Huntington, A.I. Lvovsky, eprint arXiv:1111.4012.
[8] M. Munroe, D. Boggavarapu, M.E. Anderson, M.G. Raymer, Phys. Rev. A **52**, R924 (1995).
[9] A.I. Lvovsky, M.G.Raymer, Rev. Mod. Phys. **81**, 299 (2009).

Paper E

Witnessing single-photon entanglement with local homodyne measurements: analytical bounds and robustness to losses

Melvyn Ho, Olivier Morin, Jean-Daniel Bancal, Nicolas Gisin,
Nicolas Sangouard and Julien Laurat

New Journal of Physics **16**, 103035 (2014)

New Journal of Physics
The open access journal at the forefront of physics
Deutsche Physikalische Gesellschaft DPG | IOP Institute of Physics

Witnessing single-photon entanglement with local homodyne measurements: analytical bounds and robustness to losses

Melvyn Ho[1,4,5], Olivier Morin[2,5], Jean-Daniel Bancal[1], Nicolas Gisin[3], Nicolas Sangouard[3,4] and Julien Laurat[2]

[1] Centre for Quantum Technologies, National University of Singapore, 3 Science Drive 2, Singapore 117543
[2] Laboratoire Kastler Brossel, UPMC Univ Paris 6, Ecole Normale Supérieure, CNRS, Collège de France, 4 place Jussieu, 75252 Paris Cedex 05, France
[3] Group of Applied Physics, University of Geneva, CH-1211 Geneva 4, Switzerland
[4] Department of Physics, University of Basel, CH-4056 Basel, Switzerland
E-mail: julien.laurat@upmc.fr

Received 2 June 2014, revised 25 July 2014
Accepted for publication 29 August 2014
Published 24 October 2014
New Journal of Physics **16** (2014) 103035
doi:10.1088/1367-2630/16/10/103035

Abstract

Single-photon entanglement is one of the primary resources for quantum networks, including quantum repeater architectures. Such entanglement can be revealed with only local homodyne measurements through the entanglement witness presented in Morin *et al* (2013 *Phys. Rev. Lett.* **110** 130401). Here, we provide an extended analysis of this witness by introducing analytical bounds and by reporting measurements confirming its great robustness with regard to losses. This study highlights the potential of optical hybrid methods, where discrete entanglement is characterized through continuous-variable measurements.

Keywords: entanglement witness, single-photon, homodyne detection

[5] These authors contributed equally to this work.

1. Introduction

Important developments have recently been made in the optical hybrid approach to quantum information, which consists of mixing in a protocol both discrete and continuous degrees of freedom. These developments include advancements in quantum state engineering, state characterization, and long-distance communication architectures [1–6].

Based on this approach, a witness for single-photon entanglement [7–10], namely states of the form $|1\rangle_A|0\rangle_B + |0\rangle_A|1\rangle_B$ where A and B are two spatial modes sharing a delocalized single-photon, has recently been proposed and experimentally tested [11]. It relies only on homodyne detections (i.e., on continuous quadrature measurements and not on photon counting) and offers significant advantages relative to other witnessing methods [12–15]. Indeed, unlike most steering experiments [16], it does not require postselection and does not assume knowledge of the underlying Hilbert space dimension. Also, in contrast with other entanglement witnesses [17], it specifically identifies the entanglement present in the single-photon subspace. Finally, the measurements are only operated locally on the entangled modes, an important feature if applied to large-scale networks [18, 19].

The witness presented in [11] was built up on numerical arguments. In the present work, we extend its analysis by means of analytical calculations. The aim is to gain insight into the properties of the witness with respect to various practical imperfections. In particular, we theoretically and experimentally investigate its robustness with regard to channel loss or, equivalently, to imperfect single-photon states used as the initial resource for entanglement generation. We demonstrate that even for a large admixture of vacuum, our witness reveals the presence of entanglement, confirming its suitability for use in realistic networks and entanglement distribution protocols where losses are inherent.

The paper is organized as follows. Section 2 gives an overview of the single-photon entanglement witness based on local homodyne measurements. Then, in the case where the state only contains vacuum and single-photon components (i.e., the state lies within a qubit subspace) the witness parameter is evaluated and compared to the separable bound. Symmetric and asymmetric channels are considered. In section 3, multiphoton components, which are critical in experimental realizations, are taken into account. We show, in particular, how the witness is extended to this realistic case by experimentally bounding the Hilbert space, and we then derive the effect of losses in the communication channels. This study leads to several expressions for the separable bound. The setup and experimental results are presented in section 4, and we give our conclusions in section 5.

2. Principle of the witness

This section presents the principle of the single-photon entanglement witness, which relies only on local homodyne measurements, as proposed and demonstrated in [11]. We then introduce the specific focus of this paper: the behavior of this witness in the presence of loss, coming equivalently from a single-photon generated with non-unity efficiency or subsequent losses in the communication channels. In this section, the state is assumed to belong to the qubit subspace, $\{|0\rangle, |1\rangle\}^{\otimes 2}$. This simplistic restriction allows us to understand the main features of the witness before generalizing the discussion to include multiphoton components.

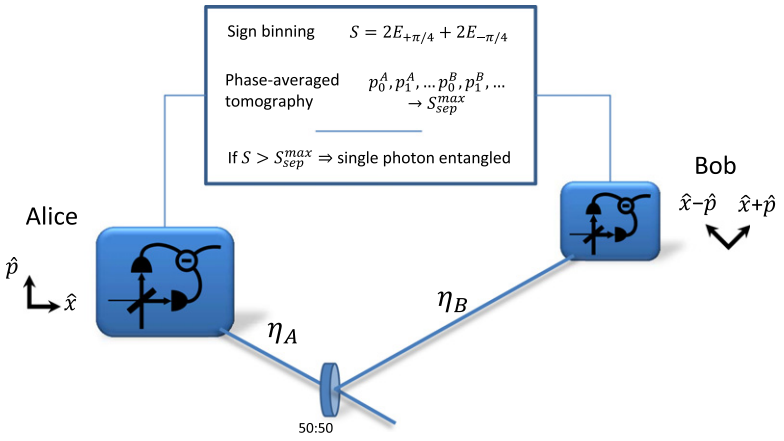

Figure 1. Principle of the entanglement witness. Single-photon entanglement is generated by impinging a single-photon state onto a 50/50 beam-splitter. Symmetric or asymmetric losses are then induced by the communication channels, with transmission efficiencies denoted by η_A and η_B. To witness the entanglement, the two distant parties, Alice and Bob, randomly choose a measurement along two quadratures (for instance, $\{X, P\}$ for Alice and $\{X + P, X - P\}$ for Bob). The phase of the local oscillators are phase averaged; only the relative phase between the two detections is fixed. Sign-binning of the quadrature measurements enables them to calculate the witness parameter S, which has to be compared to the separability bound, $S_{\text{sep}}^{\max}$. This bound depends on the multi-photon components and can be optimized by using the local probabilities, which can be directly accessed from the same data as a result of the phase-averaging.

2.1. A Bell test scenario with local homodyning

The general principle of the witness is shown in figure 1. The two distant entangled modes are detected by Alice and Bob via homodyne detection, which allows one to measure any quadrature component of the optical field (i.e., $X\cos(\phi) + P\sin(\phi)$) by varying the relative phase, ϕ, between the optical mode and the local oscillator [20]. Two phase settings are required on each side: Alice performs a measurement among two quadratures, $\{X, P\}$, while Bob makes a measurement in a basis rotated by 45° to access the quadratures $\{X + P, X - P\}$. The measurement outcomes, which are real numbers, are then sign-binned to obtain binary results ± 1. The scenario is thus similar to the usual Bell test, where two parties can perform two possible measurements of two outcomes each. From the four possible combinations of quadratures, the witness parameter, S, is finally determined from the Clauser–Horne–Shimony–Holt (CHSH) polynomial [21],

$$S = E_{X,X+P} + E_{X,X-P} + E_{P,X+P} - E_{P,X-P}, \tag{1}$$

where the correlations are defined by $E_{a,b} = p(1, 1) + p(-1, -1) - p(1, -1) - p(-1, 1)$, and $p(i, j)$ are the conditional probabilities to obtain the outcomes i and j if the quadratures a and b are chosen.

Additionally, the phase of the local oscillators can be averaged while keeping the relative phases between Alice and Bob's measurements fixed. This averaging can only lead to an underestimation of the entanglement, as it can be realized by local operations and classical communications. The S parameter reduces thus to two terms—one where the relative phase differs by $\frac{\pi}{4}$, and the other by $-\frac{\pi}{4}$:

$$S = 2E_{+\pi/4} + 2E_{-\pi/4}. \tag{2}$$

As shown in [11], this phase-averaging is actually crucial in the protocol, as it enables us to access the local photon-number probabilities with the same homodyne measurements. These probabilities are then used to further constrain the set of density matrices that we consider in our optimization of the separable bounds.

2.2. Extremal values of the witness for entangled states

Sign-binning of homodyne measurement in the qubit subspace, $\{|0\rangle, |1\rangle\}^{\otimes 2}$, is equivalent with a noisy spin measurement [22, 23]. For instance, the operator associated with a sign-binned X-measurement corresponds to $\sqrt{2/\pi}\,\hat{\sigma}_x$, where $\hat{\sigma}_x$ is the standard Pauli matrix. A maximally entangled state, $(|1\rangle|0\rangle + |0\rangle|1\rangle)/\sqrt{2}$, thus leads to $S_{\max} = 2\sqrt{2}\ .2/\pi \simeq 1.8$, the maximal value that one can obtain using the aforementioned measurements. Note that since this value is lower than 2, a violation of the well-known local bound for the CHSH polynomial is not possible in this context. While this would have been sufficient to demonstrate entanglement, it is not necessary if the separable bound is lower.

The next question that arises is the value of the separable bound. It can be shown that the maximal value over the set of all the separable states is equal to $S_{\text{sep}} = \sqrt{2}\ .2/\pi \simeq 0.9$ [24]. In the qubit space, an observed S parameter above 0.9 allows one to conclude that the two modes are entangled. Importantly, this separable bound can be optimized further if additional knowledge about the state is available, as this knowledge constrains the set of compatible separable states. In our case, the phase-averaged homodyne measurements provide the local photon number distributions. These local photon-number distributions, p_0^A, p_1^A (vacuum and single-photon component on the Alice side) and p_0^B, p_1^B (Bob side), allow us to optimize the bound, as we will now show.

First, thanks to the averaging of the local phases, many off-diagonal terms of the measured state do not contribute to the measurement results. Since our goal is to reveal entanglement, it is therefore sufficient to consider density matrices of the following form in the Fock basis [13]:

$$\hat{\rho} = \begin{pmatrix} p_{00} & 0 & 0 & 0 \\ 0 & p_{01} & \boldsymbol{d} & 0 \\ 0 & \boldsymbol{d}^* & p_{10} & 0 \\ 0 & 0 & 0 & p_{11} \end{pmatrix}. \tag{3}$$

Then, for any state within the qubit subspace, it can be shown that the S parameter can be rewritten as [11]

$$S = \frac{16}{\pi\sqrt{2}}\Re\left[\langle 01|\,\hat{\rho}\,|10\rangle\right] = \frac{16}{\pi\sqrt{2}}\Re[\boldsymbol{d}]. \tag{4}$$

When Alice and Bob measure the value of S, they can also extract the local probabilities, p_0^A and p_0^B, from the quadrature measurements. Hence, only a reduced set of states are compatible with these probabilities. It can be translated formally as:

- $p_0^A = p_{00} + p_{01}$ and $p_0^B = p_{00} + p_{10}$ (relationship between joint probabilities and local probabilities)
- $\text{Tr}\,[\hat{\rho}] = 1$ (conservation of probabilities)

- $\hat{\rho} \geqslant 0$ (physical state, all eigenvalues are positive, i.e., $p_{01}p_{10} \geqslant |\boldsymbol{d}|^2$)
- $0 \leqslant p_{ij} \leqslant 1$ (regular probabilities)

The maximization of $|\boldsymbol{d}|$ under all these constraints gives the upper bound, $S^{\max}$, for the witness parameter,

$$S^{\max} = \frac{16}{\pi\sqrt{2}} \begin{cases} \sqrt{p_0^A p_0^B} & \text{if } p_0^A + p_0^B \leqslant 1, \\ \sqrt{\left(1 - p_0^A\right)\left(1 - p_0^B\right)} & \text{if } p_0^A + p_0^B \geqslant 1. \end{cases} \tag{5}$$

We now derive the separable bound, $S_{\text{sep}}^{\max}$. Separable states remain positive under partial transposition (PPT criterion) [25, 26]. This additional constraint leads to the condition $|\boldsymbol{d}|^2 \leqslant p_{00}p_{11}$ for separable states. Hence, the maximization of $|\boldsymbol{d}|$ provides the maximal value of S but, this time, for the separable states only,

$$S_{\text{sep}}^{\max} = \frac{16}{\pi\sqrt{2}} \sqrt{p_0^A p_0^B \left(1 - p_0^A\right)\left(1 - p_0^B\right)}. \tag{6}$$

2.3. Witnessing single-photon entanglement after losses

We now study the use of the proposed witness in the case where the entangled state undergoes loss (e.g., propagates through lossy communication channels). What are the acceptable losses in this case? With the help of the analytical bounds derived previously, we detail how the proposed witness is affected.

The situation is sketched in figure 1. We consider the entanglement to be initially generated from an ideal single-photon state, and the channel transmissions are denoted by η_A from the source to Alice, and η_B from the source to Bob. One can write the full transmission between Alice and Bob as $\eta_{AB} = \eta_A\eta_B$. After propagation, the resulting state shared by Alice and Bob can be written as

$$\hat{\rho}_{AB} = \frac{1}{2} \begin{pmatrix} 2 - \eta_A - \eta_B & 0 & 0 & 0 \\ 0 & \eta_A & \sqrt{\eta_A\eta_B} & 0 \\ 0 & \sqrt{\eta_A\eta_B} & \eta_B & 0 \\ 0 & 0 & 0 & 0 \end{pmatrix}. \tag{7}$$

As given by equation (4), the CHSH polynomial value, S, can be written as

$$S\left(\hat{\rho}_{AB}\right) = \frac{16}{\pi\sqrt{2}} \frac{\sqrt{\eta_A\eta_B}}{2}. \tag{8}$$

Furthermore, the local probabilities are given by

$$p_1^A = \eta_A/2 \quad \text{and} \quad p_1^B = \eta_B/2. \tag{9}$$

The maximal value of equation (5) is saturated by the state given in equation (7), and the corresponding separable bound is

$$S_{\text{sep}}^{\max} = \frac{8}{\pi\sqrt{2}} \sqrt{\eta_A\eta_B\left(1 - \eta_A/2\right)\left(1 - \eta_B/2\right)}. \tag{10}$$

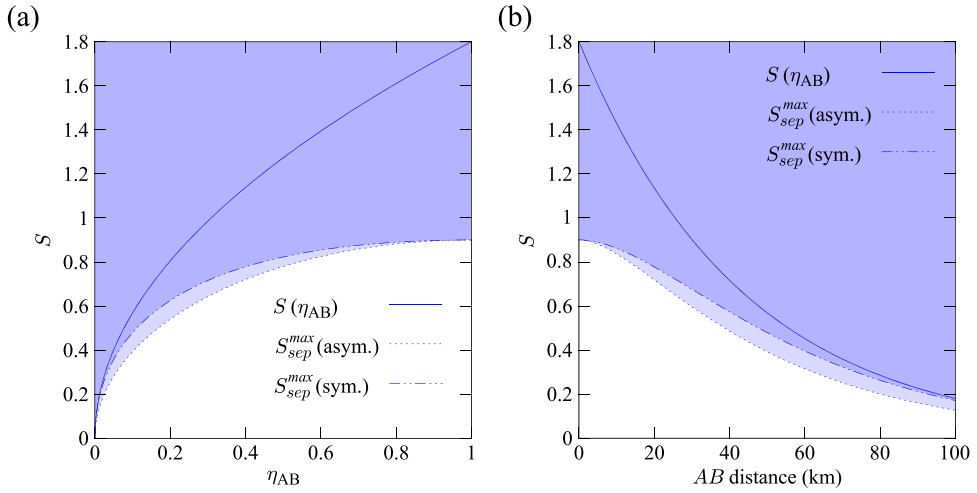

Figure 2. (a) Values of the CHSH parameter, S, and of the separable bounds, $S_{\text{sep}}^{\max}$, when applied to single-photon entanglement propagated through lossy communication channels. Two cases are considered: when the total losses are only on one transmission channel (asymmetric case, $\eta_A = 1$ and $\eta_B = \eta_{AB}$) and when the losses are symmetric on the two channels ($\eta_A = \eta_B = \sqrt{\eta_{AB}}$). (b) The figure corresponds to the same results, but with a scale given in kilometers of propagation in a fiber at telecom wavelength (0.2 dB-per-km loss).

With this simple model in hand, one can distinguish two different experimental scenarios. First, when the source is placed on Alice's site, the losses are thus asymmetric, and $\eta_A = 1$ and $\eta_B = \eta_{AB}$. For this configuration, the separable bound is

$$S_{\text{sep}}^{\max}\ (asym.\ ) = \frac{4}{\pi}\sqrt{\eta_{AB}\left(1 - \eta_{AB}/2\right)}\ . \tag{11}$$

The second scenario places the source at an equal distance from Alice and Bob, so that the state will propagate along the same distance on both arms. The two modes are thus affected by the same losses, $\eta_A = \eta_B = \sqrt{\eta_{AB}}$, leading to the following separable bound:

$$S_{\text{sep}}^{\max}\ (sym.\ ) = \frac{8}{\pi\sqrt{2}}\sqrt{\eta_{AB}}\left(1 - \sqrt{\eta_{AB}}/2\right)\ . \tag{12}$$

In order to compare both cases, we fix the full transmission, $\eta_{AB} = \eta_A\eta_B$. In other words, the position of the source changes, but the total distance between Alice and Bob does not. Furthermore, we note that the symmetric situation can equivalently correspond to losses on the source itself. Indeed, it is formally equivalent to attribute these losses to the two transmission channels.

Figure 2 provides the CHSH polynomial as a function of the transmission, together with the two separable bounds. As shown before, the parameter S depends only on the total loss, while the separable bound additionally depends on whether the losses are symmetric or asymmetric. As we can see, the distance between the witness and the bound decreases with the losses but reaches zero only for infinite ones, meaning that in principle the witness can detect entanglement for any losses. Furthermore, we note that the distance of S from the separable bound is always larger for the asymmetric case than for the symmetric case. The witness is thus slightly more efficient in the latter case.

3. Including higher photon numbers: general case

In the previous section, the separable bound was determined by considering that the state contains at most one photon per mode. However, states produced in a setup generally include multiphoton components that must be critically taken into account. We present here separable bounds, which can be used in this case. Namely, we provide three such expressions. Each one has different strengths, which we summarize in the last part of this section. We first present the approach we use to bound the possible effect of multiphoton components on the witness, S.

3.1. Bounding the Hilbert space

When the number of photons per mode is not restricted to one, we use the local photon number distributions obtained via phase-averaged quantum state tomography to determine an upper bound on the joint probability, $p_{\text{joint}} = p(n_A \geqslant 2 \cup n_B \geqslant 2)$, so that at least one of the modes is populated with more than one photon. Indeed, this probability can be bounded by the local probabilities of the zero and one-photon components on each side as

$$p_{\text{joint}} \leqslant p^{\star}, \tag{13}$$

where $p^{\star} = p_{\geqslant 2}^{A} + p_{\geqslant 2}^{B}$ and $p_{\geqslant 2}^{A(B)} = 1 - p_0^{A(B)} - p_1^{A(B)}$, denoting the probability that one party observes at least two photons.

In the following, we present some separable bounds in terms of p_{joint}. These can be re-expressed in terms of local photon distributions by substituting $p^{\star}$ for p_{joint}, thus slightly overestimating the bound.

3.2. A first separable bound as a function of the local probabilities

Following a similar argument as presented in section 2.2, we provide here a separable bound for S that is valid outside of the qubit space.

In this larger Hilbert space, S can be bounded as follows (see [11]):

$$S \leqslant \frac{16}{\pi\sqrt{2}} d + \frac{8}{\pi} e + \frac{8}{\pi} f + 2\sqrt{2}\, p_{\text{joint}}, \tag{14}$$

where $d = \Re\big[\langle 01|\hat{\rho}|10\rangle\big]$, $e = \Re\big[\langle 20|\hat{\rho}|11\rangle\big]$, and $f = \Re\big[\langle 02|\hat{\rho}|11\rangle\big]$ denote different contributions to the witness. Due to the positivity of $\hat{\rho}$ and $\hat{\rho}^{T_B(0,1)}$, each of these contributions can be bounded as a function of a single density matrix variable p_{00}:

$$d^2 \leqslant p_{01}p_{10} \leqslant \left(p_0^{A} - p_{00}\right)\left(p_0^{B} - p_{00}\right) \tag{15}$$

$$d^2 \leqslant p_{00}p_{11} \leqslant p_{00}\left[p_{00} + 1 - p_0^{A} - p_0^{B} + p_{\geqslant 2}^{A} + p_{\geqslant 2}^{B}\right] \tag{16}$$

$$e^2 \leqslant p_{02}p_{11} \leqslant p_{\geqslant 2}^{B}\left[p_{00} + 1 - p_0^{A} - p_0^{B} + p_{\geqslant 2}^{A} + p_{\geqslant 2}^{B}\right] \tag{17}$$

$$f^2 \leqslant p_{20}p_{11} \leqslant p_{\geqslant 2}^{A}\left[p_{00} + 1 - p_0^{A} - p_0^{B} + p_{\geqslant 2}^{A} + p_{\geqslant 2}^{B}\right]. \tag{18}$$

The maximum value of S_{sep} can thus be obtained by optimizing equation (14) over the p_{00} variable. Recall that here, we do not impose the state $\hat{\rho}$ to be fully PPT, but only PPT within the

0/1 subspace. This allows us to verify the presence of entanglement in the single-photon subspace [11].

For small $p_{\geqslant 2}^{A(B)}$, the choice $p_{00}^{c} = p_0^{A} p_0^{B}/z$ is optimal, where $z = 1 + p_{\geqslant 2}^{A} + p_{\geqslant 2}^{B}$. This gives the following separable bound:

$$\begin{aligned} S_{\text{sep}}^{\max} &= \frac{16}{\pi\sqrt{2}}\sqrt{p_0^{A} p_0^{B}\left(1 - \frac{p_0^{B}}{z}\right)\left(1 - \frac{p_0^{A}}{z}\right)} \\ &\quad + \frac{8}{\pi}\left(\sqrt{p_{\geqslant 2}^{A}} + \sqrt{p_{\geqslant 2}^{B}}\right)\sqrt{z + \frac{p_0^{A} p_0^{B}}{z} - p_0^{A} - p_0^{B}} \\ &\quad + 2\sqrt{2}\, p_{\text{joint}}. \end{aligned} \tag{19}$$

One can verify that this expression reduces to the qubit bound given by equation (6) in the case $p_{\geqslant 2}^{A(B)} = 0$. Equation (19) provides an analytical estimation of the value of the witness needed to demonstrate single-photon entanglement as a function of the local observed probabilities. We emphasize that this bound is also valid in the presence of multiphoton components.

3.3. Separable bound as a function of p_{joint}

Here we derive a separable bound which only depends on the p_{joint} variable. Writing matrices M and N such that

$$\begin{aligned} \text{Tr}\left(M\hat{\rho}\right) &= \frac{16}{\pi\sqrt{2}}\Re\left[\left\langle 01\middle|\hat{\rho}\middle|10\right\rangle\right] + \frac{8}{\pi}\left(\Re\left[\left\langle 20\middle|\hat{\rho}\middle|11\right\rangle\right] + \Re\left[\left\langle 02\middle|\hat{\rho}\middle|11\right\rangle\right]\right) \\ \text{Tr}\left(N\hat{\rho}\right) &= \langle 00|\hat{\rho}|00\rangle + \langle 01|\hat{\rho}|01\rangle + \langle 10|\hat{\rho}|10\rangle + \langle 11|\hat{\rho}|11\rangle, \end{aligned} \tag{20}$$

the maximum separable value of equation (14) given p_{joint} can be found by maximizing $\text{tr}\,(M\hat{\rho}) + 2\sqrt{2}p_{\text{joint}}$ under the constraints $\hat{\rho} \geqslant 0$, $\text{tr}\,(\hat{\rho}) \leqslant 1$, $\hat{\rho}^{T_B(0,1)} \geqslant 0$, and $\text{tr}\,(N\hat{\rho}) = 1 - p_{\text{joint}}$.

Any matrices A and B, and variables λ and μ that satisfy $A + B^{T_B(0,1)} - \mu N - \lambda I = -M$, $A \geqslant 0$, $B \geqslant 0$ can provide an upper bound on the result of this optimization. Indeed, these constraints guarantee that

$$\begin{aligned} \text{tr}\left(M\hat{\rho}\right) &= \text{tr}\left[\left(\lambda I + \mu N - A - B^{T_B(0,1)}\right)\hat{\rho}\right] \\ &= \lambda\ \text{tr}\left(\hat{\rho}\right) + \mu\ \text{tr}\left(N\hat{\rho}\right) - \text{tr}\left(A\hat{\rho}\right) - \text{tr}\left(B\hat{\rho}^{T_B(0,1)}\right) \\ &\leqslant \lambda + \mu\left(1 - p_{\text{joint}}\right). \end{aligned} \tag{21}$$

In the appendix, we describe matrices A and B that satisfy these constraints for $p_{\text{joint}} \leqslant 1/2$, $\lambda = \frac{2}{\pi}\sqrt{\frac{2}{p_{\text{joint}}}}x_+$, $\mu = \left(\frac{2}{\pi}\sqrt{2}x_+^2 - \lambda\right)\Big/(1 - p_{\text{joint}})$, and $x_\pm = \sqrt{1 - p_{\text{joint}}} \pm \sqrt{p_{\text{joint}}}$. This gives the following maximum for the separable bound:

$$S_{\text{sep}}^{\max} = 2\sqrt{2}\left[\frac{1}{\pi}\left(\sqrt{1 - p_{\text{joint}}} + \sqrt{p_{\text{joint}}}\right)^2 + p_{\text{joint}}\right]. \tag{22}$$

One can check that this bound is achievable for all $p_{\text{joint}} \leqslant 1/2$ by some quantum states $\hat{\rho}$, which are PPT in the single-photon subspace. This guarantees that the bound is tight as a function of p_{joint}. However, this bound does not take into account the local probabilities.

3.4. A refined semidefinite bound taking advantage of local probabilities

In [11], a semidefinite program (SDP) is presented to compute separable bounds on S as a function of the local photon number probabilities. Here, we provide a refined version of this program, including two improvements.

The first improvement is to express p_{joint} in (14) as a function of the density matrix elements, rather than bounding it according to equation (13). This allows us to perform the optimization of S across all terms together.

The second step is to take into account all information about the local probability distributions. This can be achieved by using the Frechet inequalities [36]. In the form of the disjunction[6], these inequalities can be expressed as

$$\max(0,\, p(A) + p(B) - 1) \leqslant P(A \bigcap B) \leqslant \min(p(A),\, p(B)). \tag{23}$$

Here, $A(B)$ refers to any set that includes at least one photon number on Alice's (Bob's) side. For instance, in the case that probabilities up to one photon component are observed, the possible choices for A and B consist of any nonempty combination from $\{0 \text{ photon},\ 1 \text{ photon},\ \text{more than } 1 \text{ photon}\}$. This gives us a set of $(2^3 - 1)$ by $(2^3 - 1)$ separate Frechet inequalities.

Adding the usual conditions to the two we just mentioned leads to the following formulation for the refined bound:

$$\begin{aligned}
\max \quad & S\left(p_0^A, p_1^A, p_0^B, p_1^B\right) \\
\text{s.t.} \quad & \hat{\rho} \geqslant 0 \\
& \operatorname{tr}\left(\hat{\rho}\right) \leqslant 1 \\
& \hat{\rho}^{T_b(0,1)} \geqslant 0 \\
& P(A \cap B) \geqslant \max[\,0,\, p(A) + p(B) - 1\,],\ \ \forall\, A, B \\
& P(A \cap B) \leqslant \min[\,p(A),\, p(B)\,],\ \ \forall\, A, B.
\end{aligned} \tag{24}$$

The program described in [9] can be seen as a relaxation of this program.

As presented here, it should be clear that the program 24 can be extended to take into account additional local photon numbers. In this case, the expression (14) needs to be modified to fit the newly considered Hilbert space. Similarly, the definition of p_{joint} can be adapted. However, the program remains the same. This presents the possibility of enhancing the bounds by taking into account additional information. We come back to this possibility in the experimental part of this paper.

Finally, we note that uncertainties in the local probabilities can be taken into account in this method by following the same procedure presented in [11].

[6] The conjunction and disjunction form of the Frechet inequalities can be found to be equivalent, so we use only one form.

3.5. Comparison of the separable bounds

Until now, we have presented four separable bounds for the witness. Let us briefly highlight their differences and mention the context in which it would be appropriate to use each of them.

The first bound, given in equation (6), is valid only for qubit states, and is thus not applicable in practice. However, it takes advantage of the observed local photon number distributions. This is the bound we used in section 2.3 to first illustrate the effect of losses on the witness.

The second bound, given in equation (19), also takes advantage of the knowledge of the photon number distributions and applies outside of the qubit space. However, one can check that this bound is not always tight. This stems from the fact that only some of the Frechet inequalities were taken into account in its derivation. Moreover, this bound can be very sensitive to uncertainties in the local probabilities, making it hardly applicable in practice. Nevertheless, it can be useful to quickly estimate the value of the bound that can be derived from equation (24).

The third bound, given in equation (22), is tight as a function of p_{joint} alone. It behaves well in presence of uncertainties, but does not take advantage of the knowledge of the local photon number probabilities.

The fourth bound, given in equation (24), is expressed as a semidefinite program. It does not assume a qubit structure and computes the tightest separable bound compared to all other methods by taking all physical constraints into account. Moreover, since it includes an exact modelization of the underlying quantum state, it behaves well in the presence of uncertainties on the local probabilities. Therefore, this is the kind of bound that we use in the next section to analyze the experimental data.

4. Experimental implementation of the witness

In this section, we present the experimental setup, including the single-photon source used for the entanglement generation and the practical details for implementing the witness. The experimental behavior of the witness with losses is also given.

4.1. Single-photon source and entanglement

The single-photon source is based on a type-II optical parametric oscillator (OPO) pumped far below threshold by a continuous-wave frequency-doubled Nd:YAG laser at 532 nm [27]. The frequency-degenerate signal and idler modes are orthogonally polarized and can be easily separated. The detection of a single photon on one mode then heralds the preparation of a single photon on the other mode [28–30]. Importantly, the photon is generated in a very well-defined spatiotemporal mode due to the OPO cavity. Experimental details, including the filterings required in the conditioning path and the definition of the temporal mode, have been presented elsewhere [31–34]. In the current experiment, the heralding efficiency (i.e., the single-photon component at the output of the OPO) is equal to 90 %, and the two-photon component is limited to a few percents. If one includes the total propagation and detection losses, the single-photon component reaches 68±2%. The initial effective transmission, η_{AB}, is thus ∼0.68.

Entanglement is obtained by impinging the heralded single-photon state on a balanced polarizing beam splitter. To check the entanglement, the two modes are then directed to two

homodyne detections, as shown in figure 1. By using the previous notations, without introducing additional communication channel losses, $p_1^A = p_1^B = 0.34 \pm 0.01$, in comparison to $p_1^A = p_1^B = 0.5$ for entanglement generated from an ideal single-photon source. In the following, we include additional losses to decrease the transmission in both symmetric and asymmetric ways.

4.2. Witnessing entanglement: practical realization

To perform the homodyne detections, a bright beam impinges on the balanced polarizing beam splitter mentioned above in order to distribute the two required local oscillators. Thus, the classical and quantum channels have orthogonal polarizations but the same spatial modes up to the detections. This configuration allows one to easily adjust the relative phase between the two detections by choosing an appropriate elliptical polarization for the bright beam before the splitting [9, 34]. By also sweeping its phase, both homodyne detections have a fixed relative phase but are locally phase-averaged, as required.

We now detail the full experimental procedure for implementing the proposed witness. The steps are as follows:

- *Acquiring homodyne data.* Phase-averaged homodyne tomography is performed on both modes. Four relative phase settings are required, but phase-averaging enables us to reduce them to two (i.e., $\pm\pi/4$). The recorded data are then used for the next steps.
- *Extracting the local probabilities.* The local photon-number distributions are extracted from the previous data. Importantly, no additional measurements are required. The estimation is obtained via pattern functions that relax any assumptions on the size of the Fock space [35].
- *Determining the separable bound.* The local probabilities are used to constrain the set of separable states and calculate the separable bound following the program given in equation (24).
- *Calculating the S parameter.* The homodyne data are sign-binned and the S parameter is then determined from equation (1). If S is above the separable bound, the bipartite state is entangled.

4.3. Tunable losses

We now turn to the study of the effect of losses on the proposed witness. Losses have been simulated here by changing the temporal modes. Indeed, the experiment is based on continuous-wave homodyne detection (i.e., the quadrature measurement is a continuous signal, $x(t)$). In order to measure the mode in which our state lies, a temporal filtering is required, leading to $x_\psi = \int \psi(t)x(t)dt$. The optimal temporal mode, $\psi(t)$, contains the generated state, and all the other orthogonal modes contain a vacuum state [32]. We can thus generate controlled and tunable losses by mismatching the temporal mode and the optimal mode we chose. The overlap, $\int \psi(t+\tau)\psi(t)dt$, provides the additional losses, $\eta(\tau)$, on each channel. As completed with the same raw data, the original state is always the same. Only the losses are tuned by this procedure.

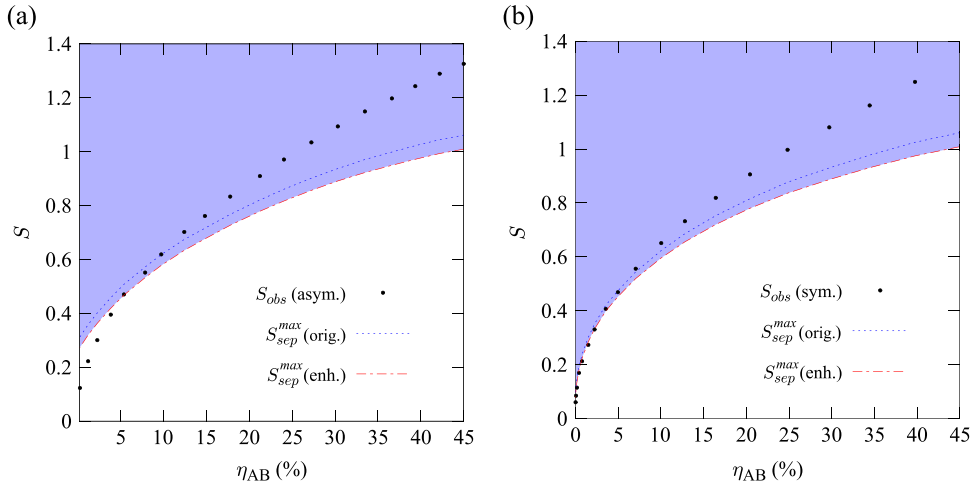

Figure 3. Experimental results. In the asymmetric case (a), additional losses are applied on one channel, whereas in the symmetric case (b), losses are applied equally on both channels. The results are given as a function of the overall transmission, $\eta_{AB} = \eta_A \eta_B$. The figures provide the measured CHSH values, S_{obs} (the size of the points accounts for statistical errors), together with two separable bounds determined using the program outlined in section 3.4. $S_{\text{sep}}^{\max}$ $(orig.)$ takes into account the multi-photon components up to one photon, as presented in [11]. $S_{\text{sep}}^{\max}$ $(enh.)$ corresponds to an enhanced separable bound, which takes into account the two-photon components as additional constraints in the optimization.

4.4. Results

Experimental results are displayed in figure 3. The measured CHSH parameter is given for different values of losses, together with the corresponding separable bounds. In the asymmetric case, the losses have been increased on one of the homodyne detections, while for the symmetric case, the losses are generated equally on both of them. However, as we did in the model, we can compare both situations in a relevant fashion only if we consider the full losses; we estimate the local losses with the help of the experimental vacuum components, $p_0^A = 1 - \eta_A$ and $p_0^B = 1 - \eta_B$, and then obtain the corresponding overall transmission, $\eta_{AB} = \eta_A \eta_B$.

The obtained results are in very good agreement with the expected behavior (i.e., $S \propto \sqrt{\eta_{AB}}$), and show that the bound of the single-photon entanglement witness can be violated unless very significant losses have ocurred. The figure provides two separable bounds determined by using the program outlined in section 3.4. The first bound takes as constraint the local probabilities up to one photon, as considered in [11], while the second bound considers the two-photon component. Clearly, more losses can be tolerated thanks to this enhanced separable bound. In the asymmetric case, the limit is pushed experimentally from 90% to 95% (corresponding to around 65 km of fiber at telecom wavelength if one starts with an ideal single-photon), while in the symmetric case a rise from 95% to 97% (77 km of fiber) is obtained. This small difference between the symmetric and asymmetric cases can be explained by the higher photon number component and the sensitivity of the bound to this parameter. Indeed, in the asymmetric case, the mode that does not experience loss keeps a larger two-photon component, which allows for a separable state with a higher S parameter.

5. Conclusion

In summary, we have presented a detailed analysis of the scheme to witness single-photon entanglement based only on the local homodyne measurements proposed in [11]. The effects of losses have been considered, and our investigation has shown the robustness of this hybrid witness. Even with communication channel losses of around 95%, entanglement can still be experimentally witnessed, both in the symmetric and asymmetric cases. The separable bound has been optimized by including local photon number distributions up to two photons. Indeed, the main contribution outside the qubit subspace comes from this component. These results confirm the efficiency of the witness and its relevance as an operational test for large-scale networks relying on single-photon entanglement.

Acknowledgements

We would like to thank Valentina Caprara Vivoli, Valerio Scarani, and Pavel Sekatski for discussions and comments on this paper. We acknowledge support from the ERC Starting Grant HybridNet, the ERA-NET CHIST-ERA under the QScale project, the Swiss NCCR QSIT, the Swiss National Science Foundation SNSF (grant PP00P2 – 150579), the European Commission (IP SIQS), the Singapore National Research Fund, and the Ministry of Education (partly through the Academic Research Fund Tier 3 MOE2012-T3–1-009). JL is a member of the Institut Universitaire de France.

Appendix

Here are the matrices we use to derive the analytical bound in section 3.3. The matrices are expressed in the natural basis for photon numbers (i.e., $\{|00\rangle, |01\rangle, |02\rangle, |10\rangle, |11\rangle, |12\rangle, |20\rangle, |21\rangle, |22\rangle\}$).

$$A = \begin{bmatrix} 0 & 0 & 0 & 0 & 0 & 0 & 0 & 0 & 0 \\ 0 & \lambda+\mu & 0 & m & 0 & 0 & 0 & 0 & 0 \\ 0 & 0 & \lambda & 0 & -\frac{4}{\pi} & 0 & 0 & 0 & 0 \\ 0 & m & 0 & \lambda+\mu & 0 & 0 & 0 & 0 & 0 \\ 0 & 0 & -\frac{4}{\pi} & 0 & \ell & 0 & -\frac{4}{\pi} & 0 & 0 \\ 0 & 0 & 0 & 0 & 0 & \lambda & 0 & 0 & 0 \\ 0 & 0 & 0 & 0 & -\frac{4}{\pi} & 0 & \lambda & 0 & 0 \\ 0 & 0 & 0 & 0 & 0 & 0 & 0 & \lambda & 0 \\ 0 & 0 & 0 & 0 & 0 & 0 & 0 & 0 & \lambda \end{bmatrix},$$

$$B = (\lambda + \mu - \ell)\begin{bmatrix} x_+^2/x_-^2 & 0 & 0 & 0 & -x_+/x_- & 0 & 0 & 0 & 0 \\ 0 & 0 & 0 & 0 & 0 & 0 & 0 & 0 & 0 \\ 0 & 0 & 0 & 0 & 0 & 0 & 0 & 0 & 0 \\ 0 & 0 & 0 & 0 & 0 & 0 & 0 & 0 & 0 \\ -x_+/x_- & 0 & 0 & 0 & 1 & 0 & 0 & 0 & 0 \\ 0 & 0 & 0 & 0 & 0 & 0 & 0 & 0 & 0 \\ 0 & 0 & 0 & 0 & 0 & 0 & 0 & 0 & 0 \\ 0 & 0 & 0 & 0 & 0 & 0 & 0 & 0 & 0 \\ 0 & 0 & 0 & 0 & 0 & 0 & 0 & 0 & 0 \end{bmatrix},$$

where

$$\ell = \frac{8\sqrt{2p_{\text{joint}}}}{\pi x_+}, \quad \text{and} \quad m = \frac{x_+}{x_-}(\lambda + \mu - \ell) - \frac{4\sqrt{2}}{\pi}.$$

References

[1] van Loock P 2011 Optical hybrid approaches to quantum information *Laser Photonics Rev.* **5** 167–200

[2] Furusawa A and van Loock P 2011 *Quantum teleportation and entanglement* (Weinheim: Wiley)

[3] Sangouard N, Simon C, Gisin N, Laurat J, Tualle-Brouri R and Grangier P 2010 Quantum repeaters with entangled coherent states *JOSA* B **27** A137–45

[4] Brask J B, Rigas I, Polzik E S, Andersen U L and Sorensen A S 2010 Hybrid long-distance entanglement distribution protocol *Phys. Rev. Lett.* **105** 160501

[5] Jeong H, Zavatta A, Kang M, Lee S W, Constanzo L S, Grandi S, Ralph T C and Bellini M 2014 Generation of hybrid entanglement of light *Nat. Photonics* **8** 564–9

[6] Morin O, Huang K, Liu J, Le Jeannic H, Fabre C and Laurat J 2014 Remote creation of hybrid entanglement between particle-like and wave-like optical qubits *Nat. Photonics* **8** 570–574

[7] Duan L M, Lukin M D, Cirac J I and Zoller P 2001 Long-distance quantum communication with atomic ensembles and linear optics *Nature* **414** 413–8

[8] van Enk S J 2005 Single-particle entanglement *Phys. Rev.* A **72** 064306

[9] Björk G, Jonsson P and Sánchez-Soto L L 2001 Single-particle nonlocality and entanglement with the vacuum *Phys. Rev.* A **64** 042106

[10] Hessmo B, Usachev P, Heydari H and Björk G 2004 Experimental demonstration of single photon nonlocality *Phys. Rev. Lett.* **92** 180401

[11] Morin O, Bancal J-D, Ho M, Sekatski P, D'Auria V, Gisin N, Laurat J and Sangouard N 2013 Witnessing trustworthy single-photon entanglement with local homodyne measurements *Phys. Rev. Lett.* **110** 130401

[12] Babichev S A, Appel J and Lvovsky A I 2004 Homodyne tomography characterization and nonlocality of a dual-mode optical qubit *Phys. Rev. Lett.* **92** 193601

[13] Chou C W, de Riedmatten H, Felinto D, Polyakov S V, van Enk S J and Kimble H J 2005 Measurement-induced entanglement for excitation stored in remote atomic ensembles *Nature* **438** 828–32

[14] Laurat J, Choi K S, Deng H, Chou C W and Kimble H J 2007 Heralded entanglement between atomic ensembles: preparation, decoherence, and scaling *Phys. Rev. Lett.* **99** 180504

[15] Laurat J, Chou C W, Deng H, Choi K S, Felinto D, de Riedmatten H and Kimble H J 2007 Towards experimental entanglement connection with atomic ensembles in the single excitation regime *New J. Phys.* **9** 207

[16] Bennet A J, Evans D A, Saunders D J, Branciard C, Cavalcanti E G, Wiseman H M and Pryde G J 2012 Arbitrarily loss-tolerant Einstein–Podolsky–Rosen steering allowing a demonstration over 1 km of optical fiber with no detection loophole *Phys. Rev.* X **2** 031003
[17] Cavalcanti E G, Drummond P D, Bachor H A and Reid M D 2009 Spin entanglement, decoherence and Bohm's EPR paradox *Opt. Express* **17** 18693–702
[18] Kimble H J 2008 The quantum internet *Nature* **453** 1023–30
[19] Sangouard N, Simon C, de Riedmatten H and Gisin N 2011 Quantum repeaters based on atomic ensembles and linear optics *Rev. Mod. Phys.* **83** 33–80
[20] Leonhardt U 1997 *Measuring the quantum state of light* (Cambridge: Cambridge University Press)
[21] Clauser J F, Horne M, Shimony A and Holt R A 1969 Proposed experiment to test local hidden-variable theories *Phys. Rev. Lett.* **23** 880–4
[22] Quintino M T, Araujo M, Cavalcanti D, Franca Santos M and Terra Cunha M 2012 Maximal CHSH violations with low efficiency photodetection and homodyne measurements *J. Phys. A: Math. Theor.* **45** 215308
[23] Sangouard N, Bancal J-D, Gisin N, Rosenfeld W, Sekatski P, Weber M and Weinfurter H 2011 Loophole-free Bell test with one atom and less than one photon on average *Phys. Rev.* A **84** 052122
[24] Roy S M 2005 Multipartite separability inequalities exponentially stronger than local reality inequalities *Phys. Rev. Lett* **94** 010402
[25] Peres A 1996 Separability criterion for density matrices *Phys. Rev. Lett.* **77** 1413
[26] Horodecki M, Horodecki P and Horodecki R 1996 Separability of mixed states: necessary and sufficient conditions *Phys. Lett.* A **223** 1–8
[27] Laurat J, Coudreau T, Keller G, Treps N and Fabre C 2004 Compact source of Einstein-Podolsky-Rosen entanglement and squeezing at very low noise frequencies *Phys. Rev.* A **70** 042315
[28] Hong C K and Mandel L 1986 Experimental realization of a localized one-photon state *Phys. Rev. Lett.* **56** 58–60
[29] D'Auria V, Lee N, Amri T, Fabre C and Laurat J 2011 Quantum decoherence of single-photon counters *Phys. Rev. Lett.* **107** 050504
[30] D'Auria V, Morin O, Fabre C and Laurat J 2012 Effect of the heralding detector properties on the conditional generation of single-photon states *Eur. Phys. J.* D **66** 249
[31] Morin O, D'Auria V, Fabre C and Laurat J 2012 High-fidelity single-photon source based on a type-II optical parametric oscillator *Optics Lett.* **37** 3738–40
[32] Morin O, Fabre C and Laurat J 2013 Experimentally accessing the optimal temporal mode of traveling quantum light states *Phys. Rev. Lett.* **111** 213602
[33] Morin O, Liu J, Huang K, Barbosa F, Fabre C and Laurat J 2014 Quantum state engineering of light with continuous-wave optical parametric oscillators *J. Vis. Exp.* **87** e51224
[34] Laurat J, Coudreau T, Keller G, Treps N and Fabre C 2005 Effects of mode coupling on the generation of quadrature Einstein-Podolsky-Rosen entanglement in a type-II optical parametric oscillator below threshold *Phys. Rev.* A **71** 022313
[35] Munroe M, Boggavarapu D, Anderson M E and Raymer M G 1995 Photon-number statistics from the phase-averaged quadrature-field distribution: theory and ultrafast measurement *Phys. Rev. A* **52** R924 R
[36] Fréchet M 1935 Généralisations du théorème des probabilités totales *Fundamenta Mathematicae* **25** 379–87

CONCLUSION

In this thesis we have presented efforts in three chapters towards different aspects of quantum repeater systems. We have discussed how it is possible to *ensure conditions* for implementing quantum repeaters with atomic ensembles, *explore the option* of optomechanical systems for implementing quantum repeaters and *verify the success* of completed quantum repeater protocols. In addition to our work, we also want to point out experimental achievements along similar directions, in addition to those already cited. For example, efforts have been made to increase the retrieval efficiency in atomic ensembles [50], going as high as 87% for gradient echo memory schemes [51, 52]. Other possibilities for the repeater nodes have been explored as well. Heralded entanglement has been experimentally shown in devices such as NV-centres in diamond [53, 54], neutral atoms [55], quantum dots [56] and recently mechanical resonators [57], demonstrating their potential for use in quantum repeaters.

There is still much that we can do to further the directions in which we have worked. For one, platforms explored as alternatives for atomic ensembles need high retrieval efficiencies to achieve entanglement connection and for the overall repeater system to be effective. To date, retrieval efficiencies from mechanical resonators stands only at about 30% [58, 59], and keeps them from being part of quantum repeater systems, due to critical efficiency requirements on the retrieval process. Finding fundamental limits for the retrieval efficiency would inform us if there are efficiency gains to be had, and would also further clarify the place of optomechanical devices in quantum repeaters.

To further our efforts in verification, we might also start to consider more

general 2-D architectures, as such architectures lend themselves more readily to real-world geographical scenarios. A natural extension of our verification of single photon entanglement is to focus on the verification of W-states, which are single photons delocalised over many paths. With an array of beamsplitters arranged so that the which-path information is erased, detector clicks can herald the sharing of a W-state between all the parties. Once this cluster has established entanglement, entanglement swapping operations could connect neighbouring clusters to complete the 2-D repeater system. Aside from W states, GHZ states have also been put forward as resources for 2-D quantum repeater systems within each link [60]. Entanglement witnesses for the GHZ state have been put forward and can even be resistant to large amounts of white noise [61, 62]. As we proceed towards real-world implementations of quantum repeaters with 2-D architectures, finding loss-resistant entanglement witnesses for the distributed states will be useful for verification, and could be a possible avenue for subsequent investigation.

Aside from the goals pursued in this thesis, other kinds of improvements have also been sought, especially with regards to the entanglement creation process in each link. The DLCZ protocol calls for a low write photon emission probability so that the heralding indicates the creation of a single delocalised excitation. Raising the write pulse laser power might increase the number of write photons, and thus increase the heralding rate, but this gives rise to multiple excitations, and erodes the quality of the distributed state. Multiplexing allows for multiple attempts at entanglement creation, while still keeping the probability of each write photon emission low. This can allow direct advantages with regards to the repeater rate [63]. or architectures to avoid memory lifetime constraints [64]. There are multiple forms of multiplexing that have already been considered. For example, atomic ensembles have demonstrated some capacity for spatial multiplexing, demonstrated in [65] with further possible improvements expected [66]. Efforts towards temporal multiplexing in atomic ensembles have been most promising as well [67, 68]. It would be valuable to explore schemes that combine different kinds of multiplexing in neighbouring links, motivated simply from an implementation of a hybrid quantum repeater system, or from advantages in more intricate multiplexing strategies.

We have come a long way from early communications systems. From the use of signal fires and semaphore devices, we have reached a point where the everyday user can possess mobile devices that can deal with bandwidth-heavy communications. Since quantum physics has given us a path towards secure communications

without assumptions on adversarial computational power, many people in this vibrant community from industry and academia alike have worked tirelessly toward this goal. The basic workings of a hybrid quantum network have already appeared in recent works, with photons from quantum dots stored in trapped ions [69] and an atomic ensemble memory shown to be suitable for storing light from quantum dots [70]. We also note the work in Ref [36], with a heralded spin excitation in an atomic ensemble retrieved, and then transferred into a rare-earth doped ion crystal with a second subsequent retrieval. Finally, let us remember that satellites have already been employed for secure communications, distributing secret keys across continents [29, 30]. It is this steady progress that suggests that quantum-enabled secure communications will be an accessible reality, and we are hopeful that our work contributes towards quantum repeater systems of the future.

BIBLIOGRAPHY

[1] M. Planck, Verhandl. Dtsch. Phys. Ges. **2**, 202 (1900)

[2] A. Einstein, Annalen der Physik **17**, 132 (1905)

[3] W. Heisenberg, Z. Phys. **33**, 879 (1925)

[4] M. Born, Z. Phys. **38**, 803 (1926)

[5] E. Schrödinger, Phys. Rev. **28**, 1049 (1926)

[6] T. Young, Phil. Trans. R. Soc. Lond. **92** 12 (1802)

[7] I. Cirac, and P. Zoller, Nature Phys. **8**, 264 (2012)

[8] D. Castelvecchi, Nature **541**, 9 (2017)

[9] R. Rivest, A. Shamir, and L Adleman, Comm. ACM **21** 120 (1978)

[10] P. Shor, J. Sci. Statist. Comput. **26** 1484 (1997)

[11] E. Martín-López, A. Laing, T. Lawson, R. Alvarez, X.-Q. Zhou, and J. L. O'Brien, Nature Phot. **6**, 773 (2012)

[12] N. Xu, J. Zhu, D. Lu, X. Zhou, X. Peng, and J. Du, Phys. Rev. Lett. **108**, 130501

[13] N. S. Dattani, and N. Bryans, arXiv:1411.6758

[14] F. Miller, *Telegraphic code to insure privacy and secrecy in the transmission of telegrams.* C.M. Cornwell. (1882)

[15] V. Scarani, H. Bechmann-Pasquinucci, N. J. Cerf, M. Dušek, Norbert Lütkenhaus, and M. Peev, Rev. Mod. Phys. **81**, 1301 (2009)

[16] C. Bennett, and G. Brassard, Proc. IEEE Int. Conf. on Comp. Sys. and Signal Process., 175 (1984)

[17] W. K. Wootters, and W. H. Zurek, Nat. **299** 802 (1982)

[18] V. Scarani, S. Iblisdir, N. Gisin, and A. Acín, Rev. Mod. Phys. **77**, 1225 (2005)

[19] A. K. Ekert, Phys. Rev. Lett. **67**, 661 (1991)

[20] J. F. Clauser, M. A. Horne, A. Shimony, and R. A. Holt, Phys. Rev. Lett. **23**, 880 (1969)

[21] D. Mayers, and A. Yao, in Proceedings of the 39th Annual Symposium on Foundations of Computer Science, Palo Alto, 1998 (IEEE, Washington, DC, 1998), p. 503

[22] S. Pironio, A. Acin, N. Brunner, N. Gisin, S. Massar, and V. Scarani, New J. Phys. **11**, 045021 (2009)

[23] U. Vazirani, and T. Vidick, Phys. Rev. Lett. **113**, 140501 (2014)

[24] C. Bennett, F. Bessette, G. Brassard, L. Salvail, and J. Smolin, J. Cryptol. **5**, 3 (1992)

[25] A. Muller, H. Zbinden, and N. Gisin, Europhys. Lett. **33**, 335 (1996)

[26] Y. Liu, T.-Y. Chen, J. Wang, W.-Q. Cai, X. Wan, L.-K. Chen, J.-H. Wang, S.-B. Liu, H. Liang, L. Yang, C.-Z. Peng, K. Chen, Z.-B. Chen, and J.-W. Pan, Opt. Express **18**, 8587 (2010)

[27] B. Korzh, C. C. W. Lim, R. Houlmann, N. Gisin, M. J. Li, D. Nolan, B. Sanguinetti, R. Thew, and H. Zbinden, Nat. Phot. **9**,163 (2015)

[28] R. Bedington, J. M. Arrazola, and A. Ling, npj Quant. Inf. **3**, 30 (2017)

[29] S.-K. Liao et. al., Nature (London) **549**, 43 (2017)

[30] S.-K. Liao et al., Phys. Rev. Lett. **120**, 030501 (2018)

[31] S.-K. Liao et. al., Nature Phot. **11**, 509 (2017)

[32] H.-J. Briegel, W. Dür, J. I. Cirac, and P. Zoller, Phys. Rev. Lett. **81**, 5932 (1998)

[33] N. Sangouard, C. Simon, H. de Riedmatten, and N. Gisin, Rev. Mod. Phys. **83**, 33 (2011)

[34] Duan L.-M., M. D. Lukin, J. I. Cirac, and P. Zoller, 2001, Nature (London) **414** 6862 (2001)

[35] H. J. Kimble, Nature (London) **453**, 1023 (2008)

[36] N. Maring, P. Farrera, K. Kutluer, M. Mazzera, G. Heinze, and H. de Riedmatten, Nature (London) **551**, 485 (2017)

[37] P. Farrera, G. Heinze, B. Albrecht, M. Ho, M. Chávez, C. Teo, and N. Sangouard, Nature Commun. **7**, 13556 (2016)

[38] M. Ho, C. Teo, H. de Riedmatten, and N. Sangouard, New J. Phys. **20**, 123018 (2018)

[39] A. V. Gorshkov, A. Andre, M. D. Lukin, and A. S. Sorensen, Phys. Rev. A **76**, 033805 (2007)

[40] J. Chan, A. H. Safavi-Naeini, J. T. Hill, S. Meenehan, and O. Painter, Appl. Phys. Lett. **101**, 081115 (2012)

[41] C. L. Yu, H. Kim, N. de Leon, I. W. Frank, J. T. Robinson, M. McCutcheon, M. Liu, M. D. Lukin, M. Loncar, and H. Park, Nano Lett. **13**, 248 (2013)

[42] M. Sumetsky, Y. Dulashko, and R. S. Windeler, Opt. Letters **35**, 1866 (2010)

[43] Z.-H. Zhou, C.-L. Zou, Y. Chen, Z. Shen, G.-C. Guo, and C.-H. Dong, Opt. Express **25**, 4046 (2017)

[44] V. Caprara Vivoli, T. Barnea, C. Galland, and N. Sangouard, Phys. Rev. Lett. **116**, 070405 (2016)

[45] M. Ho, E. Oudot, J.-D. Bancal, and N. Sangouard, Phys. Rev. Lett. **121**, 023602 (2018)

[46] C. W. Chou, H. de Riedmatten, D. Felinto, S. V. Polyakov, S. J. van Enk, and H. J. Kimble, Nature (London) **438**, 828 (2005)

[47] S.A. Babichev, J. Appel, and A.I. Lvovsky, Phys. Rev. Lett. **92**, 193601 (2004)

[48] O. Morin, J.-D. Bancal, M. Ho, P. Sekatski, V. D'Auria, N. Gisin, J. Laurat, and N. Sangouard, Phys. Rev. Lett. **110**, 130401 (2013)

[49] M. Ho, O. Morin, J.-D. Bancal, N. Gisin, N. Sangouard, and J. Laurat, New J. Phys. **16**, 103035 (2014)

[50] P. Vernaz-Gris, K. Huang, M. Cao, A. S. Sheremet, and J. Laurat, Nature Commun. **9**, 363 (2018)

[51] M. Hosseini , B. M. Sparkes, G. Campbell, P. K. Lam, and B. C. Buchler, Nature Commun. **2**, 174 (2011)

[52] Y.-W. Cho, G. T. Campbell, J. L. Everett, J. Bernu, D. B. Higginbottom, M. T. Cao, J. Geng, N. P. Robins, P. K. Lam, and B. C. Buchler, Optica **3**, 100 (2016)

[53] K. C. Lee, M. R. Sprague, B. J. Sussman, J. Nunn, N. K. Langford, X.-M. Jin, T. Champion, P. Michelberger, K. F. Reim, D. England, D. Jaksch, and I. A. Walmsley, Science **334** 1253 (2011)

[54] H. Bernien, B. Hensen, W. Pfaff, G. Koolstra, M. S. Blok, L. Robledo, T. H. Taminiau, M. Markham, D. J. Twitchen, L. Childress, and R. Hanson, Nature (London), **497**, 86 (2013)

[55] J. Hofmann, M. Krug, N. Ortegel, L. Gérard, M. Weber, W Rosenfeld, and H. Weinfurter, Science **337**, 72 (2012)

[56] A. Delteil, Z. Sun, W. Gao, E. Togan, S. Faelt, and A. Imamoğlu, Nature Phys. **12**, 218 (2016)

[57] R. Riedinger, A. Wallucks, I. Marinkovic, C. Löschnauer, M. Aspelmeyer, S. Hong, and S. Gröblacher, arXiv:1710.11147

[58] S. Hong, R. Riedinger, I. Marinkovic, A. Wallucks, S. G. Hofer, R. A. Norte, M. Aspelmeyer, and S. Gröblacher, Science **358**, 203 (2017)

[59] M. D. Anderson, S. T. Velez, K. Seibold, H. Flayac, V. Savona, N. Sangouard, and C. Galland, arXiv: 1802.04163

[60] J. Wallnöfer, M. Zwerger, C. Muschik, N. Sangouard, and W. Dür, Phys. Rev. A **94**, 052307 (2016)

[61] O. Gühne, and P. Hyllus, Int. J. Theor. Phys. **42**, 1001 (2003)

[62] C. Eltschka, and J. Siewert, Sci. Rep. **2**, 942 (2012)

[63] C. Simon, H. de Riedmatten, M. Afzelius, N. Sangouard, H. Zbinden, and N. Gisin, Phys. Rev. Lett. **98**, 190503 (2007)

[64] O. A. Collins, S. D. Jenkins, A. Kuzmich, and T. A. B. Kennedy, Phys. Rev. Lett. **98**, 060502 (2007)

[65] L. Tian, Z. Xu, L. Chen, W. Ge, H. Yuan, Y. Wen, S. Wang, S. Li, and H. Wang, Phys. Rev. Lett. **119**, 130505 (2017)

[66] A. Grodecka-Grad, E. Zeuthen, and A. S. Sørensen, Phys. Rev. Lett. **109**, 133601 (2012)

[67] I. Usmani , M. Afzelius , H. de Riedmatten, and N. Gisin, Nature Commun. **1**, 12 (2010)

[68] B. Albrecht, P. Farrera, G. Heinze, M. Cristiani, and H. de Riedmatten, Phys. Rev. Lett. **115**, 160501 (2015)

[69] H. M. Meyer, R. Stockill, M. Steiner, C. Le Gall, C. Matthiesen, E. Clarke, A. Ludwig, J. Reichel, M. Atatüre, and M. Köhl, Phys. Rev. Lett. **114**, 123001 (2015)

[70] J. Wolters, G. Buser, A. Horsley, L. Béguin, A. Jöckel, J.-P. Jahn, R. J. Warburton, and P. Treutlein, Phys. Rev. Lett. **119**, 060502 (2017)